Neuronal Activity Underlying Pathological Synchrony in the Rat Entorhinal Cortex

Li-Yuan Chen

Integrated Program in Neuroscience

McGill University

Montreal, Quebec, Canada

May 2020

A thesis submitted to McGill University in partial fulfillment of the requirements of the degree of Doctor of Philosophy.

Table of Contents

<u>Abstr</u>	ract	6
Résun	mé	8
Prefac	ce	10
Ackno	owledgements	11
Contr	ribution of original knowledge	13
Contr	ribution of authors	14
Chapt	ter 1: Background	15
1.1.	Mesial temporal lobe epilepsy	16
1.2.	Ictal activity	17
1.3.	Potassium-chloride cotransporter 2 (KCC2)	19
1.4.	Interictal activity	20
1.5.	Theta rhythm	21
1.6.	Research objectives and rationales	21
<u>Chapt</u>	ter 2: Dynamic Interneuron-Principal Cell Interplay Leads to a	a Specific Pattern of <i>In</i>
	Ictogenesis	24
2.1.	Abstract	25
2.2.	Introduction	26
2.3.	Materials and methods	26
2.3.1.	Slice preparation and maintenance	26
2.3.2.	Single-unit and field potential recording	27
2.3.3.	Clustering and identification of cell types	27
2.3.4.	Single unit-interictal discharge relationship	28
2.3.5.	Single-unit activity during ictal discharges	28
2.3.6.	Single unit-ictal discharge phase relationship	29
2.4.	Results	29
2.4.1.	Epileptiform activity induced by 4AP	29
2.4.2.	Characterization of single units	29

2.4.3.	Single-unit activity during interictal discharges	30
2.4.4.	Single-unit activity during ictal discharges	31
2.5.	Discussion	32
2.5.1.	Frequently occurring spikes are sustained by interneuron and principal cell	network
	interplay	32
2.5.2.	Sudden onset ictal discharges are initiated by principal cell activity	33
2.5.3.	Distinct patterns of epileptiform activities induced in the EC by 4AP	35
2.5.4.	Conclusions	35
2.6.	References	37
2.7.	Figures	40
Chapt	ter 3: KCC2 Antagonism Increases Neuronal Network Excitability but	Disrupts
	enesis In Vitro.	45
3.1.	Abstract	46
3.2.	Introduction	47
3.3.	Materials and methods	48
3.3.1.	Ethical approval	48
3.3.2.	Slice preparation and maintenance	48
3.3.3.	Single-unit and field potential recording	49
3.3.4.	Raw data processing for single-unit activity	49
3.3.5.	Raw data processing for field potential activity	50
3.3.6.	Qualitative analysis of single-unit activity	51
3.3.7.	Quantitative analysis of single-unit firing	51
3.3.8.	Statistical Analysis	52
3.4.	Results	53
3.4.1.	Characterization of single units	53
3.4.2.	Effects of KCC2 antagonism on 4AP-induced field activity	53
3.4.3.	Effects of KCC2 antagonism on single-unit activity during ictal discharges	54
3.4.4.	Effects of KCC2 antagonism on single-unit activity during interictal events	55
3.5.	Discussion	56
3.5.1.	KCC2 function is needed for the generation of 4AP-induced ictal discharges	56
3.5.2.	KCC2 antagonism leads to neuronal hyperexcitability	58

3.5.3.	Conclusions	59
3.6.	References	60
3.7.	Figures	64
<u>Chapt</u>	ter 4: KCC2 Antagonism and GABAergic Synchronization in the Entorhinal Cortex	x in
the Al	bsence of Ionotropic Glutamatergic Receptor Signalling.	70
4.1.	Abstract	71
4.2.	Introduction	72
4.3.	Materials and methods	73
4.3.1.	Ethical approval	73
4.3.2.	Specimen preparation and maintenance	73
4.3.3.	Tetrode recordings	74
4.3.4.	Isolation of single-unit activity	75
4.3.5.	Isolation of field potential activity	75
4.3.6.	Patterns of single-unit activity around the onset of interictal spikes	76
4.3.7.	Quantification of single-unit activity around the peak of interictal spikes	76
4.3.8.	Statistical analyses	77
4.4.	Results	77
4.4.1.	Single-unit characterization	77
4.4.2.	Alterations of interictal spikes by antagonizing KCC2 activity	77
4.4.3.	Effects of VU0463271 on single-unit activity pattern around the onset of interictal spi	kes
		78
4.4.4.	Effects of VU0463271 on the occurrence of single-unit activity during interictal spikes	, 79
4.5.	Discussion	79
4.5.1.	KCC2 antagonism alters the dynamics of interictal spikes	80
4.5.2.	KCC2 antagonism alters the pattern of single-unit activity during interictal spikes	81
4.5.3.	Conclusions	82
4.6.	References	83
4.7.	Figures	87
<u>Chapt</u>	ter 5: Single-Unit Activity in the <i>In Vitro</i> Entorhinal Cortex During Carbachol-Indu	<u>ced</u>
Field	Oscillations	91

5.1.	Abstract	92
5.2.	Introduction	
5.3.	Materials and methods	94
5.3.1.	Brain slice preparation, maintenance, and treatment	94
5.3.2.	Tetrode recordings	95
5.3.3.	Raw data processing for single-unit activity	95
5.3.4.	Raw data processing for field potential activity	96
5.3.5.	Classification of single-unit activity types	96
5.3.6.	Single-unit activities around CCh-induced oscillations	97
5.3.7.	Single-unit phase firing during CCh-induced oscillations	97
5.3.8.	Statistics	98
5.4.	Results	98
5.4.1.	Single-unit classification	98
5.4.2.	Single-unit activity during CCh-induced oscillations	99
5.4.3.	GABA _A receptor involvement in CCh-induced oscillations	100
5.4.4.	Ionotropic glutamatergic receptor involvement in CCh-induced oscillations	101
5.5.	Discussion	102
5.5.1.	CCh induced increases in single-unit activity during CCh-induced oscillations	102
5.5.2.	The role of interneurons and GABAA-receptor during CCh-induced oscillations	103
5.5.3. Ionotropic glutamatergic signaling is necessary for the generation		nduced
	oscillations	104
5.5.4.	Epileptiform synchronization and CCh-induced oscillations	104
5.6.	References	106
5.7.	Figures	111
Chapt	ter 6: General Discussion	118
6.1.	Summary of findings	119
6.2.	Seizure onset patterns and changes in neuronal activity	120
6.3.	KCC2 antagonism and dynamics of neuronal activity	120
6.4.	Interneurons in epilepsy	121
6.5.	Future perspective and concluding remarks	122

Reference List	12	5
----------------	----	---

Abstract

Mesial temporal lobe epilepsy is a debilitating disease presenting with pathological brain rhythm; however, our current understanding of the neuronal activity underlying the epileptiform activity is limited. Identifying factors that contribute to changes in neuronal activity during epileptiform events could advance our understanding of the basic mechanisms of epilepsy. Therefore, I performed *in vitro* tetrode recordings in the rat entorhinal cortex to simultaneously record single-unit and local field potential (LFP) activities during epileptiform discharges as well as theta oscillations.

First, I investigated single-unit activity underlying the *in vitro* 4-aminopyridine (4AP)-induced ictal events presented with the sudden onset pattern that are recorded in the LFP activity. The experiments demonstrated that the excitatory principal cells were involved in the generation of these epileptiform events. Together with previous studies showing the involvement of inhibitory interneurons in the generation of 4AP-induced ictal events characterized by the low-voltage fast (LVF) onset pattern, my findings suggest that different seizure onset patterns are associated with different involvements of specific neuronal populations.

Next, I studied the effects of antagonizing the K⁺-Cl⁻ cotransporter 2 (KCC2) activity on single-unit activity underlying the *in vitro* 4AP-induced LVF onset ictal events recorded in the LFP activity. I found that ictal-like events occurring during KCC2 antagonism were not associated with significant increases in interneuron and principal cell activities, suggesting that the typical 4AP-induced LVF onset ictal events were abolished. Additionally, 4AP-induced interictal events, which continued to occur during KCC2 antagonism, were associated with significant increases in interneuron and principal cell activities; during KCC2 antagonism, however, significant increases were observed in the interneuron and principal cell firing but not in their neuronal synchrony. When these 4AP-induced interictal events were recorded during the blockade of ionotropic glutamatergic signalling, interneuron action potentials were significantly more likely to occur at the beginning of the interictal events than the end, pointing to an increase in interneuron excitability. Altogether, these findings suggest that KCC2 antagonism enhances neuronal excitability.

Finally, I analyzed the interplay between inhibitory and excitatory mechanisms during carbachol (CCh)-induced theta oscillations *in vitro*. My analyses of the single-unit activity showed that, around the onsets of these theta oscillations in the LFP activity, interneuron activity increased

before principal cell activity. After γ -aminobutyric acid type A (GABA_A) signalling was antagonized, the duration of theta oscillations became more variable. Altogether, my findings highlight the role of inhibitory neurons and signalling in regulating theta rhythm and describe a neuronal interplay where interneurons fire before principal cells.

The experiments outlined in this thesis examined three factors contributing to changes in neuronal activity underlying epileptiform discharges: seizure onset pattern, KCC2 activity, and theta rhythm. By examining neuronal activity with respect to these factors, the findings presented in this thesis is part of a larger research effort devoted to understanding the basic mechanisms of epilepsy.

Résumé

L'épilepsie temporale mésiale est un désordre neurologique associé à de l'activité électroencéphalographique (EEG) pathologique. L'activité neuronale sous-jacente à l'activité épileptiforme enregistrée sur l'EEG est cependant peu connue. L'identification des facteurs qui contribuent aux changements de l'activité neuronale pendant les évènements épileptiformes pourrait contribuer à l'avancement des connaissances sur les mécanismes de base de l'épilepsie. Ainsi, j'ai effectué des enregistrements avec les tétrodes dans le cortex entorhinal du rat afin d'obtenir l'activité neuronale unitaire et l'activité des potentiels de champs locaux pendant les décharges épileptiformes ainsi que pendant les oscillations thêta.

Premièrement, j'ai étudié l'activité neuronale unitaire associée aux décharges épileptiformes induites par la 4-aminopyridine (4AP) in vitro. J'ai observé des décharges ictales qui apparaissaient soudainement (aussi nommé décharges ictales à « initiation soudaine ») et montré le rôle des neurones pyramidaux excitateurs au début de la genèse de ces décharges ictales. Les études précédentes avaient montré que les décharges ictales induites par la 4AP et caractérisées par une activité rapide à bas voltage (aussi nommées « low-voltage fast onset » ou LVF) étaient associées à l'activité d'interneurones inhibiteurs. En prenant en considération l'ensemble de ces résultats, j'ai montré que la genèse de ces deux patrons de décharges ictales est associée à une implication différente des interneurones et neurones pyramidaux.

Ensuite, j'ai étudié en *in vitro* les effets d'un antagoniste du co-transporteur K⁺-Cl⁻ (KCC2) sur l'activité neuronale unitaire associée aux décharges ictales « LVF » induites par la 4AP. J'ai observé que les décharges qui ressemblent à de l'activité ictale pendant l'application de l'antagoniste du KCC2 ne sont pas associées à des augmentations significatives de l'activité des interneurones et des neurones pyramidaux; donc, les décharges ictales sont abolies pendant l'application de l'antagoniste du KCC2. De plus, les décharges interictales induites par la 4AP qui continuaient à être présentes pendant l'application de l'antagoniste du KCC2 étaient associées à des augmentations significatives de l'activité des interneurones et neurones pyramidaux. Toutefois, pendant l'antagonisme du KCC2, des augmentations significatives étaient constatées de la décharge neuronale et non de la synchronisation neuronale. Lorsque les antagonistes de la neurotransmission ionotropique glutamatergique étaient appliqués, l'activité des interneurones était augmentée de façon significative au début des évènements interictaux plutôt qu'à la fin. En

d'autres termes, j'ai observé une augmentation de l'excitabilité des interneurones. Ainsi, l'antagoniste du KCC2 favorise l'excitabilité neuronale.

Finalement, j'ai effectué des analyses de l'interaction entre les mécanismes inhibiteurs et excitateurs pendant les oscillations thêta induites par le carbachol (CCh) *in vitro*. Au début des oscillations thêta, j'ai observé que l'augmentation de l'activité des interneurones survenait avant l'augmentation de l'activité des neurones pyramidaux. Après l'application de l'antagoniste de la neurotransmission GABAergique, la durée des oscillations thêta devenait variable. En somme, mes résultats ont permis de mieux définir le rôle des neurones inhibiteurs et de la transmission inhibitrice dans le rythme thêta et l'interaction entre les interneurones et les neurones pyramidaux.

Les procédures expérimentales présentées dans cette thèse ont permis d'étudier trois facteurs associés à des changements de l'activité neuronale lors de décharges épileptiformes : les décharges à « initiation soudaine », le KCC2, et le rythme thêta. En examinant l'activité neuronale associée à ces trois facteurs, les résultats présentés dans cette thèse contribuent au développement de connaissances sur les mécanismes de base de l'épilepsie.

Preface

This thesis is submitted for the degree of Doctor of Philosophy in the Integrated Program in Neuroscience at McGill University. The research described in this thesis was conducted under the supervision of Dr. Massimo Avoli at the Montreal Neurological Institute-Hospital in the Departments of Neurology & Neurosurgery and of Physiology at McGill University between 2015-2020. The aim of this thesis is to advance our understanding of the basic mechanisms underlying epileptiform synchronization. Parts of this thesis are published in peer-reviewed journals and referenced accordingly throughout the thesis.

Li-Yuan Chen January 2020

Acknowledgements

A PhD journey is never travelled alone. The work outlined in this thesis would not have been possible without the support from many individuals and organizations.

I would like to express my deepest gratitude and appreciation to Dr. Massimo Avoli for his guidance and mentorship during my graduate studies. His immense experience and knowledge have helped me to acquire invaluable skills and expertise under his supervision. Furthermore, his kindness, patience, and humor have created a unique training experience that will be remembered with respect and admiration for many years to come.

I am grateful to my advisory committee members Dr. David Ragsdale and Dr. Phillippe Séguéla as well as my mentor Dr. Louis Collins. Their advice and guidance during our annual advisory committee meetings and oral examinations are essential to my learning.

I would like to offer my appreciation to Dr. Maxime Lévesque. His guidance and insight during data acquisition and analysis as well as manuscript preparation are indispensable to my learning and productivity.

Throughout my graduate studies, I have worked with an insightful collaborator as well as amazing colleagues in the laboratory: Dr. Mauro Cataldi, Dr. Rochelle Herrington, Dr. Shabnam Hamidi, Dr. Zahra Shiri, Nancy Duan, Leila Leclerc, Siyan Wang, Sally Barker, and Cristen Kfoury. Notably, I am indebted to Dr. Shabnam Hamidi who patiently and meticulously taught me the electrophysiological recording techniques that are fundamental to my work. I also want to extend my gratitude to Dr. Rochelle Herrington, Nancy Duan, Leila Leclerc, and Siyan Wang for their participation in data collection and analysis of the work described in this thesis. Additionally, I am grateful for the insights offered by our collaborator Dr. Mauro Cataldi.

I would like to acknowledge Toula Papadopoulos and the Integrated Program in Neuroscience Administration for their support throughout my graduate studies. Additionally, I want to thank the Centre for Neurological Disease Models of the Montreal Neurological Institute-Hospital for ensuring the quality, safety, and responsible use of research models in my experiments.

To my friend Clemence Tam, I want to thank you for providing thorough grammatical guidance throughout my graduate studies, including this thesis. You never fail to add a little confidence in my writings.

Last but not the least, the work outlined in this thesis is made possible through the generous funding from the Savoy Foundation and the Canadian Institutes of Health Research. Their support

allowed me to acquire scientific training and to pursue my intellectual curiosity. The work presented in this thesis aims to fulfill their mission of creating new knowledge that can be translated to improve the health of people living with epilepsy.

Contribution of original knowledge

In the work described in this thesis, I utilized tetrodes to examine single-unit activity recorded from a large number of neurons with local field potential (LFP) activity in the *in vitro* brain slice preparation – an experimental protocol pioneered by Dr. Massimo Avoli – to elucidate the basic mechanisms of epilepsy. The experiments described in Chapter 2, 3, 4, and 5 demonstrated original scholarship, contributed to the existing knowledge, and were published as distinct manuscripts in peer-reviewed journals in the field of epilepsy research.

Chapter 2 describes the single-unit activity underlying a type of *in vitro* ictal events with a distinct ictal onset pattern – the sudden onset ictal events. While this ictal onset pattern was previously described, very few studies characterized the underlying neuronal activity. The work described in Chapter 2 is one of the first to add to our current understanding of the generation of sudden onset ictal events.

Chapter 3 characterizes the changes induced by the antagonism of K⁺-Cl⁻ cotransporter 2 (KCC2) to single-unit activity underlying an *in vitro* model of epileptiform activity. While KCC2 activity was known to be involved in epilepsy, its exact role remained elusive; in particular, the effects of KCC2 antagonism in *in vitro* epileptiform activity are still under debate. The work outlined in Chapter 3 – characterizing the underlying single-unit activity – provides further insights into this existing debate.

Chapter 4 continues the investigation outlined in Chapter 3 by examining the role of KCC2 in single-unit activity underlying the dynamics of interictal events occurring in the absence of ionotropic glutamatergic signalling. Previous work demonstrated that inhibitory signalling of interneurons plays a critical role in the generation of interictal events. Thus, by isolating these interictal spikes from ionotropic glutamatergic signalling, the work outlined in Chapter 4 specifically examines the relationship between KCC2 antagonism and interneuron activity during the generation of interictal events.

Chapter 5 examines the contributions of ionotropic excitatory and inhibitory signalling to the dynamics of an *in vitro* model of theta oscillations and its underlying neuronal interplay. Previously, the role of ionotropic inhibitory and excitatory signalling was independently examined from the interplay between the inhibitory interneurons and excitatory principal cells in these theta oscillations. Thus, the work outlined in Chapter 5 unifies our understanding of neuronal interplay during theta rhythm.

Contribution of authors

The work presented in Chapter 2, 3, 4, and 5 were collaborative efforts that were published as 4 distinct manuscripts. All individuals who contributed to the work were listed as authors, and their contributions are outlined here.

Chapter 2 was published as "Dynamic Interneuron-Principal Cell Interplay Leads to a Specific Pattern of *In Vitro* Ictogenesis" in 2018 in the *Neurobiology of Disease* with the following authors: Maxime Lévesque (M.L.), Li-Yuan Chen (L.-Y.C.), Shabnam Hamidi (S.H.), and Massimo Avoli (M.A.). M.A. conceived and designed research. L.-Y.C. and S.H. performed experiments. M.L. and L.-Y.C. analyzed data. M.L., L.-Y.C., and M.A. interpreted results of experiments. M.L. and M.A. prepared figures. M.L. and M.A. drafted manuscript. M.L., L.-Y.C., and M.A. edited and revised manuscript. All authors approved the final version of manuscript.

Chapter 3 was published as "KCC2 Antagonism Increases Neuronal Network Excitability but Disrupts Ictogenesis *In Vitro*" in 2019 in the *Journal of Neurophysiology* with the following authors: Li-Yuan Chen (L.-Y.C.), Maxime Lévesque (M.L.), and Massimo Avoli (M.A.). L.-Y.C. and M.A. conceived and designed research. L.-Y.C. performed experiments. L.-Y.C. and M.L. analyzed data. All authors interpreted results of experiments and prepared figures. All authors drafted, edited, and revised manuscript. All authors approved the final version of manuscript.

Chapter 4 was published as "KCC2 Antagonism and GABAergic Synchronization in the Entorhinal Cortex in the Absence of Ionotropic Glutamatergic Receptor Signalling" in 2020 in the *Neuropharmacology* with the following authors: Li-Yuan Chen (L.-Y.C.), Maxime Lévesque (M.L.), and Massimo Avoli (M.A.). M.A. conceived and designed research. L.-Y.C. performed experiments and analyzed data. All authors interpreted results of experiments and prepared figures. All authors drafted, edited, and revised manuscript. All authors approved the final version of manuscript.

Chapter 5 was published as "Single-Unit Activity in the *In Vitro* Entorhinal Cortex during Carbachol-induced Field Oscillations" in 2018 in the *Neuroscience* with the following authors: Li-Yuan Chen (L.-Y.C.), Maxime Lévesque (M.L.), Mauro Cataldi (M.C.), and Massimo Avoli (M.A.). M.C. and M.A. conceived and designed research. L.-Y.C. performed experiments. L.-Y.C. and M.L. analyzed data. L.-Y.C., M.L., and M.A. interpreted results of experiments and prepared figures. L.-Y.C., M.L., and M.A. drafted, edited, and revised manuscript. All authors approved the final version of manuscript.

Chapter 1: Background

In this first chapter, I provide the context of the work outlined in this thesis by reviewing the relevant literature and highlighting the research rationales and objectives. The chapter begins with an introduction on mesial temporal lobe epilepsy that is followed by an examination of the current understanding of the basic mechanisms of epilepsy – focusing on the existing literature on the underlying neuronal activity. The chapter then discusses the objectives and rationales of the experiments presented in this thesis.

1.1. Mesial temporal lobe epilepsy

Epilepsy is a neurological disease defined by an increased susceptibility to have seizures (Fisher et al., 2014). The worldwide median prevalence of epilepsy was recently estimated to be between 4.9-12.7 per 1,000 persons (Ngugi et al., 2010; Fiest et al., 2017). In Canada, the overall prevalence of epilepsy was estimated to be 4.0 per 1,000 persons (Gilmour et al., 2016). These numbers have motivated epilepsy research in the laboratory, but these efforts have translated to limited progress in the clinic. For instance, while novel anti-epileptic drugs were consistently introduced to the clinical setting to control seizure occurrence, the proportion of patients gaining adequate seizure control through pharmacotherapy did not increase (Löscher and Schmidt, 2011; Brodie et al., 2014; Pohlen et al., 2017; Chen et al., 2018). While epilepsy surgeries were consistently demonstrated to be a therapeutic alternative for achieving adequate seizure control (Wiebe et al., 2001; Engel et al., 2012; Jobst and Cascino, 2015), it remained underutilized in the clinic and, thus, could benefit from further advances in candidate selection and surgical technique (Engel, 2018). Altogether, epilepsy remains an active area of research in order to improve therapeutic strategies.

Epilepsy is also a heterogeneous disease that can be better described as *epilepsies* or *epileptic syndromes* rather than *epilepsy* per se. One of these epilepsies is mesial temporal lobe epilepsy (MTLE), in which seizures originate from limbic areas including the hippocampus, entorhinal cortex (EC), and amygdala (Quesney, 1986; Spencer and Spencer, 1994; Wennberg et al., 2002; Behr et al., 2014). MTLE was associated to a less favorable disease progression (Choi et al., 2016) and an increased likelihood of becoming medically refractory (Semah et al., 1998; Stephen et al., 2001; Gilioli et al., 2012), which is diagnosed when two or more pharmacotherapy attempts failed to provide adequate seizure control (Kwan et al., 2010). Consequently, a significant amount of research effort has been devoted to studying MTLE by investigating epileptiform activity generated in the limbic structures.

Epilepsy produces symptoms in the local field potential (LFP) activity of the brain – that is, synchronized activity electrographically recorded from a neuronal ensemble using electrodes inserted into the brain (Buzsáki et al., 2012; Kandel et al., 2013). These electrographic symptoms, which are distinctive from baseline LFP activity, are commonly differentiated into ictal events, which are seizures or electrographic disturbances lasting several seconds, and interictal events, which are electrographic disturbances lasting only few seconds between ictal events (Gibbs et al., 1935; Chatrian et al., 1974). To gain mechanistic insights into ictal and interictal activity of MTLE,

diverse acute and chronic models of epilepsy and of epileptiform activity were developed in the laboratory for research studies (Avoli and Jefferys, 2016; Lévesque et al., 2016a). The work conducted in this thesis is one of these investigations that aims to advance our understanding by providing insights into the basic mechanisms of MTLE.

1.2. Ictal activity

Conceptually, seizures are defined as "abnormal excessive or synchronous neuronal activity" (Fisher et al., 2005). This characterization implies that seizures – and seizure generation, or ictogenesis – involve increases in neuronal firing or synchrony. Accordingly, neurons were found to increase their firing around ictal onsets (Schmidt et al., 1959; Wenzel et al., 2019) and during ictal events (Prince and Wilder, 1967; Ishijima, 1972; Cymerblit-Sabba and Schiller, 2010). Such increases in neuronal firing were also reported in human epileptic patients (Calvin et al., 1973; Babb and Crandall, 1976; Babb et al., 1987; Bower et al., 2012; Schevon et al., 2012). In addition to firing, neuronal synchrony with the LFP activity was found to increase around ictal onsets (Bikson et al., 2003; Cohen et al., 2006; Wenzel et al., 2019) as well as during ictal events (Prince and Wilder, 1967; Ishijima, 1972; Butuzova and Kitchigina, 2008; Cymerblit-Sabba and Schiller, 2010), which were also replicated in investigations in human epileptic patients (Verzeano et al., 1971; Ishijima et al., 1975; Wyler et al., 1982; Truccolo et al., 2011; Schevon et al., 2012; Weiss et al., 2013). These findings altogether support the concept of seizures resulting from excessive or synchronous neuronal activity.

Upon closer examination, the neuronal activity – particularly with regards to neuronal firing – underlying seizures appears to be more complex than what was implied in the conceptual definition of seizures. Namely, researchers were able to record neurons that increased their firing simultaneously with neurons that decreased their firing around seizure onset in similar proportions: 39% and 37%, respectively (Bower and Buckmaster, 2008). Their reports were consistent with observations made from human epileptic patients (Truccolo et al., 2011; Weiss et al., 2016; Lambrecq et al., 2017). Altogether, the data associate seizures to bidirectional changes – namely, both increases and increases – in neuronal firing, which suggest that the underlying mechanisms of seizures and ictogenesis are more than increases in neuronal activity.

Considering that neurons could categorized based on the neurotransmitters that they release, heterogeneous neuronal activity patterns in association to ictal events could be further

characterized by examining the activities of interneurons and principal cells separately. While increases in the firing of both interneurons (Butuzova and Kitchigina, 2008; Lillis et al., 2012; Grasse et al., 2013; Toyoda et al., 2015; Lévesque et al., 2016b; Wenzel et al., 2019) and principal cells (Fujita et al., 2014; Ewell et al., 2015) were found around ictal onsets, important differences also emerged. With respect to the temporal dynamics between interneuron and principal cell firing increases, researchers found that interneuron firing increases preceded principal cell firing increases, implicating interneurons – as opposed to principal cells – in ictogenesis (Grasse et al., 2013; Lévesque et al., 2016b); these findings were corroborated by investigations in human epileptic patients (Elahian et al., 2018; Kandrács et al., 2019). Furthermore, with respect to neuronal synchrony with the LFP activity, interneurons increased their synchrony with the ongoing ictal events more than principal cells (Grasse et al., 2013; Neumann et al., 2017). These findings thus implicate increases in interneuron activity during seizures and ictogenesis.

Seemingly contradictory findings also exist in the literature. Namely, some investigators found that principal cell activity increased more than interneuron activity during seizures (Aeed et al., 2020), suggesting that principal cells were more involved in ictogenesis than interneurons. However, a difference existed among these studies – the LFP activity patterns around the onsets of seizures. Different seizure onset patterns were identified in experimental models (Avoli et al., 2013, 2016; Lévesque et al., 2016a) and in human epileptic patients (Perucca et al., 2014). Upon a closer examination, principal cell activity increased more than interneuron activity during seizures presenting with the hypersynchronous onset pattern (Aeed et al., 2020) – which is a high amplitude, low frequency discharge pattern (Engel, 2013; Avoli et al., 2016). On the contrary, some of the previously discussed studies that reported increases in interneuron firing and synchrony examined exclusively ictal events of the low-voltage fast onset pattern (Grasse et al., 2013; Lévesque et al., 2016b; Elahian et al., 2018) – which is a low amplitude, high frequency discharge pattern (Engel, 2013; Avoli et al., 2016). In other words, heterogeneous neuronal activity firing patterns can be further characterized by considering the types of neurons and seizure onset patterns involved.

At first glance, seizures appeared to be associated with heterogeneous patterns of neuronal activity, rather than the proposed increases in neuronal activity. Upon closer examination, this heterogeneity in neuronal activity pattern can be further dissected by distinguishing interneurons from principal cells and different seizure onset patterns.

1.3. Potassium-chloride cotransporter 2 (KCC2)

The electrical activity of neurons is influenced by the ionic concentration gradient across the neuronal membrane. While many proteins are expressed by neurons to control the concentration gradients of different ions, one protein of particular research interest is K⁺-Cl⁻ cotransporter 2 (KCC2). Mutations in the SLC12A5, which encodes KCC2 in humans, were identified in people living with familial epilepsy (Kahle et al., 2014; Puskarjov et al., 2014; Stödberg et al., 2015; Saitsu et al., 2016; Saito et al., 2017; Till et al., 2019). These studies associated epilepsy with impaired KCC2 function – namely, mutations disrupted the intracellular Cl⁻ extrusion and the KCC2 protein expression on the cell surface (Kahle et al., 2014; Puskarjov et al., 2014; Stödberg et al., 2015; Saitsu et al., 2016). Therefore, studies of human genetic mutations support an involvement of KCC2 in epilepsy.

In ictogenesis, the role of KCC2 was previously interrogated with regards to ionic dynamics. KCC2 extrudes Cl⁻ and K⁺ from neurons (Di Cristo et al., 2018) and is expressed by both interneurons and principal cells (Gulyás et al., 2001). Its activity was known to influence the intracellular [Cl-], which determined the integrity of γ-aminobutyric acid type A (GABA_A) signalling (Kaila et al., 2014). Accordingly, previous experiments demonstrated that, at seizure onset, there was an increase in interneuron firing concomitant with an increase in intracellular [Cl⁻] in both interneurons and principal cells (Lillis et al., 2012). Given that KCC2 activity influenced γ-aminobutyric acidergic (GABAergic) response in both interneurons and principal cells (Otsu et al., 2020), the experiments together suggested that interneuron firing at seizure onset could result in disrupted GABAergic signalling due to an intracellular increase in [Cl-] from a pathological decrease in KCC2 activity. In addition to [Cl⁻] dynamics at seizure onset, researchers correlated increases in extracellular [K⁺] to increases in the interneuron firing and the GABAergic signalling (Librizzi et al., 2017). Based on previous experiments, KCC2 activity could mediate increases in extracellular [K⁺], resulting in neuronal membrane depolarization (Viitanen et al., 2010). In other words, interneuron firing at seizure onset could depolarize local populations of neurons due to an extracellular increase in [K⁺] from a pathological increase in KCC2 activity. Taking these data together, KCC2 could be involved in ictogenesis through its ability to modulate the [Cl-] and [K+] gradients.

Experimental data from the literature implicated KCC2 in ictogenesis through GABAergic signalling of interneuron activity. More specifically, KCC2 modulated interneuron and principal

cell activities around seizure onset through its involvement in regulating intracellular [Cl⁻] and extracellular [K⁺]. In other words, increases in interneuron activity in association with ictal events, which were previously discussed (Butuzova and Kitchigina, 2008; Lillis et al., 2012; Grasse et al., 2013; Toyoda et al., 2015; Lévesque et al., 2016b; Elahian et al., 2018; Kandrács et al., 2019; Wenzel et al., 2019), could modulate the activity of downstream neurons not only through GABAergic signalling but also through KCC2 activity.

1.4. Interictal activity

Similar to the reported neuronal activity pattern associated with seizures, interictal events were found to be associated to heterogeneous changes in neuronal activity. For example, while increases in neuronal firing during interictal events were reported among investigators (Enomoto and Ajmone-Marsan, 1959; Dichter et al., 1973; Karlócai et al., 2014), decreased and unchanged neuronal firings were also noted (Enomoto and Ajmone-Marsan, 1959; Prince and Wilder, 1967; Ishijima, 1972; Dichter et al., 1973). Similarly, increases and decreases in neuronal firing were identified in interictal events recorded in human epileptic patients (Altafullah et al., 1986; Keller et al., 2010; Alvarado-Rojas et al., 2013). Therefore, heterogenous changes in neuronal activity patterns were reported to occur during interictal events.

Similar to the literature surrounding seizures and ictogenesis, some investigators also examined the interneuron and principal cell activities separately during interictal events. Notably, they found that interneurons were more likely to fire during interictal events than principal cells (Muldoon et al., 2015). Accordingly, when comparing neuronal firing during interictal events to during baseline between successive interictal events, only interneuron – not principal cell – firing significantly increased (Lévesque et al., 2016b). Taken together, interneurons play an important role in determining the dynamics of interictal events.

To summarize, heterogenous changes in neuronal activity associated with interictal events could be further characterized by considering the types of neurons involved. By examining interneuron and principal cell activities separately, investigators established increases specifically in interneuron activity during interictal events. Considering the findings of neuronal activity patterns during ictal and interictal events altogether, it is evident that interneurons are critical players in epilepsy.

1.5. Theta rhythm

Theta rhythm (4–12 Hz) is an oscillation activity commonly observed in the LFP recording of the hippocampus and is involved in physiological processes such as memory, synaptic plasticity, sensory information integration, network integration, and rapid eye movement sleep (Buzsáki, 2002; Colgin, 2016). Recent work has also implicated theta rhythm in pathological conditions. For instance, increases in the power of theta rhythm were found around ictal onset in experimental models of epilepsy (Butuzova and Kitchigina, 2008; Grasse et al., 2013; Fujita et al., 2014; Toyoda et al., 2015; Karunakaran et al., 2016). This finding was replicated in investigations of human epileptic patients (Misra et al., 2018; Naftulin et al., 2018). Altogether, these findings illuminated a new area of epilepsy research – pre-ictal theta rhythm.

Like investigations of ictal and interictal events, changes in neuronal activity in relation to pre-ictal theta rhythm were also examined and yielded insights into the mechanisms of ictogenesis. Increases in the firing of both interneurons (Ewell et al., 2015; Toyoda et al., 2015; Karunakaran et al., 2016) and principal cells (Fujita et al., 2014; Ewell et al., 2015) were identified. However, upon closer examinations, only the synchrony of interneurons with the ongoing pre-ictal theta rhythm was found to increase (Butuzova and Kitchigina, 2008; Grasse et al., 2013; Karunakaran et al., 2016). Similar increases in theta rhythm power and interneuron synchrony were also observed prior to seizure appearance in the mesial temporal lobe structures of human epileptic patients (Misra et al., 2018). Therefore, these findings – by highlighting the relationship between theta rhythm and the underlying interneuron activity before seizure onset – re-emphasize the role of interneurons in ictogenesis.

1.6. Research objectives and rationales

With the goal to advance therapeutic strategies for epilepsy, my graduate studies aim to advance our understanding of the neuronal activity associated to epileptiform activity. To this end, I utilized tetrodes to record interneuron and principal cell activities simultaneously with the LFP activity in the *in vitro* brain slice preparations.

As discussed previously, seizure onset patterns were associated to specific changes in neuronal activity, thus could be used to clarify the reported heterogeneity in neuronal activity changes associated to seizures. Therefore, as our first objective, we aim to establish the changes in neuronal activity associated to the sudden onset ictal events recorded in the LFP

activity. To this end, we utilized the *in vitro* 4-aminopyridine (4AP) model of epileptiform synchronization. In this model, brain slice preparations are bathed in artificial cerebral spinal fluid (ACSF) containing 4AP, a K⁺ channel antagonist, that induces activities resembling both ictal and interictal events recorded from human epileptic patients (Avoli and Jefferys, 2016). In this model, three types of ictal onset pattern could be observed: low-voltage fast (LVF), sudden, and hypersynchronous (Avoli et al., 2013, 2016). We specifically examined the sudden onset ictal events and interpreted the findings in light of the previous study, in which changes in neuronal activity in association to LVF onset ictal events were analyzed (Lévesque et al., 2016b). These experiments are outlined in Chapter 2 and published as a distinct manuscript.

While K⁺-Cl⁻ cotransporter 2 (KCC2) was previously implicated in epilepsy, the influence of KCC2 activity on neuronal activity during ictal and interictal events remained elusive. Therefore, as my second objective, I aim to characterize the effects of KCC2 antagonism on the neuronal activity underlying LVF onset epileptiform activity. To accomplish my objective, I utilized the 4AP model of epileptiform synchronization. To antagonize KCC2 activity, I utilized VU0463271 that was reported to be a highly specific and potent KCC2 antagonist (Delpire et al., 2012). Additionally, since interneuron activity were known to play a critical role in the generation of epileptiform activity, I pharmacologically isolated epileptiform activity generation from ionotropic glutamatergic signalling for further investigations. These experiments are outlined in Chapter 3 and 4; additionally, they are published as 2 distinct manuscripts, which separately described the influences of KCC2 antagonism on neuronal activity during 4AP-induced epileptiform events in the presence and absence of ionotropic glutamatergic signalling.

Lastly, changes in theta rhythm before seizure onset were reported by epilepsy researchers. While the synchrony of the underlying interneuron activity with the LFP activity was also identified, our understanding of theta rhythm in ictogenesis could be further complemented by examining the interplay between inhibitory and excitatory neurons with respect to the types of neuronal activity and signalling. **Therefore, for my last objective, I aim to elucidate the interplay between inhibition and excitation during theta rhythm.** For this objective, I studied the carbachol (CCh)-induced theta oscillations *in vitro*, which allowed for pharmacological dissections of ionotropic excitatory and inhibitory signalling. In this *in vitro* model of theta rhythm, periodic bursts of oscillatory activity between 4–15 Hz – which is similar to the frequency range of theta rhythm – were induced in brain slice preparations by adding CCh, a muscarinic

acetylcholine receptor agonist, to ACSF (Kowalczyk et al., 2013; Lévesque and Avoli, 2018). These experiments are outlined in Chapter 5 and published as a distinct manuscript.

Altogether, my research objectives will enhance our understanding of the basic mechanism of epilepsy by investigating the relationship between neuronal action potentials and their resulting epileptiform activity. Furthermore, the work conducted according to the research objectives will highlight the power and versatility of the methodology – the *in vitro* tetrode recordings in brain slice preparations for simultaneous investigation of single-unit and LFP activities – in epilepsy research. Lastly, the findings presented in this thesis will provide fundamental knowledge necessary for the advancement of therapeutic strategies for epilepsy.

Chapter 2: Dynamic Interneuron-Principal Cell Interplay Leads to a Specific Pattern of *In Vitro* Ictogenesis

Previous experiments revealed that the increase in interneuron activity preceded principal cell activity around the initiation of low-voltage fast (LVF) onset ictal events. These important experiments added to a wealth of experimental work showing that interneurons actively contribute to the generation of seizures. However, epilepsy is a well-known heterogeneous disease with many different seizure onset patterns; thus, my colleagues and I investigated whether specific seizure onset patterns could be associated to specific neuronal interplay by utilizing tetrodes to characterize the 4-aminopyridine (4AP)-induced sudden onset ictal events in the rat entorhinal cortex (EC). This work was published in 2018 in the *Neurobiology of Disease* as a manuscript titled "Dynamic Interneuron-Principal Cell Interplay Leads to a Specific Pattern of *In Vitro* Ictogenesis."

Lévesque M, Chen L-Y, Hamidi S, Avoli M (2018) Dynamic interneuron-principal cell interplay leads to a specific pattern of in vitro ictogenesis. Neurobiol Dis 115:92–100.

2.1. Abstract

Ictal discharges induced by 4-aminopyridine in the *in vitro* rodent entorhinal cortex present with either low-voltage fast or sudden onset patterns. The role of interneurons in initiating low-voltage fast onset ictal discharges is well established but the processes leading to sudden onset ictal discharges remain unclear. We analyzed here the participation of interneurons (n = 75) and principal cells (n = 13) in the *sudden* onset pattern by employing *in vitro* tetrode wire recordings in the entorhinal cortex of brain slices from Sprague-Dawley rats. Ictal discharges emerged from a background of frequently occurring interictal spikes that were associated to a specific interneuron/principal cell interplay. High rates of interneuron firing occurred 12 ms before interictal spike onset while principal cells fired later during low interneuron firing. In contrast, the onset of sudden ictal discharges was characterized by increased firing from principal cells 627 ms before ictal onset whereas interneurons increased their firing rates 161 ms before ictal onset. Our data show that *sudden* onset ictogenesis is associated with frequently occurring interictal spikes resting on the interplay between interneurons and principal cells while ictal discharges stem from enhanced principal cell firing leading to increased interneuron activity. These findings indicate that specific patterns of interactions between interneurons and principal cells shape interictal and ictal discharges with sudden onset in the rodent entorhinal cortex. We propose that specific neuronal interactions lead to the generation of distinct onset patterns in focal epileptic disorders.

2.2. Introduction

A commonly used pharmacological tool to induce epileptiform synchronization is the potassium channel blocker 4-aminopyridine (4AP); this pharmacological manipulation makes interictal and ictal discharges occur in the rodent or guinea pig entorhinal cortex (EC) maintained *in vitro* (Avoli and de Curtis, 2011; de Curtis and Avoli, 2016). The EC is known to play a role in the generation of seizures in patients presenting with temporal lobe epilepsy (Rutecki et al., 1989; Deutch et al., 1991; Spencer and Spencer, 1994; Bartolomei et al., 2005).

Field potential recordings have shown that ictal activity generated by the EC during application of 4AP presents with two main onset patterns (Avoli et al., 2013): (i) *low-voltage fast* (LVF) onset ictal discharges that are heralded by a 'sentinel' spike, and (ii) *sudden* onset ictal discharges that emerge abruptly from a continuous background of frequently occurring interictal spikes. The onset of LVF ictal discharges mainly depends on GABAA receptor signalling (see for review: Avoli and de Curtis, 2011; Avoli et al., 2016). In line with this view, in the presence of 4AP, LVF ictal discharges are triggered in the rodent EC by optogenetic stimulation of parvalbumin-positive or somatostatin-positive inhibitory cells (Shiri et al., 2015, 2016; Yekhlef et al., 2015; Lévesque et al., 2016). Moreover, tetrode wire recordings from the EC have shown that interneuron activity increases shortly before the onset of 4AP-induced LVF ictal events whereas principal cell activity remains unchanged (Lévesque et al., 2016).

With the exception of one intracellular study that addressed the activity generated by EC regular firing and thus presumptive principal cells (Lopantsev and Avoli, 1998), the participation of interneurons and principal cells to *sudden* onset ictal discharges (and to the accompanying, frequently occurring interictal spikes) remains to date unexplored. Therefore, we used here tetrode wire recordings in the rat EC to establish the involvement of these two cell types in this specific pattern of 4AP-induced epileptiform synchronization.

2.3. Materials and methods

2.3.1. Slice preparation and maintenance

Male Sprague-Dawley rats (250–275 g; Charles River Laboratories, Saint Constant, QC, Canada) were deeply anaesthetized under 3% isoflurane in 100% O₂, and then decapitated. The brain was removed and placed in ice-cold, oxygenated artificial cerebrospinal fluid (ACSF) (124 mM NaCl, 2 mM KCl, 2 mM CaCl₂, 2 mM MgSO₄, 1.25 mM KH₂PO₄, 26 mM NaHCO₃, and 10 mM p-

glucose). The ACSF was bubbled with an O_2/CO_2 (95%/5%) gas mixture to maintain its pH at 7.4. The brain was then mounted on a vibratome (VT1000S; Leica, Concord, ON, Canada) and the obtained slices (thickness = 450 µm) were transferred to an interface chamber where they were maintained between warm (32 ± 1 °C) ACSF (305 mOSM/kg) and humidified gas (O_2/CO_2 , 95%/5%). Following a recovery period of approximately 1 h, epileptiform activity was induced by continuous bath application of 4AP (50 µM; Sigma-Aldrich, Oakville, ON, Canada) at a flow rate of 2 ml/min. All procedures were carried out in accordance with directives approved by the Canadian Council of Animal Care and by the McGill Animal Care Committee.

2.3.2. Single-unit and field potential recording

We used tetrode wire recordings in brain slices since it allowed us to analyze the activity of multiple single units in relationship with epileptiform activities induced with 4AP. Tetrode wires $(0.05 \text{ mm}, 0.5-1.2 \text{ M}\Omega)$ were mounted into a drive (NLX-18) (Neuralynx, Bozeman, MT, USA). In some experiments, up to 8 tetrodes were used. Tetrodes were placed above the horizontal slice (see Lévesque et al., 2016), slowly lowered using a micromanipulator into the EC and left in place for approximately 1 min. The region of the EC sampled by tetrodes was <500 μ M in diameter. If no single-unit activity was recorded, tetrodes were moved to another region of the EC. The entire EC was sampled in one recording session. When single-unit activity was visible, it was recorded for 10 min after which the tetrode wires were moved to another region of the EC. Up to 3 single units could be recorded per tetrode, although in most cases only one single unit per tetrode was visible. A ground wire was connected to a screw on the table, to which the bath solution was grounded. One channel of the tetrode wire assembly, which was also placed in the medial EC, was used as reference. Recordings were performed with the software Neuroware (2.1) from Triangle Biosystems (Durham, NC, USA). Data were acquired at a sampling rate of 20 kHz with a recording bandwidth between 0.8 to 22,000 Hz.

2.3.3. Clustering and identification of cell types

Filtered signals (300–3,000 Hz) were analyzed with an unsupervised cluster cutting algorithm (WaveClus) (Quiroga et al., 2004). Peaks that were 5 standard deviations above the threshold were considered as action potentials generated from single units and were merged according to selected sets of wavelet coefficients. This step was followed by manual clustering, during which the

experimenter selected for further analysis single units with <2% of discharges in the refractory period (<3 ms) (Lévesque et al., 2016). The action potential of a single unit was visible on at least 2 channels, and differed in amplitude between channels (Gray et al., 1995; Lévesque et al., 2016).

Based on the channel in which action potentials with the highest amplitude were observed, we calculated the amplitude from the trough to the following peak, the peak amplitude asymmetry, the duration of the repolarization time and the width of the action potential at 50% amplitude (Sakata and Harris, 2009; Lévesque et al., 2016). Then, using *k*-means clustering, we classified single units as interneurons or principal cells. Units that could not be categorized as interneurons or principal cells were defined as unclassified. Auto-correlograms were computed with action potentials occurring outside of ictal discharges for each recorded unit.

2.3.4. Single unit-interictal discharge relationship

The first deflection from the field baseline was considered as the onset of the interictal spike (**Figure 2.1Ba**, arrowhead). Perievent time histograms were built for each single unit, with *time* 0 representing the onset of interictal discharge. Histograms from interneurons and principal cells were averaged and consecutive bins, with amplitude >99% confidence interval of the mean, were considered as significant increases of firing rates. This procedure was performed for a time period of 100 ms before and after the onset of interictal spikes.

Cross-correlations were obtained from pairs of single units that were simultaneously recorded during interictal spikes. To determine significant cross-correlation peaks, we compared the average cross-correlogram to the average cross-correlogram obtained from shuffled spike trains (repeated 10 times for each pair). Consecutive peaks separated by <3 ms in the cross-correlogram that exceeded or were lower in amplitude than the 99% confidence interval around the mean of the shuffled cross-correlogram were considered as significant.

2.3.5. Single-unit activity during ictal discharges

The first field deflection from the baseline was considered as the onset of ictal discharges (**Figure 2.1Bb**, arrowhead). Moreover, by employing spectrogram analysis (**Figure 2.1A**), we were able to identify the change in frequency that marked the onset of the tonic and clonic phase of *sudden* onset ictal discharges (**Figure 2.1A** and **Bc**, arrows). The return to baseline activity was considered as the end of the ictal discharge.

Perievent time histograms were built for each single unit, with *time* 0 representing the onset of ictal discharges. Histograms from interneurons and principal cells were averaged, and consecutive bins with amplitude greater or lower than 99% confidence interval of the mean and separated by <3 ms were considered as significant increases or decreases of firing rates. This procedure was performed for a time period of 2 s before and after the onset of ictal discharges.

2.3.6. Single unit-ictal discharge phase relationship

To estimate the relationship between single-unit firing and field transients at the onset of ictal discharges, we calculated the Hilbert transform of processed field potentials filtered between 9 and 10 Hz, with 0° and 360° representing the peaks of the oscillations. The probability that single-unit discharges would fire at distinct phases was displayed in polar plots to examine the phase firing of single units during these oscillations. We used the Watson-Williams test to compare the mean angle vector in interneurons and principal cells.

2.4. Results

2.4.1. Epileptiform activity induced by 4AP

As previously reported (Avoli et al., 2013), bath application of 4AP induced either LVF or *sudden* onset ictal discharges. In this study, however, we selected for analysis only brain slices (n = 22, 13 animals) in which *sudden* onset ictal discharges along with a pattern of frequently occurring interictal spikes occurred (**Figure 2.1A**). These interictal spikes (n = 238) lasted $0.7 \pm 0.02 \text{ s}$, and occurred every $2.2 \pm 0.2 \text{ s}$, while ictal discharges (n = 28) lasted $28.8 \pm 3.04 \text{ s}$ and had an interval of occurrence of $144.7 \pm 22.2 \text{ s}$. Ictal discharges were characterized by an initial tonic phase with fast, large amplitude transients recurring on average at $9.7 \pm 0.3 \text{ Hz}$ that was followed by a clonic phase with ictal spikes occurring at $3.07 \pm 0.26 \text{ Hz}$. The tonic and clonic phases lasted $8.5 \pm 0.6 \text{ s}$ and $20.2 \pm 2.7 \text{ s}$, respectively.

2.4.2. Characterization of single units

We recorded a total 94 single units during bath application of 4AP. An average of 7 (\pm 7) single units were recorded per slice. As specified in the Methods section, several criteria were used to classify single units as putative interneurons or principal cells, but combining the width of the action potential measured at 50%, the amplitude from the trough to peak, and the peak amplitude

asymmetry provided the best separation (**Figure 2.2A**) (Sakata and Harris, 2009; Lévesque et al., 2016). Employing the k-means clustering analysis on these variables, we could identify two groups of units that presumably reflected the activity generated by interneurons (n = 75) and principal cells (n = 13); six units were considered as unclassified because they could not be categorized in either group and were excluded from further analysis (**Figure 2.2A**).

Panels B and C in **Figure 2.2** show representative waveforms of the action potentials generated by a presumptive interneuron and a presumptive principal cell, respectively, along with their auto-correlogram. It should be noted that the auto-correlograms obtained from principal cell activity showed peaks surrounded by fast decays between 0 and 100 ms (**Figure 2.2C**); in contrast, this pattern was not observed in auto-correlograms obtained from the single-unit activity generated by presumptive interneurons (**Figure 2.2B**) (Csicsvari et al., 1998; Karunakaran et al., 2016; Lévesque et al., 2016).

2.4.3. Single-unit activity during interictal discharges

Figure 2.3 shows the activity of an interneuron (A) and a principal cell (B) during frequently occurring interictal spikes. The activity of both interneurons (n = 22) (Figure 2.3C) and principal cells (n = 13) (Figure 2.3D) was highly correlated with the field potentials corresponding to the frequently occurring interictal spikes (n = 6838 interictal spikes, 5 ms bins). Analysis performed by using 1 ms bins revealed that the firing rate of interneurons, but not of principal cells, significantly increased within a time period of 12 ms before the onset of the field interictal event (Figure 2.3C INT, inset). In addition, interneuron firing occurring during these interictal spikes was characterized by two peaks of significant increase: the first peak occurred between 22 and 54 ms after the interictal field onset, and it was followed by a pause and a subsequent rebound increase in firing rate between 68 and 87 ms after onset (Figure 2.3C INT, inset). In contrast, the firing rates of principal cells significantly increased between 26 and 50 ms, a time corresponding to the first peak of interneuron firing (Figure 2.3D PC, inset). However, we could also identify a significant increase that peaked between 56 and 62 ms after the field potential onset, and thus it corresponded to a period of low interneuron firing (Figure 2.3D PC, inset).

We also performed cross-correlation analyses between single units to further characterize their activity during interictal spikes, using pairs of interneurons (n = 26), pairs of interneurons and principal cells (n = 9) and pairs of principal cells (n = 3) that were recorded during periods of

frequently occurring interictal activity. We found that interneurons fired in synchrony, as depicted in the cross-correlogram by a single peak centered around 0 (**Figure 2.3E**). In contrast, interneurons and principal cells revealed an anti-phase relationship, since a trough between two significant peaks was observed in the cross-correlogram (**Figure 2.3F**), consistent with the idea that principal cells fired during periods of low interneuron firing. Finally, principal cells tended to fire in synchrony, with significant peaks in the cross-correlogram near 0 ms time lag (**Figure 2.3G**).

2.4.4. Single-unit activity during ictal discharges

Next, we investigated the relationship between single-unit activity and sudden onset ictal discharges. We selected for analysis only interneurons (n = 37 single units, 19 ictal discharges) and principal cells (n = 9 single units, 9 ictal discharges) that could be followed throughout the ictal activity (cf., Truccolo et al., 2011) (Figure 2.4A). This analysis indicated that principal cell firing preceded that of interneuron since the firing rates of principal cells significantly increased 627 ms before the onset of the ictal field event compared to 161 ms for interneurons (Figure 2.4B, C, solid lines). The significant increase in firing rates of principal cells was accompanied by a significant decrease in interneuron firing from 627 to 160 ms before onset (Figure 2.4B, dashed line). Moreover, during the initial phase of the ictal discharges, principal cell activity preceded interneuron firing since principal firing significantly increased from 254 to 918 ms after onset compared to 636 and 1693 ms for interneurons (Figure 2.4B, C, solid lines). Principal cell firing then decreased from 929 to 1682 ms after onset (dashed line), during which interneuron firing increased (from 929 to 1687 ms after onset, solid line). A second increase in principal cell firing was observed between 1739 ms and 2 s after onset (Figure 2.4C, solid line), and it was accompanied by a significant decrease in interneuron firing between 1694 ms and 2 s after onset (Figure 2.4B, dashed line).

We next analyzed the relationship between single-unit firing and the large amplitude field transients occurring at 9.7 ± 0.3 Hz during the tonic phase of *sudden* onset ictal discharges. **Figure 2.5A** shows the activity of an interneuron during a *sudden* onset ictal discharge whereas **Figure 2.5B** shows the activity of a principal cell. Note that principal cell firing (**Figure 2.5B**, inset) tended to precede interneuron firing (**Figure 2.5A**, inset) during the tonic phase. Circular statistics indeed revealed that interneurons (n = 37 single units, 1392 action potentials) tended to fire during the rising phase of the field transients (mean direction = 234.95°) (**Figure 2.5C**), whereas principal

cells (n = 9 single units, 328 action potentials) fired after the peak of field oscillations (mean direction = 124.96°) (**Figure 2.5D**). The direction of the mean angle vector was significantly different between interneurons and principal cells (p < 0.01).

2.5. Discussion

This is presumably the first study to address the participation of presumptive interneurons and principal cells of the EC to a specific pattern of *in vitro* epileptiform synchronization termed *sudden* onset ictal discharges; this pattern emerges abruptly from a continuous background of frequently occurring interictal spikes. It must be remarked that the EC is a structure that plays a prominent role in the generation and maintenance of ictal activity *in vitro* in the 4AP model (Avoli et al., 2002), and often corresponds to the seizure onset zone in temporal lobe epilepsy patients (Rutecki et al., 1989; Deutch et al., 1991; Goldring et al., 1992; Spencer and Spencer, 1994; Bartolomei et al., 2005) and in animal models mimicking this disorder (Lévesque et al., 2012).

Our main findings can be summarized as follows. First, interneurons consistently fire action potentials shortly before interictal spike onset, whereas principal cells fire during the interictal spikes once interneuron firing has decreased. Second, the onset of ictal discharges is heralded by principal cell firing, and this appears to lead to interneuron firing. Third, just after ictal onset, a further increase in principal firing precedes an increase in interneuron firing. Fourth, principal cell firing preceded interneuron firing during field transients occurring at 9 Hz during the tonic phase of *sudden* onset ictal discharges. Therefore, these findings strongly suggest that specific patterns of interplay characterize the frequently occurring interictal spikes and the *sudden* onset ictal discharges. Indeed, these patterns of firing activity during *sudden* onset ictal discharges and frequently occurring interictal spikes differ from what was observed during slow interictal spikes and LVF ictal discharges also induced by 4AP in the EC (Lévesque et al., 2016).

2.5.1. Frequently occurring spikes are sustained by interneuron and principal cell network interplay

In the experiments included in this study, 4AP application to brain slices induced in the EC frequently occurring interictal discharges, similar to what was previously reported by us (Lopantsev and Avoli, 1998; Avoli et al., 2013; Herrington et al., 2015). This pattern is different

from the typical interictal spikes induced by 4AP that occur with intervals of several or even tens of seconds and that can lead to the initiation of ictal discharges (Avoli et al., 2013, 2016).

By employing tetrode recordings, we now demonstrate that the frequently occurring interictal spikes are initiated by interneurons, which is similar to what was reported for the slow and isolated interictal spikes typically induced by 4AP (Lévesque et al., 2016). However, we now provide evidence that the frequently occurring interictal spikes depend on a specific interplay between interneurons and principal cells, which is consistent with a previous study by Ziburkus *et al.* (2006), who also showed that principal cells tend to fire during periods of inactivation of interneurons. Karlócai *et al.* (2014) have also reported that during interictal epileptiform events induced by high potassium, parvalbumin-positive cells fire at onset whereas principal cells fire during periods of parvalbumin-positive cell silence. A decreased in principal cell firing then followed and was associated with a recovery in parvalbumin-positive cell firing, similar to what we have reported here.

The active contribution of principal cells to the frequently occurring interictal spikes is therefore in contrast to their relatively low firing rate occurring during the slow interictal spikes recorded in brain slices generating LVF onset ictal discharges; these slow interictal events are usually associated to high firing from interneurons (Lévesque et al., 2016). This evidence is in line with the view that the slow interictal spikes induced by 4AP mirror GABAergic inhibitory network synchrony (Avoli and de Curtis, 2011) whereas frequently occurring interictal spikes would reflect the active contribution of interneurons and principal cells (Avoli et al., 2013). Accordingly, these frequently occurring interictal spikes are readily abolished by the concomitant application of NMDA and non-NMDA glutamate receptor antagonists (Lopantsev and Avoli, 1998; Avoli et al., 2013; Herrington et al., 2015) whereas slow interictal spikes continue to occur (Avoli et al., 1996).

2.5.2. Sudden onset ictal discharges are initiated by principal cell activity

We have previously reported that LVF ictal discharges are initiated by high firing rates from interneurons whereas principal cell activity did not change before ictal onset (Lévesque et al., 2016). Similar findings were obtained by Quilichini *et al.* (2012) in the low Mg²⁺ model of epileptiform synchronization, by de Curtis and Gnatkovsky (2009) and by Gnatkovsky *et al.* (2008) in the whole brain preparation, and *in vivo* by Grasse *et al.* (2013). It has been proposed that LVF

activity at ictal onset could result from sustained inhibitory firing from interneurons (Wendling et al., 2003). We now report that *sudden* onset ictal discharges, which are also likely to be recorded in the EC under 4AP (Lopantsev and Avoli, 1998; Avoli et al., 2013; Herrington et al., 2015), are triggered by principal cell activity. Furthermore, the tonic phase of *sudden* onset ictal discharges is characterized by 9 Hz oscillations, during which principal cell firing precedes interneuron firing. This pattern is different from what was obtained during LVF ictal discharges, in which interneurons tended to fire near the trough of oscillations at onset, at a preferred phase between 90° and 150° (Lévesque et al., 2016). These findings are therefore consistent with the idea that the *sudden* onset ictal pattern may be dependent on glutamatergic synaptic transmission (Avoli et al., 2013).

The neuronal mechanisms that underlie the transition from an interictal to an ictal state under 4AP are currently unknown, but some evidence suggests that somatostatin-positive interneurons, highly coupled through gap junctions, may be highly sensitive to an increase of excitability induced by 4AP (Lillis et al., 2012). The recruitment of a sufficiently high number of interneurons during interictal spikes could therefore induce in some cases highly synchronized firing across large populations of interneurons, which would activate post-synaptic GABAergic receptors on principal glutamatergic cells and trigger depolarizations due to the activity of the potassium-chloride cotransporter 2 (KCC2) (Hamidi and Avoli, 2015). The cotransport of potassium and chloride out of principal neurons following the activation of GABAA receptors would cause increases in extracellular potassium that will facilitate the recruitment of more principal cells and lead to the generation of an ictal discharge (Hamidi and Avoli, 2015). The increase in excitation in principal cells that was triggered by the synchronization of interneuron firing under 4AP could therefore lead to the generation of sudden onset ictal discharges in the EC in vitro. In line with this view, changes in excitatory and inhibitory conductances in principal cells were reported in rodent brain slices under 4AP; principal cells showed an increase in excitation at ictal onset but were dominated by inhibition from interneurons during interictal periods (Žiburkus et al., 2013).

We have previously reported that the activity of interneurons in the EC under 4AP is strongly phase locked to the field potentials during the tonic phase of LVF ictal discharges (Lévesque et al., 2016). We now provide evidence that under the same preparation, both interneurons and principal cells fired in phase with field transients at approximately 9 Hz during

the tonic phase of *sudden* onset ictal discharges. These findings provide further support to the hypothesis that the mechanisms that are involved in the generation and maintenance of *sudden* onset ictal discharges differ from the ones associated to LVF ictal discharges and highly depend on the contribution of principal cell network activity.

2.5.3. Distinct patterns of epileptiform activities induced in the EC by 4AP

It is unclear why 4AP can induce these two patterns of epileptiform synchronization in animals of the same age and strain. It is well known that 4AP blocks outward potassium currents and slows action potential repolarization (Storm, 1987), which affects neuronal firing and enhances the release of neurotransmitters at both the glutamatergic and GABAergic terminals (Avoli et al., 2002). We have previously proposed that the occurrence of distinct patterns of interictal and ictal activities with similar concentrations of 4AP in the EC of brain slices reflects the different involvement of GABAergic networks, which should result from their different preservation following brain slicing (Avoli et al., 2013). The present study provides further evidence that the contribution of interneurons and principal cells differs between the frequently occurring interictal spikes and the slow interictal discharges as well as during the *sudden* onset and the LVF ictal discharges (Lévesque et al., 2016). Different patterns of interactions between interneurons and principal cells could therefore lead to distinct interictal activity and ictal onset patterns in the same region *in vitro*.

2.5.4. Conclusions

Our findings highlight the existence of a pattern of 4AP-induced epileptiform activity that relies on the dynamic interplay between interneuron and principal cell firings. We provide evidence that firmly establish the role of interneuron in initiating the frequently occurring interictal discharges but also the active contribution of principal cells to their generation. We also demonstrate that during *sudden* onset ictal discharges, principal cell activity leads the activity of interneurons but that both types of single units can fire in phase with the field potentials at ictal onset. Our findings therefore strongly suggest that distinct patterns of interictal and ictal activities recorded in the EC in the 4AP model of epileptiform synchronization depend on specific neuronal mechanisms.

Future studies should investigate whether these findings could be applied to seizures recorded in animal models of mesial temporal lobe epilepsy since it has already been shown that

distinct types of seizure onset patterns may depend on specific neuronal mechanisms (Lévesque et al., 2012; Avoli et al., 2013, 2016). Recent studies have also demonstrated that the optogenetic stimulation of interneurons and principal cells may lead to the generation of different ictal onset patterns (Shiri et al., 2015, 2016). Overall, these findings could contribute to the development of therapies that are targeted toward the neuronal mechanisms of seizure onset patterns in epileptic patients.

2.6. References

- Avoli M, Barbarosie M, Lücke A, Nagao T, Lopantsev V, Köhling R (1996) Synchronous GABA-Mediated Potentials and Epileptiform Discharges in the Rat Limbic System In Vitro. J Neurosci 16:3912–3924.
- Avoli M, D'Antuono M, Louvel J, Köhling R, Biagini G, Pumain R, D'Arcangelo G, Tancredi V (2002) Network and pharmacological mechanisms leading to epileptiform synchronization in the limbic system in vitro. Prog Neurobiol 68:167–207.
- Avoli M, de Curtis M (2011) GABAergic synchronization in the limbic system and its role in the generation of epileptiform activity. Progress in Neurobiology 95:104–132.
- Avoli M, de Curtis M, Gnatkovsky V, Gotman J, Köhling R, Lévesque M, Manseau F, Shiri Z, Williams S (2016) Specific imbalance of excitatory/inhibitory signaling establishes seizure onset pattern in temporal lobe epilepsy. Journal of Neurophysiology 115:3229–3237.
- Avoli M, Panuccio G, Herrington R, D'Antuono M, de Guzman P, Lévesque M (2013) Two different interictal spike patterns anticipate ictal activity in vitro. Neurobiology of Disease 52:168–176.
- Bartolomei F, Khalil M, Wendling F, Sontheimer A, Régis J, Ranjeva J-P, Guye M, Chauvel P (2005) Entorhinal Cortex Involvement in Human Mesial Temporal Lobe Epilepsy: An Electrophysiologic and Volumetric Study. Epilepsia 46:677–687.
- Csicsvari J, Hirase H, Czurko A, Buzsáki G (1998) Reliability and State Dependence of Pyramidal Cell–Interneuron Synapses in the Hippocampus. Neuron 21:179–189.
- de Curtis M, Avoli M (2016) GABAergic networks jump-start focal seizures. Epilepsia 57:679–687.
- de Curtis M, Gnatkovsky V (2009) Reevaluating the mechanisms of focal ictogenesis: The role of low-voltage fast activity. Epilepsia 50:2514–2525.
- Deutch C, Spencer S, Robbins R, Cicchetti D, Spencer D (1991) Interictal Spikes and Hippocampal Somatostatin Levels in Temporal Lobe Epilepsy. Epilepsia 32:174–178.
- Gnatkovsky V, Librizzi L, Trombin F, Curtis M de (2008) Fast activity at seizure onset is mediated by inhibitory circuits in the entorhinal cortex in vitro. Annals of Neurology 64:674–686.
- Goldring S, Edwards I, Harding GW, Bernardo KL (1992) Results of anterior temporal lobectomy that spares the amygdala in patients with complex partial seizures. Journal of Neurosurgery 77:185–193.
- Grasse DW, Karunakaran S, Moxon KA (2013) Neuronal synchrony and the transition to spontaneous seizures. Exp Neurol 248:72–84.

- Gray CM, Maldonado PE, Wilson M, McNaughton B (1995) Tetrodes markedly improve the reliability and yield of multiple single-unit isolation from multi-unit recordings in cat striate cortex. Journal of Neuroscience Methods 63:43–54.
- Hamidi S, Avoli M (2015) KCC2 function modulates in vitro ictogenesis. Neurobiology of Disease 79:51–58.
- Herrington R, Lévesque M, Avoli M (2015) Subiculum–entorhinal cortex interactions during in vitro ictogenesis. Seizure European Journal of Epilepsy 31:33–40.
- Karlócai MR, Kohus Z, Káli S, Ulbert I, Szabó G, Máté Z, Freund TF, Gulyás AI (2014) Physiological sharp wave-ripples and interictal events in vitro: what's the difference? Brain 137:463–485.
- Karunakaran S, Grasse DW, Moxon KA (2016) Role of CA3 theta-modulated interneurons during the transition to spontaneous seizures. Exp Neurol 283:341–352.
- Lévesque M, Herrington R, Hamidi S, Avoli M (2016) Interneurons spark seizure-like activity in the entorhinal cortex. Neurobiology of Disease 87:91–101.
- Lévesque M, Salami P, Gotman J, Avoli M (2012) Two Seizure-Onset Types Reveal Specific Patterns of High-Frequency Oscillations in a Model of Temporal Lobe Epilepsy. J Neurosci 32:13264–13272.
- Lillis KP, Kramer MA, Mertz J, Staley KJ, White JA (2012) Pyramidal cells accumulate chloride at seizure onset. Neurobiology of Disease 47:358–366.
- Lopantsev V, Avoli M (1998) Laminar organization of epileptiform discharges in the rat entorhinal cortex in vitro. The Journal of Physiology 509:785–796.
- Quilichini PP, Le Van Quyen M, Ivanov A, Turner DA, Carabalona A, Gozlan H, Esclapez M, Bernard C (2012) Hub GABA Neurons Mediate Gamma-Frequency Oscillations at Ictal-like Event Onset in the Immature Hippocampus. Neuron 74:57–64.
- Quiroga RQ, Nadasdy Z, Ben-Shaul Y (2004) Unsupervised spike detection and sorting with wavelets and superparamagnetic clustering. Neural Comput 16:1661–1687.
- Rutecki PA, Grossman RG, Armstrong D, Irish-Loewen S (1989) Electrophysiological connections between the hippocampus and entorhinal cortex in patients with complex partial seizures. Journal of Neurosurgery 70:667–675.
- Sakata S, Harris KD (2009) Laminar Structure of Spontaneous and Sensory-Evoked Population Activity in Auditory Cortex. Neuron 64:404–418.
- Shiri Z, Manseau F, Lévesque M, Williams S, Avoli M (2015) Interneuron activity leads to initiation of low-voltage fast-onset seizures. Annals of Neurology 77:541–546.

- Shiri Z, Manseau F, Lévesque M, Williams S, Avoli M (2016) Activation of specific neuronal networks leads to different seizure onset types. Ann Neurol 79:354–365.
- Spencer SS, Spencer DD (1994) Entorhinal-Hippocampal Interactions in Medial Temporal Lobe Epilepsy. Epilepsia 35:721–727.
- Storm JF (1987) Action potential repolarization and a fast after-hyperpolarization in rat hippocampal pyramidal cells. The Journal of Physiology 385:733–759.
- Truccolo W, Donoghue JA, Hochberg LR, Eskandar EN, Madsen JR, Anderson WS, Brown EN, Halgren E, Cash SS (2011) Single-neuron dynamics in human focal epilepsy. Nature Neuroscience 14:635–641.
- Wendling F, Bartolomei F, Bellanger JJ, Bourien J, Chauvel P (2003) Epileptic fast intracerebral EEG activity: evidence for spatial decorrelation at seizure onset. Brain 126:1449–1459.
- Yekhlef L, Breschi GL, Lagostena L, Russo G, Taverna S (2015) Selective activation of parvalbumin- or somatostatin-expressing interneurons triggers epileptic seizurelike activity in mouse medial entorhinal cortex. Journal of Neurophysiology 113:1616–1630.
- Ziburkus J, Cressman JR, Barreto E, Schiff SJ (2006) Interneuron and Pyramidal Cell Interplay During In Vitro Seizure-Like Events. Journal of Neurophysiology 95:3948–3954.
- Žiburkus J, Cressman JR, Schiff SJ (2013) Seizures as imbalanced up states: excitatory and inhibitory conductances during seizure-like events. Journal of Neurophysiology 109:1296–1306.

2.7. Figures

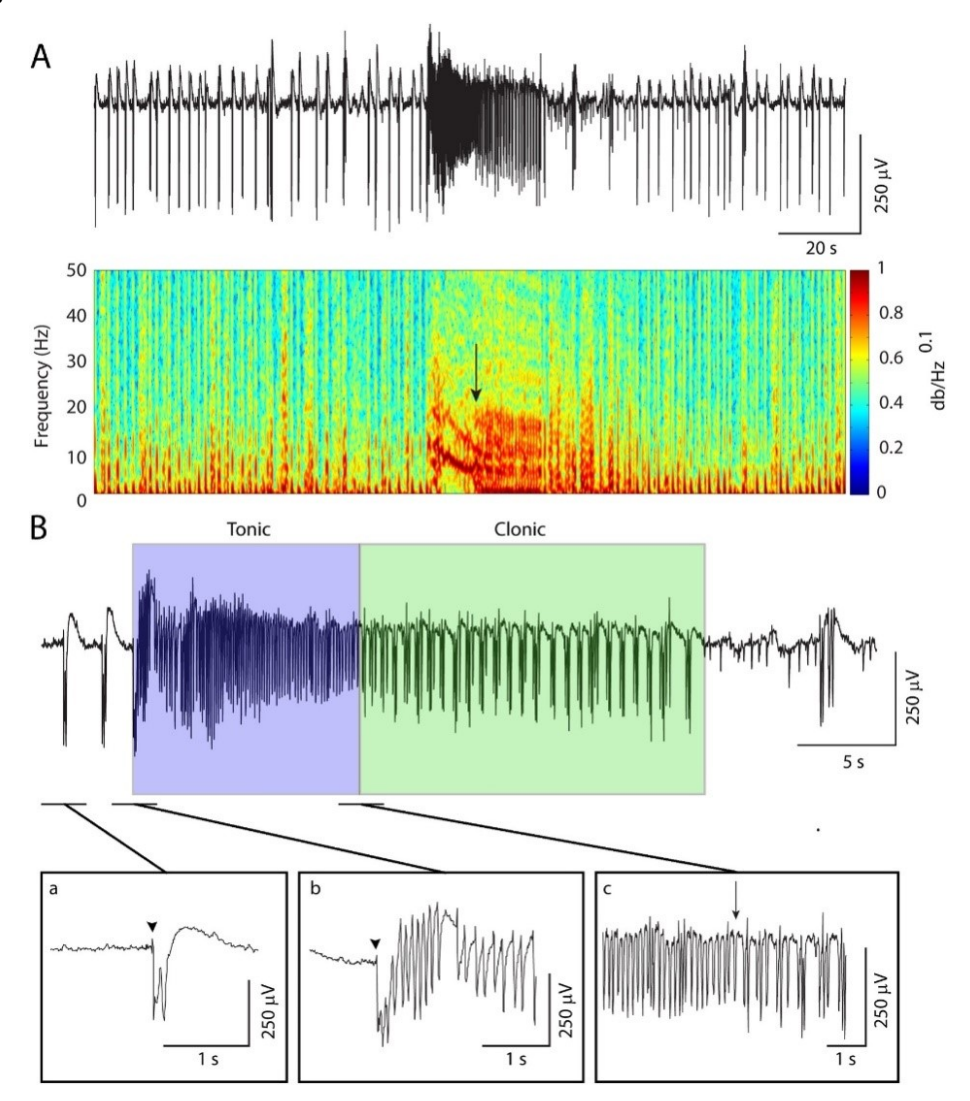


Figure 2.1. A: Representative example of a *sudden* onset ictal discharge recorded in the EC during bath application of 4AP, along with its corresponding power spectrogram. Note that *sudden* onset ictal discharges emerged from a background of frequently occurring interictal spikes. The arrow in this and following panels points to the transition from the tonic to the clonic phase, which was identified with the use of the power spectrogram. The spectrogram was computed using a frequency range from 1 to 50 Hz. To enhance the detection of seizure onsets, a gamma correction with a factor 0.2 was applied to the spectrogram to improve the contrast to random noise. **B**: Tonic (violet) and clonic (green) phases of the ictal discharge shown in **A**. The enlarged samples correspond to a frequently occurring interictal spike (**Ba**), the onset of a *sudden* onset ictal discharge (**Bb**), and the transition from the tonic to the clonic phase of an ictal discharge (**Bc**). The first deflection from baseline (arrowheads) was considered as the onset of interictal spikes (**Ba**) and the onset of ictal discharges (**Bb**). The transition from the tonic to the clonic phase (arrow) is shown in **Bc**.

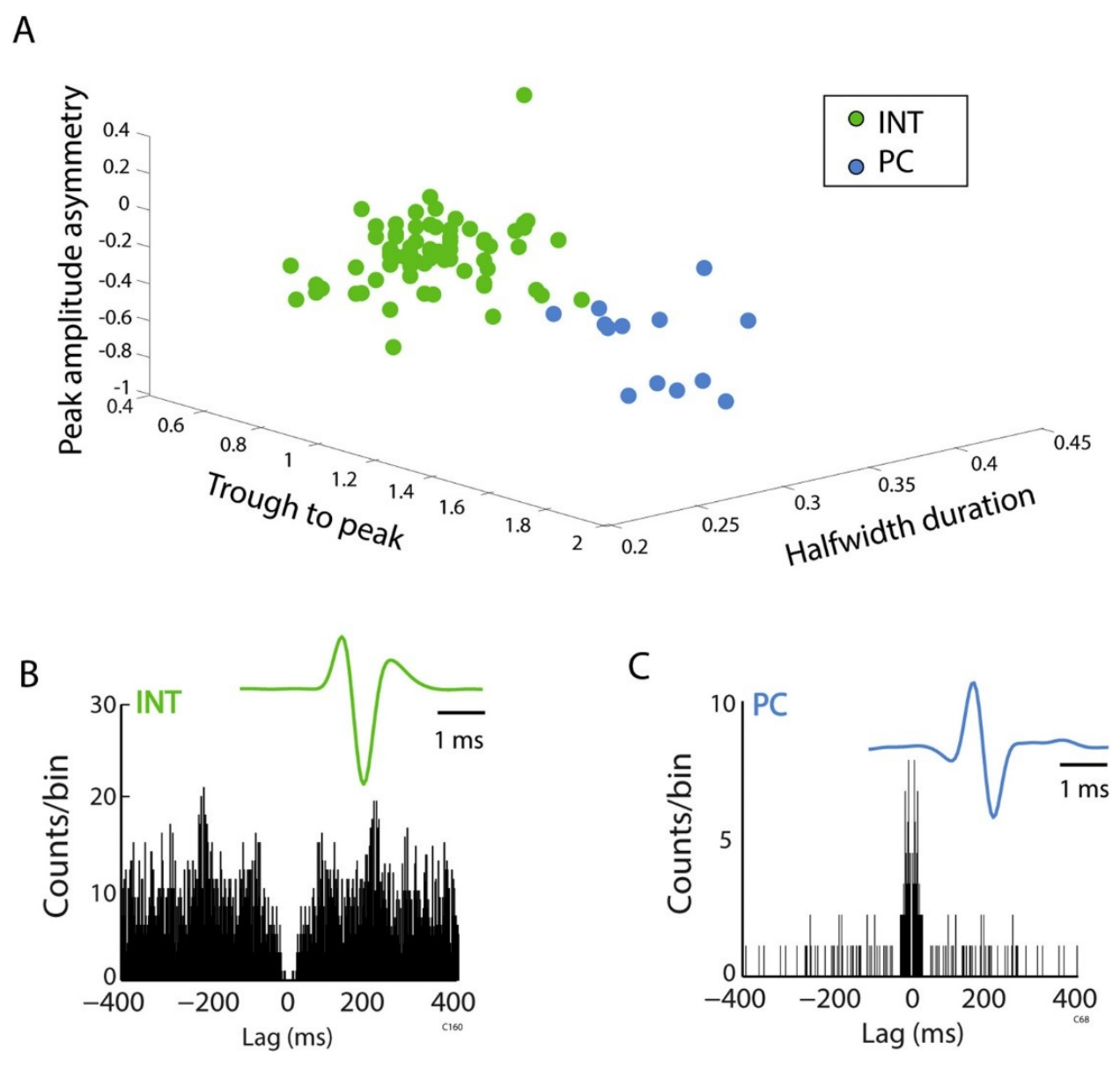


Figure 2.2. A: Three-dimensional representation of the k-means clustering analysis showing interneurons (green circles, n = 75) and principal cells (blue circles, n = 13). Single units that could not be categorized as either interneurons or principal cells were considered as unclassified and removed from further analysis (*i.e.*, they are not shown). **B**: Autocorrelogram and average waveform shape of action potentials from a presumptive interneuron. **C**: Autocorrelogram and average waveform shape of action potentials from a presumptive principal cell. Note that the principal cell shows a fast decay in the autocorrelogram between 0 and 100 ms; this phenomenon is not observed in the interneuron.

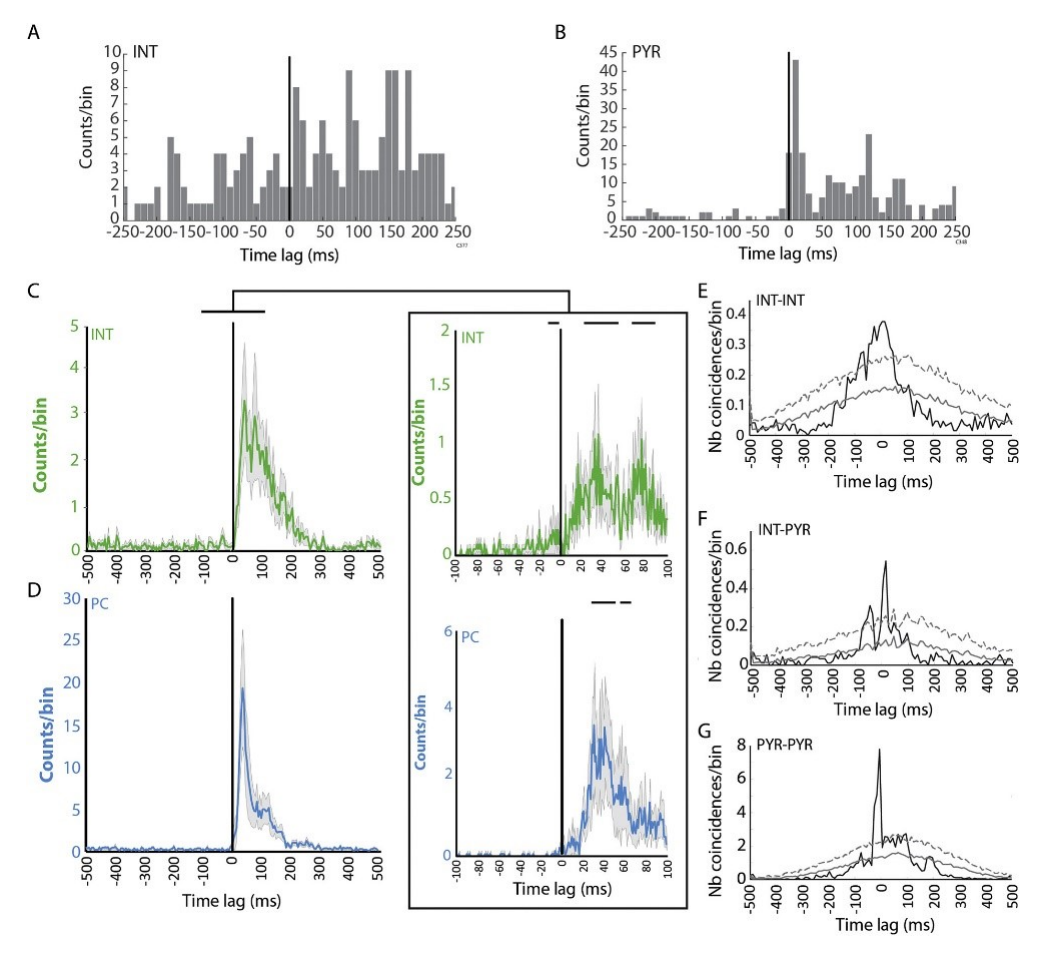


Figure 2.3. A: Peri-event histogram of a presumptive interneuron, with time 0 representing the onset of interictal spikes. Note the increase in firing rate before the onset of interictal spikes (n = 279). **B**: Peri-event histogram of a presumptive principal cell. Note the increase in principal cell activity after the onset of interictal spikes (n = 254). C, D: Peri-event time histograms of interneuron (n = 22) (C) and principal cell (D) (n = 13) firing with time 0 representing the onset of interictal spikes (n = 6838) (5 ms bins). Note that both interneurons and principal cells fired at high rates during interictal spikes. The insets show the same analysis but with smaller bin size (1 ms). Note that interneuron firing significantly increased 12 ms before the onset of interictal spikes, from 22 to 54 ms and from 68 to 87 ms after onset (solid lines). Principal cell firing significantly increased during periods of high (from 26 to 50 ms) but also low interneuron firing (from 56 to 62 ms) (solid lines). The dashed line represents the 99% confidence interval around the mean. Shading represents SEM. E: Cross-correlogram obtained from pairs of interneurons (n = 26) during interictal spikes. Interneurons tended to fire in synchrony, with significant peaks around 0 ms time lags. F: Crosscorrelogram between pairs of interneurons and principal cells (n=9). Note the anti-phase relationship, which is consistent with the idea that principal cells fire during period of low interneuron action potential discharge. G: Cross-correlogram between pairs of principal cells (n = 3) showing that they tended to fire in synchrony during interictal spikes.

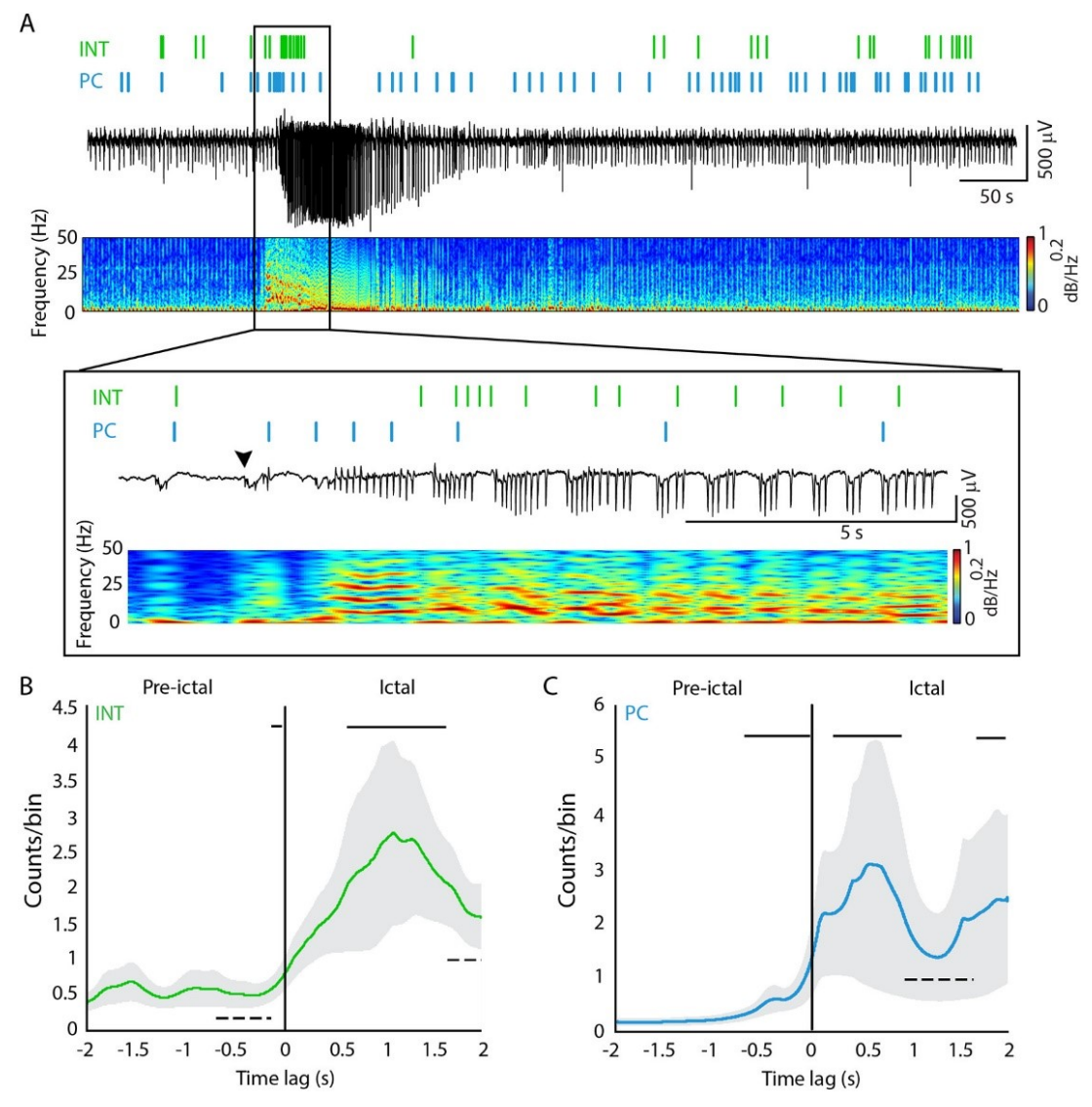


Figure 2.4. A: Representative recordings from an interneuron (INT) and a principal cell (PC) recorded on the same tetrode with the field potentials and its corresponding power spectrogram. Note that single units could be recorded over prolonged period of time, during the interictal and ictal activity patterns. The inset shows the onset (arrowhead) of the ictal discharge. Note that the principal cell firing leads interneuron firing. **B:** Peri-event histogram showing the activity of interneurons (n = 37) 2 s before and after ictal onset, which is represented as *time* 0. Note that the firing rate of interneurons significantly increases 161 ms before ictal onset and from 636 to 1693 ms after onset (solid line) but showed a significant decrease from 627 to 160 ms before onset (dashed line). A significant decrease in interneuron firing was observed between 1694 ms and 2 s after onset. **C:** Peri-event histogram showing the activity of principal cells (n = 9) 2 s before and after ictal onset (*time* 0). Principal cell firing significantly increased 627 ms before ictal onset, from 254 to 918 ms and from 1739 ms to 2 s after onset (solid lines). A significant decrease was observed from 929 to 1682 ms after onset (dashed line). Shading represents SEM.

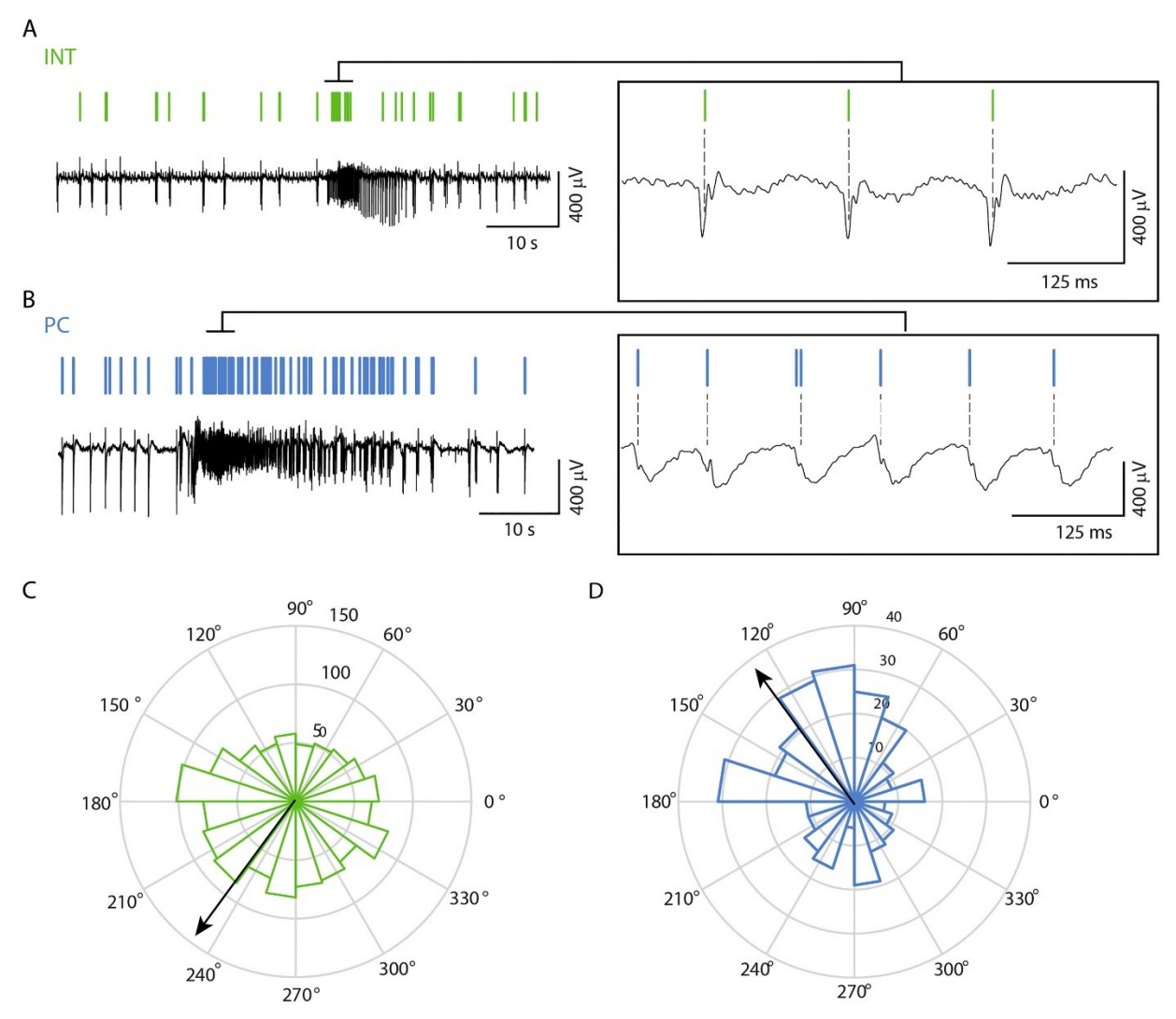


Figure 2.5. A: Representative recording of an interneuron during a *sudden* onset ictal discharge. Note in the inset that interneurons could fire in phase with the field transients at ± 9 Hz during the tonic phase of ictal discharges. **B**: Representative recording of a principal cell during a *sudden* onset ictal discharge. Note that principal cell firing tended to precede interneuron firing. **C**: Polar plot showing the distribution of phase angles for each action potential (n = 1392) from interneurons (n = 37) during the tonic phase of *sudden* onset ictal discharges. *Time* 0 represents the peak of oscillations (8–10 Hz) occurring during the tonic phase of ictal discharges. Note that interneurons tended to fire during the rising phase of field transients, at a mean angle of 234.95°. **D**: Polar plot showing the distribution of phase angles for each action potential (n = 328) from principal cells (n = 9). Note that principal cells tended to fire before interneurons, at a mean angle of 124.96°. The direction of the mean vector was significantly different between interneurons and principal cells (p < 0.01).

Chapter 3: KCC2 Antagonism Increases Neuronal Network Excitability but Disrupts Ictogenesis *In Vitro*.

K⁺-Cl⁻ cotransporter 2 (KCC2) is a known player in the epileptic pathology. However, its exact role of KCC2 remained elusive with many seemingly conflicting reports, which existed in not only *in vivo* experiments but also in the simpler *in vitro* studies. These diverse reports thus point to the need for further research to elucidate the role of KCC2 in epilepsy. In order to extend our current understanding, I antagonized KCC2 activity by applying VU0463271 to the 4-aminopyridine (4AP) model of epileptiform activity and studied the changes in neuronal activity induced by KCC2 antagonism. In part 1 of my experiments, I examined the 4AP-induced low-voltage fast (LVF) onset ictal events as well as the accompanying interictal events with tetrodes placed in the rat entorhinal cortex (EC). This work was published in 2019 in the *Journal of Neurophysiology* as a manuscript titled "KCC2 Antagonism Increases Neuronal Network Excitability but Disrupts Ictogenesis *In Vitro*."

Chen L-Y, Lévesque M, Avoli M (2019) KCC2 antagonism increases neuronal network excitability but disrupts ictogenesis in vitro. Journal of Neurophysiology 122:1163–1173.

3.1. Abstract

The potassium-chloride cotransporter 2 (KCC2) plays a role in epileptiform synchronization, but it remains unclear how it influence such a process. Here, we used tetrode recordings in the *in vitro* rat entorhinal cortex (EC), to analyze the effects of the KCC2 antagonist VU0463271 on 4-aminopyridine (4AP)-induced ictal and interictal activity. During 4AP application, ictal events were associated with significant increases in interneuron and principal cell activities. VU0463271 application transformed ictal discharges to shorter ictal-like events that were not accompanied by significant increases in interneuron or principal cell firing. Interictal events persisted during VU0463271 application at an accelerated frequency of occurrence with significant increases in interneuron and principal cell activities. Further analysis revealed that interneuron and principal cell firing rates during 4AP-induced interictal events were increased after VU0463271 application without changes in synchronicity. Overall, our results demonstrate that in the EC, KCC2 antagonism enhances both interneuron and principal cell excitabilities while paradoxically decreasing the ability of neuronal networks to generate structured ictal events.

3.2. Introduction

Application of 4-aminopyridine (4AP) in *in vitro* brain preparations induces electrographic interictal and ictal events (Avoli and de Curtis, 2011). Several studies have reported that the generation of these epileptiform events is contributed by γ-aminobutyric acid type A (GABA_A) receptor signalling resulting from interneuron firing (Avoli et al., 1996; Uva et al., 2015; Lévesque et al., 2016). This conclusion is supported by *in vitro* and *in vivo* optogenetic studies showing that interneuron activation in the 4AP model can trigger ictal discharges (Sessolo et al., 2015; Shiri et al., 2015, 2016; Yekhlef et al., 2015; Chang et al., 2018). In addition, results obtained from animal models of mesial temporal lobe epilepsy (Grasse et al., 2013; Toyoda et al., 2015; Karunakaran et al., 2016) and from epileptic patients (Elahian et al., 2018; Misra et al., 2018) have revealed that interneurons increase their firing rates at seizure onsets. Altogether, these findings suggest that synchronous interneuron activity paradoxically contributes to ictogenesis through the release of GABA, thus activating (mainly) postsynaptic GABA_A receptors.

Activated GABA_A receptor is permeable to Cl⁻ and, to a lesser extent, to HCO₃⁻ (Farrant and Kaila, 2007). In this context, the hyperpolarizing nature of GABA_A receptor-mediated currents in the mature brain depends on a low intracellular [Cl⁻] that is maintained by the K⁺-Cl⁻ cotransporter 2 (KCC2). KCC2 is a neuron-specific Cl⁻ extruder that uses [K⁺] gradient to maintain low intracellular [Cl⁻] (Viitanen et al., 2010). Indeed, it has been proposed that the excessive activity of KCC2 leads to substantial elevations in extracellular [K⁺] similar to those occurring during synchronous activation of GABA_A receptors caused by the intense firing of interneurons in the 4AP model (Avoli et al., 1996; Lévesque et al., 2016; Librizzi et al., 2017; González et al., 2018). Therefore, KCC2 function may play an important role in epileptiform synchronization (Kaila et al., 2014; Di Cristo et al., 2018).

Several KCC2 antagonists have been developed over the last few years (Delpire et al., 2009; Lebon et al., 2012; Delpire and Weaver, 2016; Delpire et al., 2012), and these molecules have been tested in *in vitro* models of epileptiform synchronization such as the 4AP and the 0-Mg²⁺. One study reported that application of the KCC2 antagonist VU0240551, which was introduced by Delpire *et al.* (2009), transformed 4AP-induced ictal activity generated by neuronal networks in the rodent entorhinal cortex (EC) into a pattern of recurrent interictal events (Hamidi and Avoli, 2015). More recently, VU0240551 was further optimized to produce VU0463271 that exhibits improved potency and selectivity for antagonizing KCC2 (Delpire et al., 2012). This new KCC2

antagonist was found, in Moss's laboratory, to enhance the excitability of cultured hippocampal neurons and to induce recurrent field spiking in *in vitro* in the 0-Mg²⁺ and 4AP models as well as *in vivo* during acute intrahippocampal administration (Sivakumaran et al., 2015; Moore et al., 2018). However, in one *in vitro* study performed by the same group, VU0463271 could prolong the ictal events induced by 4AP in the EC (Kelley et al., 2016); such finding was at odds with those obtained by us using VU0240551 to antagonize KCC2 (Hamidi and Avoli, 2015). Therefore, by employing tetrode wire recordings to dissect the underlying single-unit activity, we aimed to establish whether and how antagonizing KCC2 function with VU0463271 alter the epileptiform activity elicited *in vitro* by 4AP in the rat EC.

3.3. Materials and methods

3.3.1. Ethical approval

All procedures were performed in compliance with the guidelines of the Canadian Council on Animal Care and were approved by the McGill University Animal Care Committee.

3.3.2. Slice preparation and maintenance

Male Sprague-Dawley rats (250–275 g; Charles River Laboratories, Saint Constant, QC, Canada) were decapitated under anaesthesia induced by 5% isoflurane. Following decapitation, the brains were extracted and placed in ice-cold artificial cerebrospinal fluid (ACSF; 124 mM NaCl, 2 mM KCl, 2 mM CaCl₂, 2mM MgSO₄, 1.25 mM KH₂PO₄, 26 mM NaHCO₃, and 10 mM p-glucose) oxygenated with O₂/CO₂ (95%/5%) gas mixture to maintain a pH level of 7.4. The brains were then mounted on a vibratome (VT1000S; Leica, Concord, ON, Canada) to obtain brain slices with a thickness of 450 μm. Slices were then transferred to an interface chamber where they were maintained between warm ACSF (32 ± 1°C) and humidified O₂/CO₂ gas mixture (95%/5%). Following a recovery period of ~1 h, epileptiform activity was induced by continuous bath application of 4AP (50 μM; Sigma-Aldrich, Oakville, ON, Canada) at a flow rate of 2 ml/min. To investigate the contribution of KCC2 to 4AP-induced epileptiform synchronization, *N*-Cyclopropyl-*N*-(4-methyl-2-thiazolyl)-2-[(6-phenyl-3-pyridazinyl)thio]acetamide (VU0463271; Tocris, Canada), a KCC2 antagonist (Delpire et al., 2012), was applied (4AP + VU0463271) at a concentration of 10 μM to fully antagonize KCC2 activity.

3.3.3. Single-unit and field potential recording

The collection and analysis of single-unit activity was adapted from the protocol of Lévesque *et al.* (2016). Seven tetrodes, each made of four twisted tungsten wires (tip diameter = 50 μm, California Fine Wire Company, Grover Beach, California, USA), were inserted into individual microdrives (NLX-18; Neuralynx, Bozeman, MT, USA). A ground wire was connected between the board of the tetrode and the vibration isolation table (Newport, CA, USA) while a channel of a tetrode, placed in the EC, was used as reference. Tetrodes were lowered into the EC to record neuronal activity at a sampling rate of 20 kHz with a recording bandwidth between 0.8 to 22,000 Hz using the Neuroware (2.1) software from Triangle Biosystems (Durham, NC, USA). Because of limitations in computer processing power, we only sampled 10 min of neuronal activity for each recording epoch. Off-line data analysis was performed with MATLAB (Mathworks, Natick, MA, USA; RRID: SCR 001622).

3.3.4. Raw data processing for single-unit activity

Raw tetrode data were filtered between 300 and 3,000 Hz to visualize single-unit activity (**Figure 3.1Aa**) that was then analyzed with WaveClus (Quiroga et al., 2004). The unsupervised cluster cutting algorithm considered peaks that were five standard deviations (SDs) above the baseline as putative action potential discharges and clustered according to selected sets of wavelet coefficients (Quiroga et al., 2004). Then, the experimenter visually verified that 1) the putative single-unit clusters were distinct from the noise clusters, 2) the putative action potential discharges were visible on at least two channels of a tetrode wire, 3) the amplitudes of the putative discharges were different on different channels of the tetrode wire, and 4) less than 2% of the total number of putative discharges from the single-unit clusters occur during the refractory period (<3 ms) (Csicsvari et al., 1998).

Single units were classified as presumptive interneurons or principal cells based on characteristics used in previously published studies (Freund and Buzsáki, 1996; Csicsvari et al., 1998; Sirota et al., 2008; Sakata and Harris, 2009; Lévesque et al., 2016). From the averaged action potential waveforms of putative single units, three variables were computed: 1) the amplitude from the trough to the peak, 2) the asymmetry between the amplitudes of the peaks, and 3) the action potential width at 50% of amplitude (**Figure 3.1Ab**). Since our recordings appeared to be stable during the 10-min recording epoch – as revealed by the similarity in the averaged waveforms of

the first and last 50 action potentials (**Figure 3.1Ac**) – and between pharmacological manipulations – as revealed by the averaged waveforms of the same single unit under two different conditions (**Figure 3.1Ad**) – we clustered all single units together. We first excluded outliers, defined as data points that were 5 SDs above the mean, then applied the k-means clustering to separate the single units into two groups – presumably reflecting interneuron and principal cell populations (**Figure 3.1B**).

3.3.5. Raw data processing for field potential activity

Raw data were filtered between 1 and 500 Hz and down sampled to 2,000 Hz to visualize the field potential activity. The four channels of the tetrode were averaged together and normalized against an average of all field potentials recorded from all tetrodes used in the recording session, creating the final processed field potential (**Figure 3.1Aa**). In all conditions, interictal events were manually detected by an experimenter blind to the pharmacological manipulations; the onset was defined as the first deflection from baseline, whereas the termination was defined as the return to baseline activity (**Figures 3.2Aa** and **3.5Ba**, arrowheads). The amplitude was defined as the difference between the maximum and minimum values during the event of interest. The onset of ictal events was defined as the onset of sentinel spike observed in the low-voltage fast-activity (LVF) onset pattern, while the termination was defined as the return to baseline activity. Finally, the onset of ictal-like events occurring during application of VU0463271 was defined by the occurrence of at least 10 spikes within a time window of 2 s, which was independently assessed by at least two experimenters.

Statistical comparisons were performed as the following. The duration of ictal events in the 4AP condition was compared with the duration of ictal-like events in the 4AP + VU0463271 condition. Since most recordings only captured one ictal or ictal-like event, it was not possible to quantify the interval of occurrence of ictal and ictal-like events. Interictal duration, interval of occurrence, and amplitude were first averaged within a recording, then averages of the same pharmacological condition were pooled together and compared with other pharmacological conditions.

3.3.6. Qualitative analysis of single-unit activity

To characterize the changes in single-unit activity around the events of interest in real time, raster plots and peri-event histograms were used. For the onsets of ictal events in the 4AP condition and ictal-like events in the 4AP + VU0463271 condition, raster plots were built by extracting single-unit action potential discharges 10 s before and after the onset, defined as *time 0*, of events of interest. To reveal their distribution, the extracted action potentials were summed in 200-ms bins to generate ictal and ictal-like real-time peri-event histograms displayed below the raster plots. For interictal events, action potentials 1 s before to 2 s after the onset of interictal events, defined as *time 0*, were extracted to generate the raster plots and summed in 25-ms bins for real-time peri-event histograms.

Since events of interest had different durations, normalized peri-event histograms were also generated. Single-unit activity epochs were extracted around the events of interest to include pre-and post-event baselines of the same duration as the events of interest. The duration of the single-unit activity epoch was normalized with 0% and 100% as the onset and termination of the events of interest, respectively. The spike density of each single unit was calculated by averaging the number of action potentials that occurred in each 1% bin. Average spike densities of single units of the same neuronal type in the same pharmacological conditions were averaged to produce the normalized peri-event histograms. For visual representation, the averaged spike densities were smoothed using a moving average filter with bin width of 11 data points.

3.3.7. Quantitative analysis of single-unit firing

To assess whether application of VU0463271 induced changes in single-unit firing rate during interictal events, we calculated the delay time from the onset of an interictal event to the first action potential that occurred during the interictal event as well as the change in firing rate for each interictal event (Figure 3.5B). The average interictal firing rate was calculated by dividing the number of action potentials that occurred during an interictal event by the duration of the interictal event (Figure 3.5Ba). Using a baseline period taken immediately before each interictal event onset with the same duration as the interictal event, the average baseline firing rate was calculated by dividing the number of action potentials that occurred during the baseline period by the duration of this period (Figure 3.5Ba). The firing rate change represents the difference between the average interictal firing rate and the average baseline firing rate (Figure 3.5Bb). The firing rate changes of

the same neuron type were pooled together and compared before and after the addition of VU04632371.

To assess whether VU0463271 application changes the firing relationship between single units, we performed cross-correlation analysis on pairs of simultaneously recorded single units during interictal events. In recordings where two single units could be identified, action potentials from 1 s before to 2 s after the onsets of interictal events, defined as *time* θ , were extracted. Binary action potential discharge data were generated using the timestamps of extracted action potentials. Cross correlations were performed using the binary action potential discharge data with the MATLAB function xcorr. They were then averaged to produce the average coincidence of simultaneously recorded pairs of single units. The Monte Carlo methods were used to correct for event-related increases in the action potential discharge that could artificially increase crosscorrelation coincidence. Action potential timestamps were randomly shuffled 5,000 times while maintaining the total number of action potentials for the given epoch. Simulated binary action potential discharge data were generated for calculating the cross correlations between simulated pairs of single units using the same procedure mentioned above, then averaged. The averaged simulated coincidence was subtracted from the average coincidence of the simultaneously recorded pairs of single units. The maximum of the corrected average coincidence was identified for subsequent statistical analysis.

We displayed our quantitative data in box-and-whisker plots where the box captures the 25 to 75 percentile range of the data distribution, while the line indicates the median. The ends of the whiskers represent the entire range of the data.

3.3.8. Statistical Analysis

To compare data central tendencies, we first assessed data normality using the Shapiro-Wilks Test. For data that were not normally distributed, we used the Mann-Whitney U-Test, or the Wilcoxon Rank-Sum Test. For normally distributed data, Two-Sample T-Tests were use. Statistical significance was established at p < 0.05. Since some data were not normally distributed, throughout the text, data central tendencies are expressed as median (interquartile range, IQR). We applied the Brown-Forsythe test to compare data variances in the real-time peri-event histograms. To express the variances in distribution, the width of the distribution at half of the peak distribution was computed.

To assess for statistical significance in the normalized peri-event histograms, the Monte Carlo methods were applied. For each extracted single-unit activity epochs, action potential timestamps were randomly shuffled 5,000 times to simulate spontaneous single-unit discharge patterns. Average spike densities for simulated single-unit activity epochs were calculated using the same procedure mentioned above. Average spike densities of the acquired data that were 2.50 SDs above the average spike densities of simulated activity were considered to be statistically significant changes in single-unit discharge activity.

3.4. Results

3.4.1. Characterization of single units

We identified 171 single units recorded from 37 slices that were obtained from 23 animals. We excluded 2 single units from k-means clustering analysis since they were considered as outliers (**Figure 3.1B**). Using previously published guidelines aimed at characterizing action potential waveform shape (Freund and Buzsáki, 1996; Csicsvari et al., 1998; Sirota et al., 2008; Sakata and Harris, 2009; Lévesque et al., 2016), we identified 138 putative interneurons and 31 putative principal cells from our tetrode recordings (4AP: n = 80 interneurons, n = 12 principal cells; 4AP + VU0463271: n = 58 interneurons, n = 19 principal cells). As illustrated in **Figure 3.1B**, insets, the action potential waveforms of putative interneurons were narrower and more symmetrical than those of putative principal cells.

3.4.2. Effects of KCC2 antagonism on 4AP-induced field activity

As previously reported (Avoli et al., 2013; Lévesque et al., 2016), interictal (**Figure 3.2Aa**) and ictal events with LVF onset pattern (**Figure 3.2Ab**) occurred in our experiments during bath application of 4AP (n = 22 animals). LVF ictal events often initiated with a sentinel spike, whose shape was similar to an interictal event, and were characterized by electrographic tonic and clonic phases. The duration of LVF ictal events (n = 91 events, n = 28 slices) was 90.97 s (IQR = 42.51–126.26 s). The duration and the interval of occurrence of interictal events recorded in the 4AP condition (n = 1690 events, n = 32 slices) were 1.15 s (IQR = 0.97–1.39 s) and 23.79 s (IQR = 16.09–31.50 s), respectively.

Application of the KCC2 antagonist VU0463271 (n = 6 animals) changed the 4AP-induced activity to continuous interictal spiking (**Figure 3.2Ac** and **3.2Ad**). These persistent interictal

events (n = 2960, n = 10 slices) had a duration of 0.28 s (IQR = 0.23–0.37 s) and interval of occurrence of 0.66 s (IQR = 0.54–0.95 s). Therefore, both the duration and the interval of occurrence of the interictal events recorded from the EC in 4AP + VU0463271 condition were significantly shorter than those occurring in the 4AP condition (duration: Mann-Whitney *U*-Test, $p = 5.50 \times 10^{-27}$, W = 2523.00, z = -10.76; interval of occurrence: Mann-Whitney *U*-Test, $p = 1.35 \times 10^{-27}$, W = 2485.00, z = -10.89; **Figure 3.2A**).

This continuous interictal activity appeared to be a consistent finding, since it was observed in all slices during bath application of VU0463271 (**Figure 3.2A**). However, in seven of these slices, we could also identify sporadic accelerations in interictal spiking, which made this electrographic pattern resemble an ictal event, hereafter referred to as ictal-like event (n = 38 events; **Figure 3.2B**). These ictal-like events had a duration of 62.31 s (IQR = 48.80-74.74 s), which was significantly shorter than the duration of the ictal events that were recorded during bath application of only 4AP (Mann-Whitney *U*-Test, p = 0.02, W = 2014.00, z = -2.35). In addition, as illustrated in the enlarged sample in **Figure 3.2B**, the electrographic pattern of the ictal-like events occurring during applications of 4AP + VU0463271 was less structured (*i.e.*, it was not characterized by an initial sentinel spike nor by any subsequent electrographic tonic-to-clonic phase transition), as compared to the ictal events that were recorded in the presence of only 4AP.

3.4.3. Effects of KCC2 antagonism on single-unit activity during ictal discharges

First, we analyzed single-unit activity around the time of initiation of the ictal events recorded under 4AP and of the ictal-like events occurring under 4AP + VU0463271. In **Figure 3.3Ab**, the raster plot indicates that interneuron (n = 65) and principal cell (n = 10) firings increased at the onsets of the ictal events occurring during 4AP application (n = 91). In contrast, single-unit activities generated by interneurons (n = 16) and principal cells (n = 8) did not appear to change at the initiation of ictal-like events (n = 38) occurring in the 4AP + VU0463271 condition. The real-time peri-event histograms further showed that both interneurons and principal cells increased their firings at the onsets of ictal events recorded during 4AP application; however, interneurons and principal cells did not increase their firings at the onsets of the ictal-like events occurring in the presence of 4AP + VU0463271 (**Figure 3.3Ac**).

To statistically assess for changes in interneuron and principal cell activities during ictal and ictal-like events of different durations, we also constructed normalized peri-event histograms;

these histograms revealed significant increases in the firings of both interneurons and principal cells only during the LVF ictal events that were recorded during application of 4AP but not during the ictal-like events occurring during application of medium containing 4AP + VU0463271 (**Figure 3.3B**).

3.4.4. Effects of KCC2 antagonism on single-unit activity during interictal events

Next, we analyzed the effects of VU0463271 on the single-unit activity occurring during 4AP-induced interictal events. As illustrated in **Figure 3.4Ab**, both interneurons and principal cells fired action potentials at the onsets of interictal events in the presence of 4AP (n = 1690 events, n = 80 interneurons, n = 12 principal cells) as well as during the application of medium containing 4AP + VU0463271 (n = 2960 events, n = 58 interneurons, n = 19 principal cells). The real-time peri-event histograms revealed that action potentials were concentrated at the onsets of interictal events under both pharmacological conditions (**Figure 3.4Ac**). However, the distribution of interneuron action potentials in the 4AP + VU0463271 (0.15 s) condition was less variable than that in the 4AP (0.58 s) condition (Brown- Forsythe Test, $p = 1.76 \times 10^{-82}$, F(1, 6300) = 381.24); this difference was not observed in the distribution of principal cell action potentials (4AP: 0.30 s; 4AP + VU0463271: 0.13 s). To statistically assess the increase in single-unit activity during interictal events of different durations, we also constructed normalized peri-event histograms that revealed significant increases in interneuron and principal cell activities during interictal events under both 4AP and 4AP + VU0463271 (**Figure 3.4B**).

The peaks of interneuron and principal cell activities in the real-time and normalized perievent histograms prompted us to also quantify and compare the changes in single-unit firing associated to interictal events recorded in the 4AP and 4AP + VU0463271 conditions. We found a significant decrease in the delay time from the onsets of interictal events to the first interneuron action potentials between the 4AP (0.19 s, IQR: 0.08–0.36 s) and 4AP + VU0463271 (0.09 s, IQR: 0.06–0.14 s) conditions (Mann-Whitney *U*-Test, $p = 3.05 \times 10^{-44}$, W = 591837.50, z = -13.95; **Figure 3.5A**). A similar significant decrease was also observed for principal cells between the 4AP (0.16 s, IQR: 0.09–0.30 s) and the 4AP + VU0463271 (0.10 s, IQR: 0.08–0.13 s) conditions (Mann-Whitney *U*-Test, $p = 8.51 \times 10^{-7}$, W = 33340.50, z = 4.92; **Figure 3.5A**).

Since the delay time between the interictal event onset and the first action potential does not provide information regarding the neuronal firing rate throughout the interictal events, we also calculated the change in firing rate (**Figure 3.5B**). As shown in **Figure 3.5C**, we found that the change in interneuron firing rate in the 4AP condition (1.85 Hz, IQR = 0.98–4.23 Hz) was significantly lower than what was observed in the 4AP + VU0463271 condition (4.01 Hz, IQR = 2.80-5.69 Hz; Mann-Whitney *U*-Test, $p = 3.75 \times 10^{-52}$, W = 481950.00, z = -15.20). The principal cell firing rate change in the 4AP condition (1.82 Hz, IQR = 1.02-3.73 Hz) was also significantly lower than the one in the 4AP + VU0463271 condition (4.12 Hz, IQR = 3.07-5.26 Hz; Mann-Whitney *U*-Test, $p = 1.77 \times 10^{-17}$, W = 18258.50, z = -8.51; **Figure 3.5C**).

Finally, we performed cross-correlation analyses on pairs of simultaneously recorded single units during interictal events recorded in 4AP and 4AP + VU0463271 conditions to assess for cell synchrony (**Figure 3.6A**). We found no significant changes in the average coincidence between pairs of single units recorded under the bath application of 4AP (n = 47) condition and those recorded under 4AP + VU0463271 (n = 40) condition (**Figure 3.6B**).

3.5. Discussion

In this study, we performed tetrode wire recordings in the *in vitro* model of 4AP-induced epileptiform synchronization to examine the effects of the KCC2 antagonist VU0463271 on the field and single-unit activities that were recorded in the rat EC. The main findings of our study can be summarized as follows. First, the typical LVF onset ictal discharges that are induced *in vitro* by bath application of 4AP were replaced, during application of VU0463271, by continuous interictal spikes that could, at times, accelerate in frequency of occurrence thus resembling an electrographic ictal-like discharge pattern. Second, significant increases in both interneuron and principal cell activities were only identified at the onsets of 4AP-induced ictal events and not at the onsets of ictal-like events recorded under 4AP + VU0463271. Third, 4AP-induced interictal events after the addition of VU0463271 were associated with significant increases in both interneuron and principal cell firings, while no change in synchronicity was observed.

3.5.1. KCC2 function is needed for the generation of 4AP-induced ictal discharges

As reported by Lévesque *et al.* (2016), EC interneurons and principal cells increased their firings at the onsets of 4AP-induced ictal events, which were consistently characterized by an LVF onset pattern followed by tonic and clonic electrographic phases. By normalizing the duration of these ictal events, we found significant increases in interneuron and principal cell activities. In contrast,

during application of the KCC2 antagonist VU0463271, interictal events became the predominant activity pattern. Although they could, at times, show increased frequency of occurrence – which made them resemble ictal events lacking both the sentinel spike and the electrographic tonic-clonic transition – these ictal-like events were not associated with significant increases in interneuron or principal cell activities at onset. Thus, the recruitment of neuronal networks during ictal events appeared to be disrupted by KCC2 antagonism. Our results are in agreement with those obtained by Hamidi and Avoli (2015), who employed VU0240551 to demonstrate that antagonizing KCC2 function unravels the structured pattern of ictal events induced by 4AP to disclose a continuous pattern of recurrent interictal spiking.

The recurrent interictal activity identified in our experiments during the application of 4AP + VU0463271 has been previously described in the *in vitro* 0-Mg²⁺ model of epileptiform synchronization (Sivakumaran et al., 2015; Kelley et al., 2016). Similar continuous interictal spiking activity was also induced *in vivo* during acute unilateral intrahippocampal administration of VU0463271 (Sivakumaran et al., 2015). However, the same group of investigators has also reported that in the *in vitro* 4AP model, application of VU0463271 increases the duration of ictal events without disrupting their structure – which is different than our results – and proposed that KCC2 antagonism could exacerbate ictal activity (Kelley et al., 2016). More recently, Moore *et al.* (2018) have found that 4AP- or 0-Mg²⁺-induced ictal activity were attenuated in slices obtained from mice with genetic mutations that enhanced KCC2 function. While the literature suggests that KCC2 antagonism through the application of VU0463271 may induce variable effects in epileptiform synchronization, our data propose that antagonizing KCC2 function disrupts ictal events and produces a continuous pattern of recurrent interictal spiking.

Indeed, the ability of KCC2 antagonism to de-structure the pattern of ictal activity recorded during 4AP treatment, is not in conflict with its capacity to enhance neuronal excitability. Supported by *in silico* results (González et al., 2018), previous experiments have established that an increase in extracellular [K⁺] – as a consequence of synchronous firing of interneurons releasing GABA that activates postsynaptic GABA_A receptors – is needed for the initiation and maintenance of 4AP-induced ictal activity (Avoli et al., 1996; Librizzi et al., 2017). Given that KCC2 function is responsible for the GABA_A receptor-dependent increases in extracellular [K⁺] (Viitanen et al., 2010), we propose here that an overall downregulation of KCC2 function should disrupt ictal synchronization even though, as further discussed below, the concomitant increase of intracellular

[Cl⁻] causes a positive shift of the GABA_A receptor reversal potential, thus inducing neuronal hyperexcitability (Sivakumaran et al., 2015; Kelley et al., 2018; Moore et al., 2018). In line with this hypothesis, mice with KCC2 downregulation in principal cells have been found to develop spontaneous seizures *in vivo* (Kelley et al., 2018).

3.5.2. KCC2 antagonism leads to neuronal hyperexcitability

Interictal events recorded during the 4AP + VU0463271 condition were shorter and more frequent than those observed in the 4AP condition. Real-time peri-event histograms revealed that interneuron action potentials were more concentrated after the application of VU0463271 and that these interictal events were associated to significant increases in single-unit activity. In addition, the decreased delay time between the onsets of interictal events and the first action potentials as well as the increased change in firing rate associated with interictal events upon VU0463271 application for both principal cells and interneurons suggest an increase in neuronal excitability. Concomitant to these changes, no change in synchronicity was observed. Together, these findings suggest that KCC2 antagonism induced hyperexcitability in both principal cells and interneurons, possibly by depolarizing GABAA reversal potential, and not hypersynchrony between neurons, thus disrupting ictogenesis.

Neuronal hyperexcitability due to KCC2 antagonism has been reported in the literature. Several studies have shown that in cultured hippocampal neurons, downregulating KCC2 increases neuronal excitability by inducing a depolarizing shift in the GABAA reversal potential (Sivakumaran et al., 2015; Kelley et al., 2018; Moore et al., 2018). Moreover, cell cultures expressing mutated SLC12A5 genes showed reduced KCC2 cell surface expression along with a depolarization of the GABAA reversal potential (Puskarjov et al., 2014). In line with these findings, the hippocampal formation of brain slices obtained from pilocarpine-treated animals exhibits a decrease in KCC2 expression as well as a depolarized GABAA reversal potential (Pathak et al., 2007). Furthermore, GABAergic-dependent synchronized activity has been demonstrated in resected human epileptic brain tissues (Schwartzkroin and Haglund, 1986; Köhling et al., 1998; Huberfeld et al., 2007). Together, these studies indicate that KCC2 downregulation can indeed promote neuronal hyperexcitability.

3.5.3. Conclusions

Our findings highlight the paradoxical effects induced by KCC2 antagonism on the 4AP-induced epileptiform activity generated by EC neuronal networks *in vitro*. We found that although antagonizing KCC2 leads to persistent and frequent interictal events – which should reflect neuronal hyperexcitability caused by a depolarizing shift of the GABA_A receptor reversal potential – it abolished ictal activity. This effect should result from the abated increases in extracellular [K⁺] that result from KCC2 activity due to the postsynaptic activation of GABA_A receptors. These seemingly conflicting results underscore the complex roles played by KCC2 activity in modulating GABA_A receptor signalling along with *in vitro* epileptiform synchronization.

3.6. References

- Avoli M, Barbarosie M, Lücke A, Nagao T, Lopantsev V, Köhling R (1996) Synchronous GABA-Mediated Potentials and Epileptiform Discharges in the Rat Limbic System In Vitro. J Neurosci 16:3912–3924.
- Avoli M, de Curtis M (2011) GABAergic synchronization in the limbic system and its role in the generation of epileptiform activity. Prog Neurobiol 95:104–132.
- Avoli M, Panuccio G, Herrington R, D'Antuono M, de Guzman P, Lévesque M (2013) Two different interictal spike patterns anticipate ictal activity in vitro. Neurobiol Dis 52:168–176.
- Chang M, Dian JA, Dufour S, Wang L, Moradi Chameh H, Ramani M, Zhang L, Carlen PL, Womelsdorf T, Valiante TA (2018) Brief activation of GABAergic interneurons initiates the transition to ictal events through post-inhibitory rebound excitation. Neurobiol Dis 109:102–116.
- Csicsvari J, Hirase H, Czurko A, Buzsáki G (1998) Reliability and State Dependence of Pyramidal Cell–Interneuron Synapses in the Hippocampus. Neuron 21:179–189.
- Delpire E, Baranczak A, Waterson AG, Kim K, Kett N, Morrison RD, Scott Daniels J, David Weaver C, Lindsley CW (2012) Further optimization of the K-Cl cotransporter KCC2 antagonist ML077: Development of a highly selective and more potent in vitro probe. Bioorg Med Chem Lett 22:4532–4535.
- Delpire E, Days E, Lewis LM, Mi D, Kim K, Lindsley CW, Weaver CD (2009) Small-molecule screen identifies inhibitors of the neuronal K-Cl cotransporter KCC2. Proc Natl Acad Sci 106:5383–5388.
- Delpire E, Weaver CD (2016) Challenges of finding novel drugs targeting the K-Cl cotransporter. ACS Chem Neurosci 7:1624–1627.
- Di Cristo G, Awad PN, Hamidi S, Avoli M (2018) KCC2, epileptiform synchronization, and epileptic disorders. Prog Neurobiol 162:1–16.
- Elahian B, Lado NE, Mankin E, Vangala S, Misra A, Moxon K, Fried I, Sharan A, Yeasin M, Staba R, Bragin A, Avoli M, Sperling MR, Engel J, Weiss SA (2018) Low-Voltage Fast Seizures in Humans Begin With Increased Interneuron Firing. Ann Neurol 0 Available at: https://onlinelibrary.wiley.com/doi/abs/10.1002/ana.25325 [Accessed September 26, 2018].
- Farrant M, Kaila K (2007) The cellular, molecular and ionic basis of GABAA receptor signalling. In: Progress in Brain Research (Tepper JM, Abercrombie ED, Bolam JP, eds), pp 59–87 Gaba and the Basal Ganglia. Elsevier. Available at: http://www.sciencedirect.com/science/article/pii/S0079612306600058 [Accessed July 12, 2018].

- Freund T f., Buzsáki G (1996) Interneurons of the hippocampus. Hippocampus 6:347–470.
- González OC, Shiri Z, Krishnan GP, Myers TL, Williams S, Avoli M, Bazhenov M (2018) Role of KCC2-dependent potassium efflux in 4-Aminopyridine-induced Epileptiform synchronization. Neurobiol Dis 109:137–147.
- Grasse DW, Karunakaran S, Moxon KA (2013) Neuronal synchrony and the transition to spontaneous seizures. Exp Neurol 248:72–84.
- Hamidi S, Avoli M (2015) KCC2 function modulates in vitro ictogenesis. Neurobiol Dis 79:51–58.
- Huberfeld G, Wittner L, Clemenceau S, Baulac M, Kaila K, Miles R, Rivera C (2007) Perturbed Chloride Homeostasis and GABAergic Signaling in Human Temporal Lobe Epilepsy. J Neurosci 27:9866–9873.
- Kaila K, Price TJ, Payne JA, Puskarjov M, Voipio J (2014) Cation-chloride cotransporters in neuronal development, plasticity and disease. Nat Rev Neurosci 15:637–654.
- Karunakaran S, Grasse DW, Moxon KA (2016) Role of CA3 theta-modulated interneurons during the transition to spontaneous seizures. Exp Neurol 283:341–352.
- Kelley MR, Cardarelli RA, Smalley JL, Ollerhead TA, Andrew PM, Brandon NJ, Deeb TZ, Moss SJ (2018) Locally Reducing KCC2 Activity in the Hippocampus is Sufficient to Induce Temporal Lobe Epilepsy. EBioMedicine 32:62–71.
- Kelley MR, Deeb TZ, Brandon NJ, Dunlop J, Davies PA, Moss SJ (2016) Compromising KCC2 transporter activity enhances the development of continuous seizure activity. Neuropharmacology 108:103–110.
- Köhling R, Lücke A, Straub H, Speckmann EJ, Tuxhorn I, Wolf P, Pannek H, Oppel F (1998) Spontaneous sharp waves in human neocortical slices excised from epileptic patients. Brain 121:1073–1087.
- Lebon F, Pégurier C, Ledecq M, Mathieu B, Bosman N, Frycia A, Lengelé S, Dhurke K, Kanduluru AK, Meunier S, Wagner A, Wolff C, Provins L (2012) Towards a KCC2 blocker pharmacophore model. Bioorg Med Chem Lett 22:3978–3982.
- Lévesque M, Herrington R, Hamidi S, Avoli M (2016) Interneurons spark seizure-like activity in the entorhinal cortex. Neurobiol Dis 87:91–101.
- Librizzi L, Losi G, Marcon I, Sessolo M, Scalmani P, Carmignoto G, Curtis M de (2017) Interneuronal Network Activity at the Onset of Seizure-Like Events in Entorhinal Cortex Slices. J Neurosci 37:10398–10407.
- Misra A, Long X, Sperling MR, Sharan AD, Moxon KA (2018) Increased neuronal synchrony prepares mesial temporal networks for seizures of neocortical origin. Epilepsia 59:636–649.

- Moore YE, Deeb TZ, Chadchankar H, Brandon NJ, Moss SJ (2018) Potentiating KCC2 activity is sufficient to limit the onset and severity of seizures. Proc Natl Acad Sci:201810134.
- Pathak HR, Weissinger F, Terunuma M, Carlson GC, Hsu F-C, Moss SJ, Coulter DA (2007) Disrupted Dentate Granule Cell Chloride Regulation Enhances Synaptic Excitability during Development of Temporal Lobe Epilepsy. J Neurosci 27:14012–14022.
- Puskarjov M, Seja P, Heron SE, Williams TC, Ahmad F, Iona X, Oliver KL, Grinton BE, Vutskits L, Scheffer IE, Petrou S, Blaesse P, Dibbens LM, Berkovic SF, Kaila K (2014) A variant of KCC2 from patients with febrile seizures impairs neuronal Cl– extrusion and dendritic spine formation. EMBO Rep 15:723–729.
- Quiroga RQ, Nadasdy Z, Ben-Shaul Y (2004) Unsupervised spike detection and sorting with wavelets and superparamagnetic clustering. Neural Comput 16:1661–1687.
- Sakata S, Harris KD (2009) Laminar Structure of Spontaneous and Sensory-Evoked Population Activity in Auditory Cortex. Neuron 64:404–418.
- Schwartzkroin PA, Haglund MM (1986) Spontaneous Rhythmic Synchronous Activity in Epileptic Human and Normal Monkey Temporal Lobe. Epilepsia 27:523–533.
- Sessolo M, Marcon I, Bovetti S, Losi G, Cammarota M, Ratto GM, Fellin T, Carmignoto G (2015) Parvalbumin-Positive Inhibitory Interneurons Oppose Propagation But Favor Generation of Focal Epileptiform Activity. J Neurosci 35:9544–9557.
- Shiri Z, Manseau F, Lévesque M, Williams S, Avoli M (2015) Interneuron activity leads to initiation of low-voltage fast-onset seizures. Ann Neurol 77:541–546.
- Shiri Z, Manseau F, Lévesque M, Williams S, Avoli M (2016) Activation of specific neuronal networks leads to different seizure onset types. Ann Neurol 79:354–365.
- Sirota A, Montgomery S, Fujisawa S, Isomura Y, Zugaro M, Buzsáki G (2008) Entrainment of neocortical neurons and gamma oscillations by the hippocampal theta rhythm. Neuron 60:683–697.
- Sivakumaran S, Cardarelli RA, Maguire J, Kelley MR, Silayeva L, Morrow DH, Mukherjee J, Moore YE, Mather RJ, Duggan ME, Brandon NJ, Dunlop J, Zicha S, Moss SJ, Deeb TZ (2015) Selective Inhibition of KCC2 Leads to Hyperexcitability and Epileptiform Discharges in Hippocampal Slices and In Vivo. J Neurosci 35:8291–8296.
- Toyoda I, Fujita S, Thamattoor AK, Buckmaster PS (2015) Unit Activity of Hippocampal Interneurons before Spontaneous Seizures in an Animal Model of Temporal Lobe Epilepsy. J Neurosci Off J Soc Neurosci 35:6600–6618.
- Uva L, Breschi GL, Gnatkovsky V, Taverna S, Curtis M de (2015) Synchronous Inhibitory Potentials Precede Seizure-Like Events in Acute Models of Focal Limbic Seizures. J Neurosci 35:3048–3055.

- Viitanen T, Ruusuvuori E, Kaila K, Voipio J (2010) The K+–Cl– cotransporter KCC2 promotes GABAergic excitation in the mature rat hippocampus. J Physiol 588:1527–1540.
- Yekhlef L, Breschi GL, Lagostena L, Russo G, Taverna S (2015) Selective activation of parvalbumin- or somatostatin-expressing interneurons triggers epileptic seizurelike activity in mouse medial entorhinal cortex. J Neurophysiol 113:1616–1630.

3.7. Figures

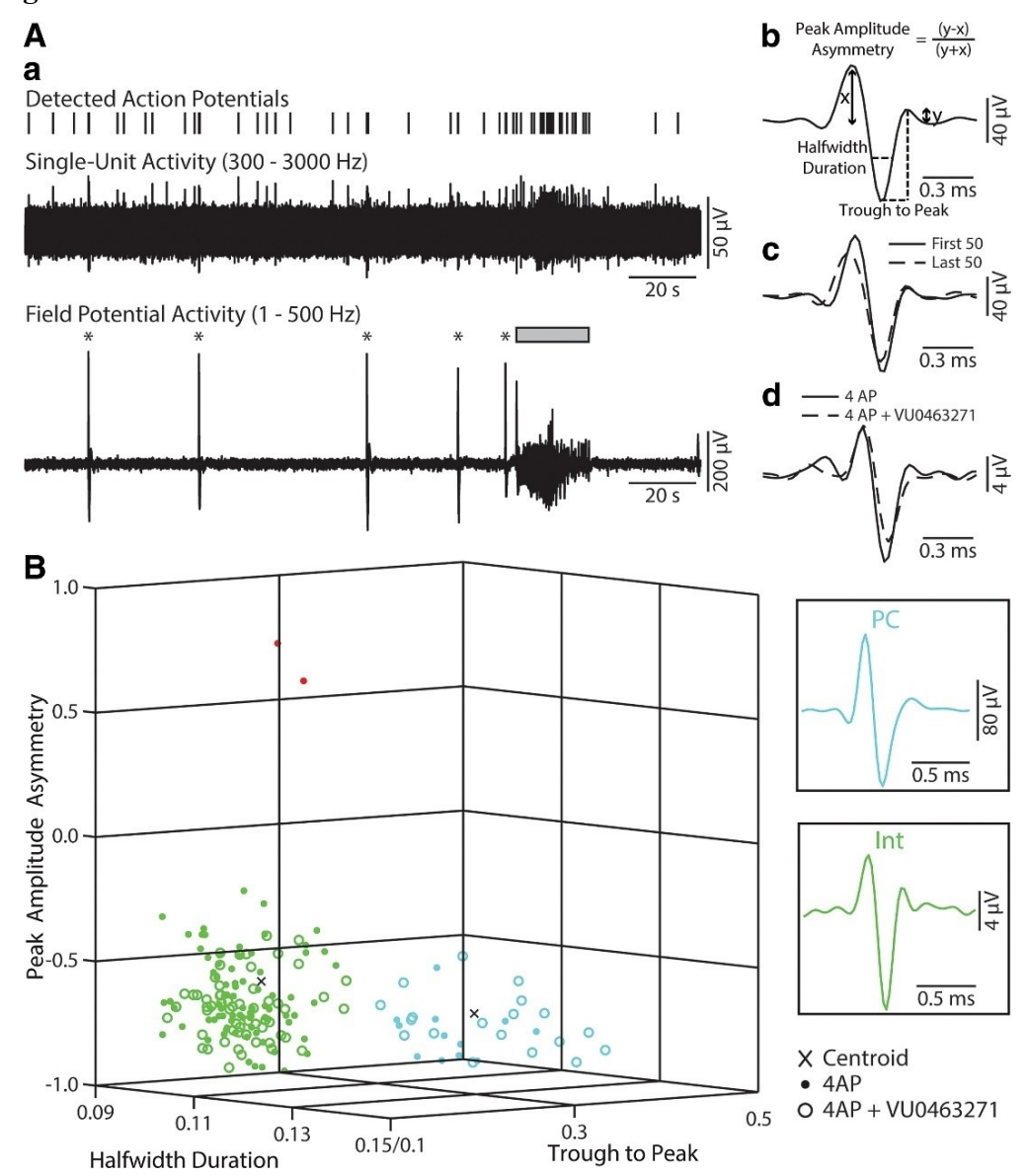


Figure 3.1. Single-unit classification. **A:** Tetrode wire recording of single-unit and field potential activity in the rat entorhinal (EC) during application of 4-aminopyridine (4AP). (a) Examples of interictal discharges (asterisks) and of a low-voltage fast-activity (LVF) ictal discharge (grey line). (b) To cluster single-unit activity, the waveform shape of action potentials was quantified using three variables: trough to peak, peak amplitude asymmetry, and half-width duration. (c) Averaged waveform shapes of the first (solid line) and last (dashed line) 50 action potentials during a 10-min recording period. (d) Averaged waveform shape of the action potentials under 4AP (solid line; n = 254) and after the addition of VU0463271 (dashed line; n = 195). **B:** Three-dimensional representation of the k-means clustering analysis showing interneurons (Int; green), principal cells (PC; blue), and outliers (red) under 4AP (dots) and 4AP + VU0463271 (circles). The centroids of the clusters are marked with x.

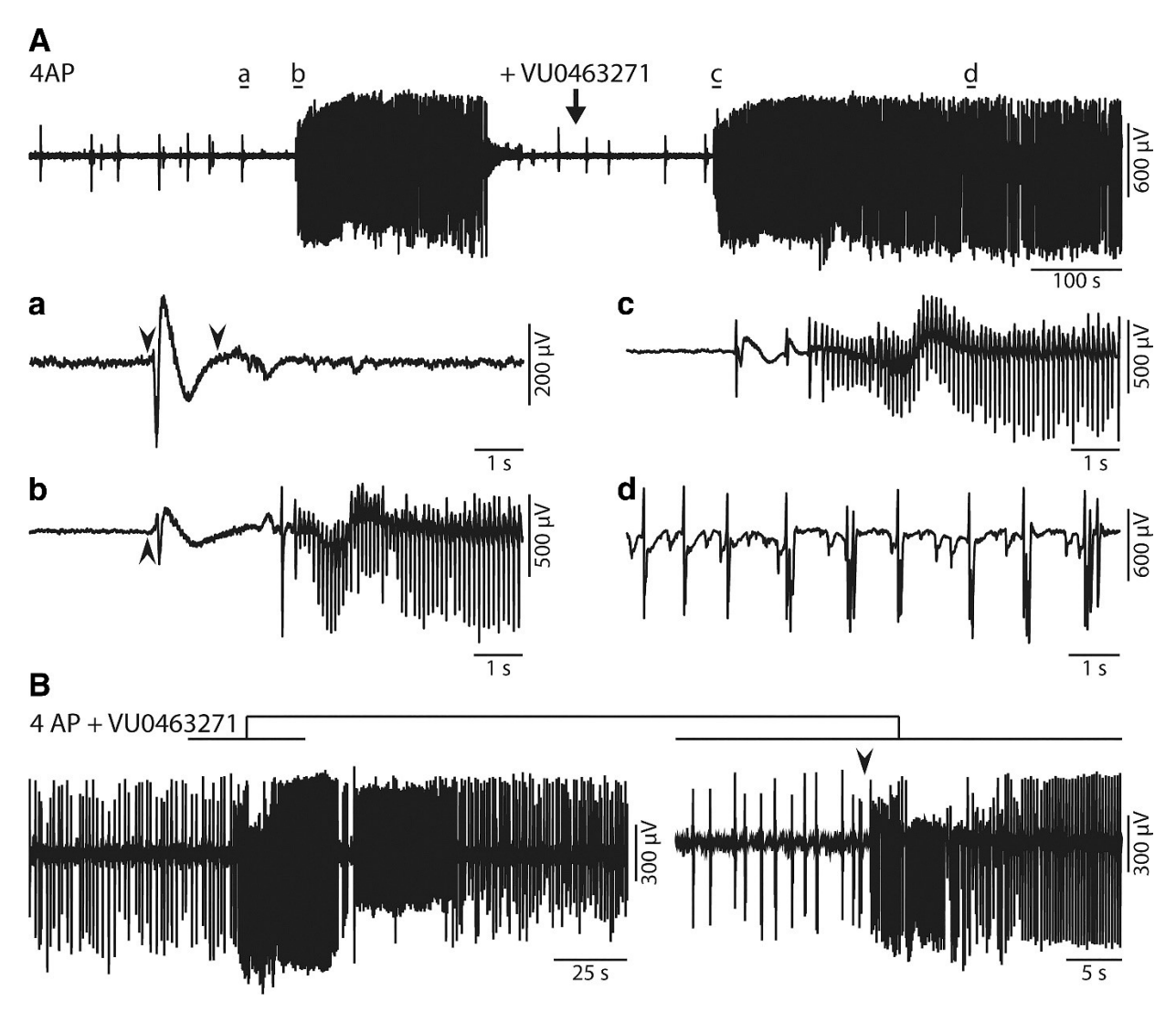


Figure 3.2. Effects of VU0463271 on the field potential activity recorded from the entorhinal cortex (EC) during different pharmacological conditions. **A:** Addition of VU0463271 to the 4-aminopyridine (4AP) medium induces a pattern of continuous interictal spikes in the field potential recording. (**a**) Enlarged example of the interictal event recorded under 4AP; the onset and termination of this interictal event are indicated by arrowheads. (**b**) Low-voltage fast-activity (LVF) ictal event recorded under 4AP, with the onset indicated by the arrowhead. (**c**) Onset of continuous interictal activity recorded in the 4AP + VU0463271 condition. (**d**) An example of interictal events recorded ~300 s after the onset of continuous interictal activity under 4AP + VU0463271. **B:** An example of ictal-like activity in the 4AP + VU0463271 condition; the arrowhead in the enlarged example identifies its onset.

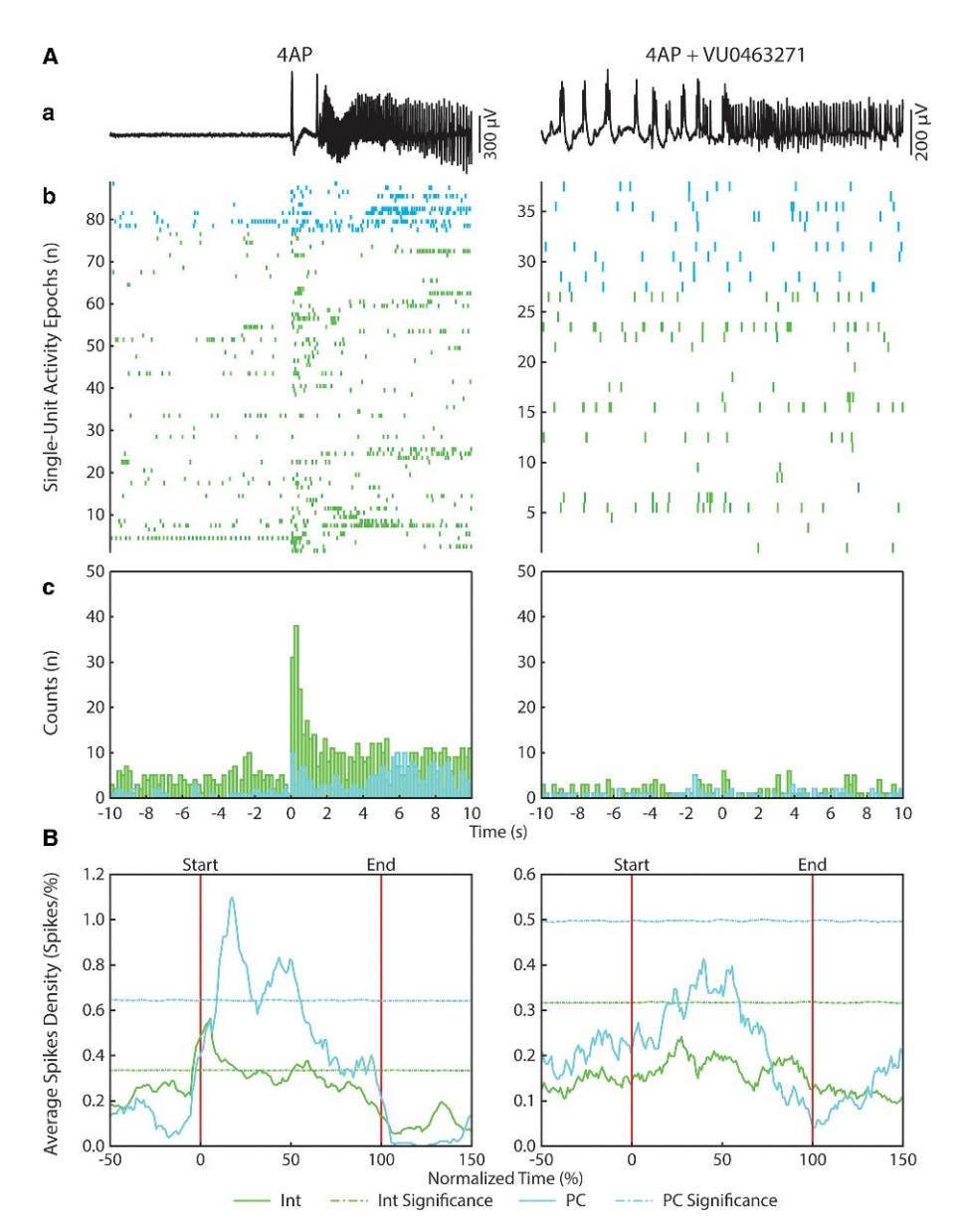


Figure 3.3. Qualitative analysis of single-unit activity during epileptiform activity recorded under 4-aminopyridine (4AP) and 4AP + VU0463271. **A**: Real-time analyses of single-unit activity during 4AP and 4AP + VU0463271 epileptiform activities. A low-voltage fast-activity (LVF) ictal event in the 4AP condition and an ictal-like event in the 4AP + VU0463271 condition are shown in **a**, while raster plots and real-time peri-event histograms (200-ms bins) are illustrated in **b** and **c**, respectively. In the real-time peri-event histograms, peaks of interneurons and principal cell firing occurred at 0.30 s and 0.10 s, respectively, after the ictal onset in the 4AP condition. **B**: Normalized peri-event histograms with *time 0* representing the onset of the ictal events (interneurons: n = 76; principal cells: n = 12) recorded under 4AP and ictal-like events (interneuron: n = 26; principal cell: n = 11) recorded under 4AP + VU0463271. In the 4AP condition, the peak of interneuron activity occurred at 5.50% of the normalized ictal events, while the peak of principal cell activity could be identified at 17.50%. Dashed lines indicate the significance thresholds.

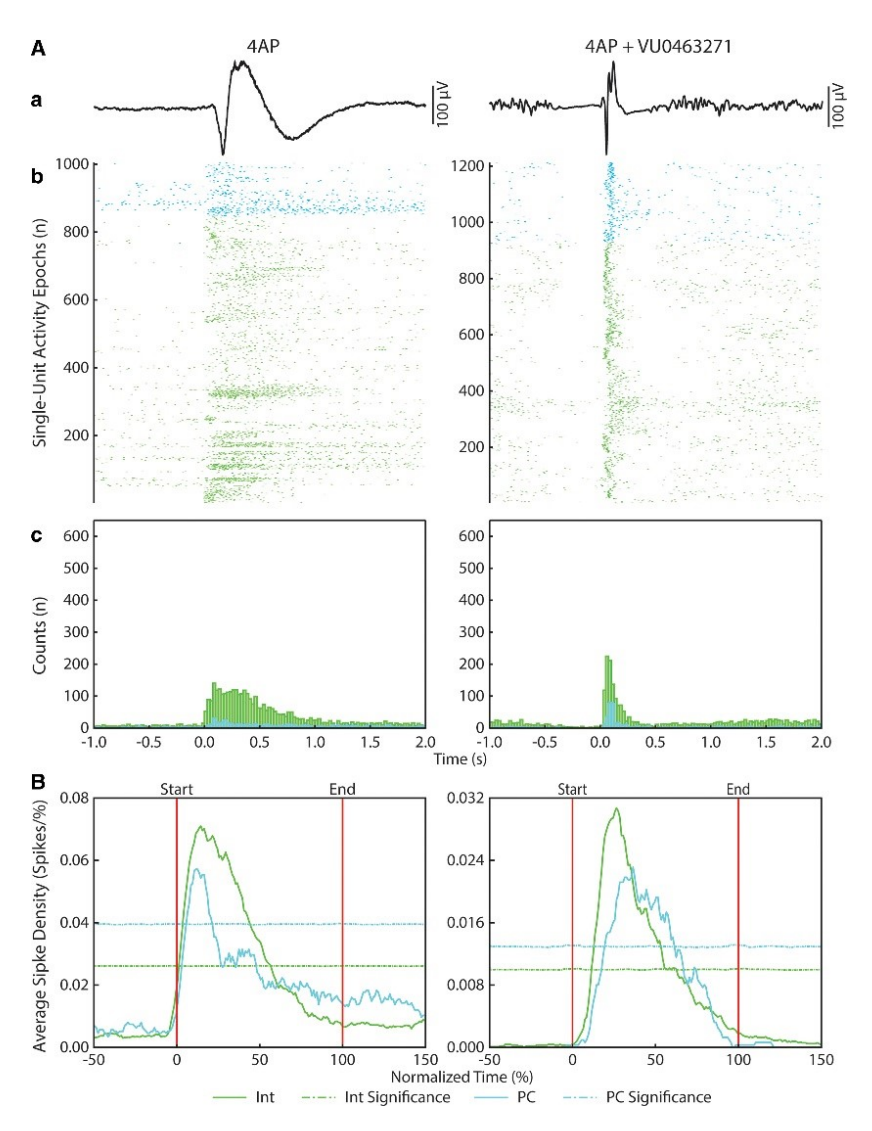


Figure 3.4. Qualitative analysis of single-unit activity during interictal events in the 4-aminopyridine (4AP) and 4AP + VU0463271 conditions. **A**: Real-time analyses of single-unit activity during interictal events in the 4AP and 4AP + VU0463271 conditions. Interictal events (**a**) along with corresponding raster plots (**b**) and real-time peri-event histograms (25-ms bins; **c**), are illustrated. In the real-time peri-event histogram, peaks of interneuron and principal cell action potential distributions in the 4AP condition were identified at 0.09 s after the onset of interictal events. In the 4AP + VU0463271 condition, peaks of interneuron and principal cell action potential distributions were identified at 0.06 s and 0.09 s, respectively, after the onset of interictal events. **B**: Normalized peri-event histograms with *time* θ representing the onset of interictal events. Note that in the 4AP condition, the peak of interneuron activity during interictal events (n = 845) occurred at 14.50% of the normalized duration, whereas the peak of principal cell activity during interictal events (n = 929) occurred at 26.50% whereas the peak of principal cell activity during interictal events (n = 929) occurred at 26.50% whereas the peak of principal cell activity during interictal events (n = 929) occurred at 36.50%. Dashed lines indicate the significance thresholds.

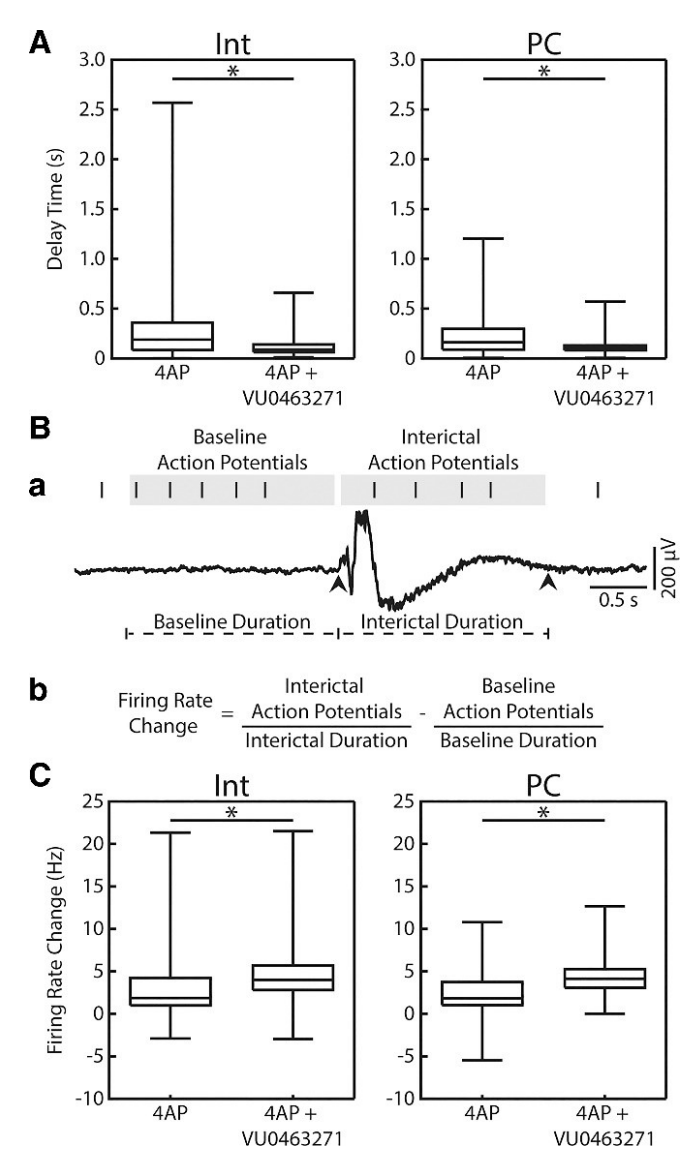


Figure 3.5. Quantitative analysis of single-unit firing during interictal events recorded in the 4-aminoypyridine (4AP) and 4AP + VU0463271 conditions. A: The delay time between the onsets of interictal events and the first interneuron (Int) and principal cell (PC) action potential occurring during the respective interictal events in the 4AP and the 4AP + VU0463271 conditions. Note that there is a decrease in the delay time between the onset of interictal events and both the first interneuron and principal cell action potential after the application of VU0463271. B: Analysis of the changes in firing rate. (a) Single-unit action potentials recorded before and during an interictal event. Arrowheads in the field potential recording denote the onset and termination of the interictal event. (b) The mathematical formula for calculating the change in firing rate. (C) Changes in interneuron (Int) and principal cell (PC) firing rate during interictal events in the 4AP and 4AP + VU0463271 conditions. Note that there is an increase in the change in firing rate of both interneurons and principal cells upon the addition of VU0463271. Mann-Whitney *U*-Test was used to established statistical significance, *p < 0.05.

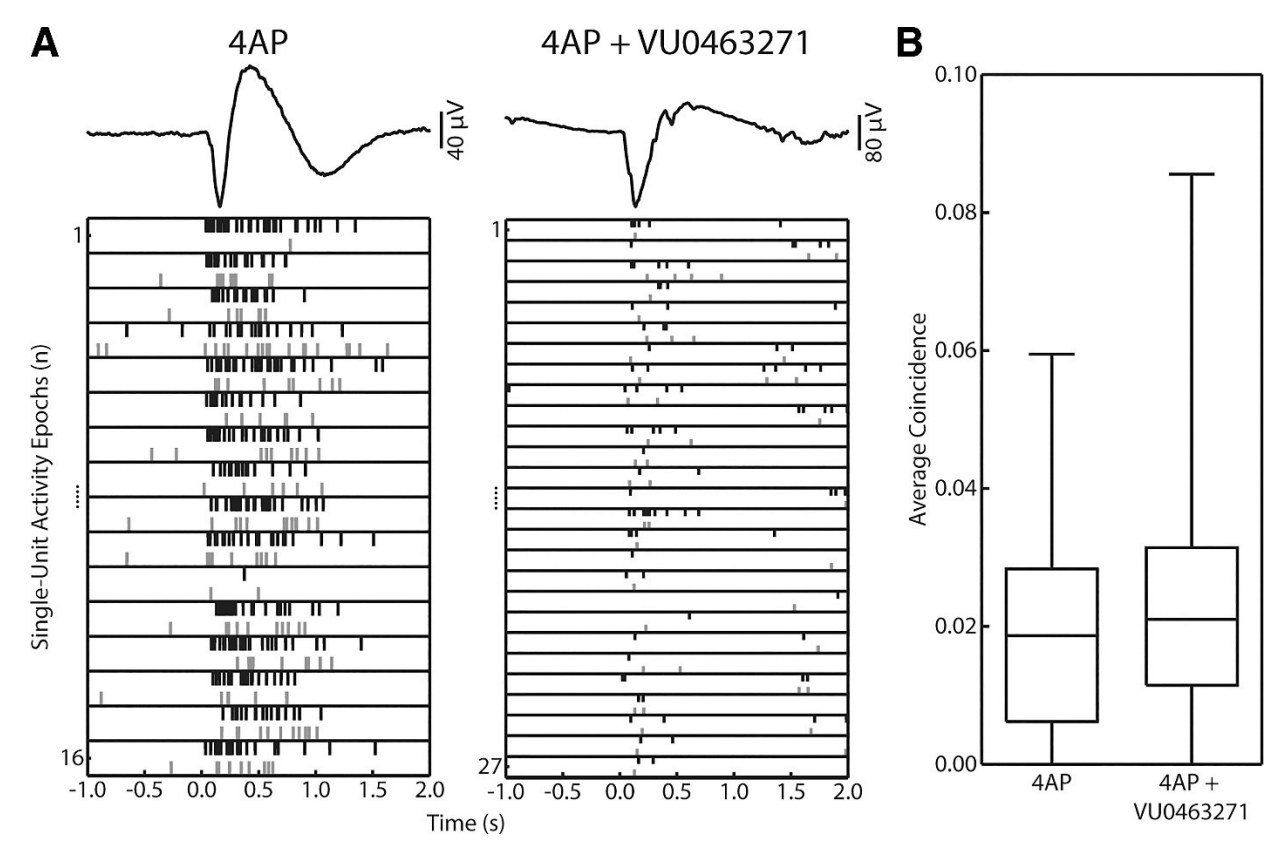


Figure 3.6. Cross-correlation analysis of pairs of simultaneously recorded single units during interictal events in the 4-aminopyridine (4AP) and 4AP + VU0463271 conditions. **A**: Sample pairs of simultaneously recorded single units during successive interictal events in the 4AP and 4AP + VU0463271 conditions. The action potential discharges of two different single units was represented by black (4AP: Int; 4AP + VU0463271: Int) and gray (4AP: Int; 4AP + VU0463271: PC). **B**: The average coincidence of the action potentials of pairs of simultaneously recorded single units during interictal events in the 4AP (n = 47) and 4AP + VU0463271 (n = 40) conditions. Note that there was no significant change in the average coincidences of action potential discharge pattern between pairs of simultaneously recorded single units between the 4AP and 4AP + VU0463271 conditions.

Chapter 4: KCC2 Antagonism and GABAergic Synchronization in the Entorhinal Cortex in the Absence of Ionotropic Glutamatergic Receptor Signalling.

Interneurons actively participate in epileptiform activity. Therefore, investigations of the epileptiform activity also need to characterize the role of inhibitory signalling of γ -aminobutyric acid (GABA). Thus, in part 2 of my experiments investigating the role of K⁺-Cl⁻ cotransporter 2 (KCC2) in epilepsy, I applied KCC2 antagonist VU0463271 to 4-aminopyridine (4AP)-induced epileptiform activity that was pharmacologically isolated from ionotropic glutamatergic signalling in the rat entorhinal cortex (EC) and studied the underlying neuronal activity using tetrodes. This work was published in 2020 in the *Neuropharmacology* as a manuscript titled "KCC2 Antagonism and GABAergic Synchronization in the Entorhinal Cortex in the Absence of Ionotropic Glutamatergic Receptor Signalling."

Chen L-Y, Lévesque M, Avoli M (2020) KCC2 antagonism and GABAergic synchronization in the entorhinal cortex in the absence of ionotropic glutamatergic signalling. Neuropharmacology 167:107982.

4.1. Abstract

γ-Aminobutyric acid (GABA), which is released by interneurons, plays an active role in generating interictal epileptiform spikes during blockade of ionotropic glutamatergic signalling, but it remains unclear whether and how the K⁺-Cl⁻ cotransporter 2 (KCC2) influences these paroxysmal events. Therefore, we employed tetrode recordings in the *in vitro* rat entorhinal cortex (EC) to analyze the effects of the KCC2 antagonist VU0463271 on 4-aminopyridine (4AP)-induced interictal spikes that were pharmacologically isolated by applying ionotropic glutamatergic receptor antagonists. After the addition of VU0463271, these interictal spikes continued to occur at similar rates as in control (i.e., during application of 4AP with ionotropic glutamatergic receptor antagonists) but were smaller and shorter. Despite the absence of ionotropic glutamatergic receptor signalling, both interneurons and principal cells increased their firing during interictal spikes. Moreover, we found that KCC2 antagonism increased interneuron firing but decreased principal cell firing during the interictal spike rising phase; in contrast, during the falling phase, interneuron firing decreased in the presence of VU0463271, while no change was observed in principal cell firing. Overall, our results show that KCC2 antagonism enhances interneuron excitability at the onset of interictal spikes generated by the EC neuronal networks during blockade of ionotropic glutamatergic transmission but disrupts later neuronal recruitment.

4.2. Introduction

While focal seizures are the hallmark of an epileptic condition, interictal epileptiform discharges (hereafter termed interictal spikes) are valuable to clinicians. For instance, they help clinicians to diagnose focal epilepsy and to identify epilepsy subtypes (Fisher et al., 2017; Tatum et al., 2018). Moreover, for epilepsy surgery, they have been used as markers of seizure onset zones (Jacobs et al., 2011; Tatum et al., 2018) and predictors of post-operative outcome (Rosati et al., 2003; Dworetzky and Reinsberger, 2011; Coutin-Churchman et al., 2012; Tatum et al., 2018; Mehvari Habibabadi et al., 2019). Therefore, identifying the fundamental mechanisms underlying interictal spikes in experimental epilepsy models should lead to improved epilepsy diagnosis and treatment in humans. To this end, basic science researchers have reproduced electrographic interictal spikes in the laboratory by applying drugs such as the K⁺ channel blocker 4-aminopyridine (4AP) to *in vitro* brain preparations (Avoli and de Curtis, 2011).

These studies have revealed excessive firing of interneurons, which release γ-aminobutyric acid (GABA) in coincidence with 4AP-induced interictal spikes, thus pointing to the involvement of inhibitory mechanisms in their generation (Avoli et al., 1996; Lévesque et al., 2016; Librizzi et al., 2017; González et al., 2018). In addition, these interictal spikes continue to occur in the absence of ionotropic glutamatergic receptor signalling, and they could be abolished upon blockade of GABA_A signalling (Avoli et al., 1996, 2013; Sudbury and Avoli, 2007; Panuccio et al., 2010; Hamidi and Avoli, 2015; Lévesque et al., 2016). Hence, this evidence suggests that interneuron firing and subsequent GABA_A signalling contribute to interictal spike generation, at least in *in vitro* models of epileptiform synchronization.

An important consequence of GABA released from interneurons is the activation of GABA_A receptors and the resulting Cl⁻ influx into neurons that causes hyperpolarization of the neuronal membrane potential (Farrant and Kaila, 2007; Avoli and de Curtis, 2011; Kaila et al., 2014; Di Cristo et al., 2018). To ensure GABA_A receptor-mediated Cl⁻ influx, neurons in the mature brain maintain a low intracellular [Cl⁻] using the K⁺-Cl⁻ cotransporter 2 (KCC2); thus, in order to extrude Cl⁻ from the neuron, KCC2 uses the [K⁺] gradient (Viitanen et al., 2010). Accordingly, excessive interneuron activity occurring at the onset of 4AP-induced ictal activity causes substantial elevations in extracellular [K⁺], presumably through KCC2 activity (Avoli et al., 1996; Librizzi et al., 2017; González et al., 2018). Taken together, KCC2 activity and the

subsequent elevations in extracellular [K⁺] may have important implications in epileptiform synchronization (Kaila et al., 2014; Di Cristo et al., 2018).

To study the role of KCC2 in epileptic disorders, KCC2 antagonists (Delpire et al., 2009, 2012; Lebon et al., 2012; Delpire and Weaver, 2016) have been used in models of epileptiform synchronization. These experiments have established that antagonizing KCC2 enhances neuronal excitability by depolarizing the reversal potential of GABA_A signalling (Sivakumaran et al., 2015; Moore et al., 2018; Chen et al., 2019). In addition, in many cases, KCC2 antagonism blocked ictal activity while enhancing interictal spike generation (Hamidi and Avoli, 2015; Sivakumaran et al., 2015; Kelley et al., 2016; Moore et al., 2018; Chen et al., 2019). However, while previous studies have shown that GABAA signalling generates interictal spikes in the in vitro 4AP model of epileptiform synchronization (see for review de Curtis and Avoli, 2016), the role of KCC2 antagonism during interictal spikes in the presence of ionotropic glutamatergic receptor antagonists was investigated in only one study using VU0240551 (Hamidi and Avoli, 2015), a less potent and selective predecessor of VU0463271 (Delpire et al., 2012). Therefore, we employed here tetrode wire recordings to understand whether and how the KCC2 antagonist VU0463271 modifies the activity of presumptive interneurons and principal cells in the rat entorhinal cortex (EC) during interictal spikes occurring in the presence of 4AP and ionotropic glutamatergic receptor antagonists in an in vitro brain slice preparation.

4.3. Materials and methods

4.3.1. Ethical approval

All procedures complied with the guidelines of the Canadian Council on Animal Care and were approved by the McGill University Animal Care Committee. All efforts were made to minimize the suffering and the number of animals used in the experiments.

4.3.2. Specimen preparation and maintenance

Brains of male Sprague-Dawley rats (250–275 g; Charles River Laboratories, Saint Constant, QC, Canada) – anaesthetized using 5% isoflurane (Fresenius Kabi Canada Limited, Toronto, ON, Canada) – were extracted and placed in ice-cold artificial cerebrospinal fluid (ACSF; 124 mM NaCl, 2 mM KCl, 2 mM CaCl₂, 2 mM MgSO₄, 1.25 mM KH₂PO₄, 26 mM NaHCO₃, and 10 mM D-glucose; Sigma-Aldrich, Oakville, ON, Canada) that was oxygenated with O₂/CO₂ (95%/5%)

gas mixture to maintain a pH of 7.4. Brains were sliced with a vibratome (VT1000S; Leica, Concord, ON, Canada) to obtain slices containing hippocampus and EC (thickness = 450 μm) and then transferred to an interface chamber to be maintained between warm ACSF (32 ± 1°C) and humidified O₂/CO₂ (95%/5%) gas mixture. Following approximately 1-h recovery period, epileptiform activity was induced by continuous bath application of ACSF containing 4AP (50 μM; Sigma-Aldrich, Oakville, ON, Canada) at a flow rate of approximately 2 ml/min (see also Chen et al., 2019). After the occurrence of baseline activity, NMDA receptor antagonist (*RS*)-3-(2-carboxypiperazin-4-yl)-propyl-1-phosphonate (CPP; 10 μM; Tocris, Canada) and AMPA receptor antagonist 6-Cyano-7-nitroquinoxaline-2,3-dione disodium salt (CNQX; 10 μM; Tocris, Oakville, ON, Canada) were added to ACSF containing 4AP (4AP + CPP + CNQX) to isolate GABAergic synchronous events. To establish the role of KCC2 in these ionotropic glutamatergic signalling-independent interictal spikes, *N*-Cyclo-propyl-*N*-(4-methyl-2-thiazolyl)-2-[(6-phenyl-3-pyridazinyl)thio]acetamide (10 μM; VU0463271; Tocris, Oakville, ON, Canada; Delpire et al., 2012) was then added (4AP + CPP + CNQX + VU0463271).

4.3.3. Tetrode recordings

Collection and analysis of single-unit activity were based on previous studies from our laboratory (Lévesque et al., 2016, 2018; Chen et al., 2018, 2019). Four tungsten wires (tip diameter = 50 µm, California Fine Wire Company, Grover Beach, CA, USA) were twisted together to make a tetrode wire; seven tetrode wires were inserted into a microdrive (NLX-18; Neuralynx, Bozeman, MT, USA). A ground wire was connected from the drive (EIB-36-18 Drive; Neuralynx, Bozeman, MT, USA) mounted on the microdrive to the vibration isolation table (Newport; Irvine, CA, USA). A channel of one tetrode was used as the reference. All tetrodes were placed in the EC to record neuronal activity at a sampling rate of 20 kHz with a recording bandwidth between 0.8 to 22,000 Hz using the Neuroware system (2.1; Triangle Biosystems, Durham, NC, USA). Due to limitations in computer performance, neuronal activity was sampled in 10-min epochs. We performed repeated sampling to minimize the number of animals used in our study. Off-line data analysis was performed with MATLAB (Mathworks, Natick, MA, USA; RRID:SCR 001622).

4.3.4. Isolation of single-unit activity

Raw tetrode recordings, which were filtered between 300 and 3,000 Hz (**Figure 4.1A**), were analyzed with WaveClus (Quiroga et al., 2004), an unsupervised cluster cutting algorithm. Peaks in the filtered signal that were 5 standard deviations (SDs) above the baseline were presumed to be action potentials and sorted based on sets of wavelet coefficients (Quiroga et al., 2004). For each identified cluster of action potentials, the experimenter visually verified that (i) it was distinct from the noise, (ii) action potentials were visible on at least two channels of a tetrode wire, (iii) action potentials were of different amplitudes between channels of the tetrode, and (iv) less than 2% of the total number of action potentials occurred during the refractory period (<3 ms) (Csicsvari et al., 1998).

Verified single-unit clusters were characterized using three variables based on previously published guidelines (Freund and Buzsáki, 1996; Csicsvari et al., 1998; Sirota et al., 2008; Sakata and Harris, 2009; Lévesque et al., 2016; Chen et al., 2019): first, the amplitude from the trough to the peak; second, the asymmetry between the amplitudes of the peaks; third, the action potential width at 50% of amplitude (**Figure 4.1C**). To cluster presumptive single units, we fitted Gaussian mixture models of various orders then selected the best model using Bayesian information criterion (**Figure 4.1D**).

4.3.5. Isolation of field potential activity

To visualize the field potential activity generated by the EC, raw tetrode recordings were filtered between 1 and 500 Hz and down sampled to 2,000 Hz. Then, the four channels of the tetrodes were averaged together and normalized against the average of all signals from all tetrodes used during the recording session. Using this final processed field activity (**Figure 4.1A**), an experimenter manually detected interictal spikes, of which the onset was defined as the first deflection from baseline and the termination as the return to baseline activity. The duration of interictal spikes was defined as the difference between the onset and termination times. The amplitude of interictal spikes was defined as the difference between the maximum and minimum values during each interictal spike.

4.3.6. Patterns of single-unit activity around the onset of interictal spikes

We used raster plots, that are summarized in real-time peri-event histograms, and normalized peri-event histograms to characterize the changes in single-unit activity around the onset of interictal spikes. The raster plots were built by extracting single-unit action potentials from 1 s before to 2 s after the onset, *time* 0, of the interictal spikes. The action potentials in the raster plots were summed in 25-ms bins and normalized to the total sum to generate real-time peri-event histograms. Since interictal spikes differed in durations, normalized peri-event histograms were generated by extracting epochs of single-unit activity around interictal spikes. These single-unit activity epochs included pre- and post-event baselines with duration same to that of interictal spikes. The duration of the entire single-unit activity epoch was normalized with 0% and 100% representing the onset and termination of interictal spikes, respectively. Action potentials generated by the same single-unit type, interneurons or principal cells, in the same pharmacological condition, 4AP + CPP + CNQX or 4AP + CPP + CNQX + VU0463271, were summed in 1% bin and averaged to produce the averaged action potential densities in the normalized peri-event histograms. For visual representation, the averaged action potential densities were smoothed using MATLAB function *movmean* with bin width of 11 data points.

4.3.7. Quantification of single-unit activity around the peak of interictal spikes

We calculated the proportions of action potentials that occurred during the rising and the falling phases for all interictal spikes recorded for all single units. Specifically, the rising phase of interictal spikes was defined as the period between the onset and peak of interictal spikes, whereas the falling phase was defined as the period between the peak and end of interictal spikes (**Figure 4.4A**). The number of action potentials that occurred in the rising and falling phases were normalized against the total number of action potentials generated by the single units during the interictal spikes to calculate the proportion of action potentials in the rising and falling phases, respectively. We then compared the total of the proportions of action potentials generated by the same type of single unit, either interneurons or principal cells, in the same phase, either rising or falling phases, across pharmacological conditions, between 4AP + CPP + CNQX and 4AP + CPP + CNQX + VU0463271.

4.3.8. Statistical analyses

For statistical comparisons between pharmacological conditions, we first assessed data normality using the Shapiro-Wilks Test and found that data were not normally distributed. Therefore, we expressed the data central tendencies as median (interquartile range) and used the Wilcoxon Rank-Sum Test for hypothesis testing. Since Wilcoxon Rank-Sum Test compares sums of rank, we also reported the mean ranks (R) of our data.

We performed Monte Carlo analysis to assess for statistical significance in the normalized peri-event histograms. For each extracted single-unit activity epochs, action potential timestamps were randomly shuffled 5,000 times to simulate random single-unit activity patterns. Using the simulated single-unit activity epochs, average action potential densities of the normalized peri-event histograms were considered to be significant when they were 2.50 SDs above the average action potential densities of simulated activity.

4.4. Results

4.4.1. Single-unit characterization

In the EC of 25 brain slices obtained from 12 animals, we performed tetrode recordings to study the relationship between field activity and action potentials generated by single units during interictal spikes generated during the application of 4AP and ionotropic glutamatergic receptor antagonists (**Figure 4.1A**). We recorded a total of 187 single units, for which the averaged action potential waveforms of the first and last 50 action potentials appeared to be similar (**Figure 4.1Ba**). Additionally, the shapes of the action potential waveform in the presence and absence of VU0463271 appeared to be similar (**Figure 4.1Bb**). As in previous studies from our laboratory (Lévesque et al., 2016, 2018; Chen et al., 2018, 2019), we used well-established characterizations of action potential waveform (Freund and Buzsáki, 1996; Csicsvari et al., 1998; Sirota et al., 2008; Sakata and Harris, 2009) to cluster the recorded single units into presumptive interneurons (4AP + CPP + CNQX: n = 80; 4AP + CPP + CNQX + VU0463271: n = 85) or principal cells (4AP + CPP + CNQX: n = 14; 4AP + CPP + CNQX + VU0463271: n = 8) (**Figure 4.1D**).

4.4.2. Alterations of interictal spikes by antagonizing KCC2 activity

As previously reported (Avoli et al., 1996, 2013; Hamidi and Avoli, 2015; Lévesque et al., 2016), interictal spikes in the EC continued to occur during the application of the ionotropic glutamatergic

receptor antagonists CPP and CNQX (n = 2480 spikes, n = 21 slices, n = 12 animals; **Figure 4.2A**). The interictal spikes had a median interval of occurrence of 20.17 s (10.72–30.28 s), a median duration of 0.97 s (0.67–1.19 s), and a median amplitude of 22.97 μ V (13.79–52.49 μ V). Interictal spikes continued to occur at a similar interval of occurrence (20.65 s, 11.59–28.20 s) following the application of the KCC2 antagonist VU0463271 (n = 2560 spikes; n = 13 slices, n = 7 animals; **Figure 4.2A** and **4.2B**); however, their median duration (0.86 s, 0.59–1.07 s) along with their median amplitude (13.35 μ V, 9.33–18.97 μ V) were significantly decreased (duration: $R_{4AP+CPP+CNQX+VU0463271} = 2.31 \times 10^3$, $p = 1.64 \times 10^{-25}$, $W = 5.91 \times 10^6$, z = -1.04; amplitude: $R_{4AP+CPP+CNQX+VU0463271} = 2.31 \times 10^3$, $R_{4AP+CPP+CNQX+VU0463271} = 1.94 \times 10^3$, $p = 4.26 \times 10^{-184}$, $p = 4.96 \times 10^6$, $p = 4.26 \times 10^{-184}$, $p = 4.96 \times 10^6$, p = 2.289) (**Figure 4.2B**).

4.4.3. Effects of VU0463271 on single-unit activity pattern around the onset of interictal spikes

Next, we characterized the pattern of single-unit activity around the onset of interictal spikes generated during application of 4AP and ionotropic glutamatergic receptor antagonists with and without VU0463271 in the medium. Examples of interictal spikes are illustrated in Figure 4.3Aa. As illustrated in Figure 4.3Ab, both interneurons and principal cells started firing around the onset of interictal spikes in both absence and presence of VU0463271 (4AP + CPP + CNQX: n = 1588interictal spikes for interneurons, n = 185 interictal spikes for principal cells; 4AP + CPP + CNOX+ VU0463271: n = 1764 interictal spikes for interneurons, n = 134 interictal spikes for principal cells). When we examined the action potential density in the real-time peri-event histograms, we noted that the peak of interneuron action potential density was higher in the 4AP + CPP + CNQX + VU0463271 condition than in the 4AP + CPP + CNQX condition (Figure 4.3Ac). Moreover, in the normalized peri-event histograms, we found that single-unit action potential densities of both interneurons and principal cells significantly increased after the onset of interictal spikes under both the 4AP + CPP + CNQX and the 4AP + CPP + CNQX + VU0463271 conditions (Figure **4.3B**). Moreover, by performing this type of analysis, we noted that the peak of interneuron action potential density in the 4AP + CPP + CNQX + VU0463271 condition was higher than that in the 4AP + CPP + CNQX condition.

4.4.4. Effects of VU0463271 on the occurrence of single-unit activity during interictal spikes

As shown in the real-time and normalized peri-event histograms in **Figure 4.3**, interneuron action potentials after the onset of interictal spikes were more concentrated after the addition of VU0463271, suggesting that the pattern of interneuron activity was altered upon the antagonism of KCC2. Therefore, we adapted the methods outlined by Spoljaric *et al.* (2019) to quantify single-unit activity around the peak of interictal spikes recorded with and without VU0463271 in the medium. Specifically, we calculated the proportion of single-unit action potentials that occurred in the rising and falling phase of interictal spikes (**Figure 4.4A**). As shown in **Figure 4.4B**, the proportion of interneuron action potentials in the rising phase was significantly higher in the presence than in the absence of VU0463271 (4AP + CPP + CNQX: 0.00%, 0.00–50.00%; 4AP + CPP + CNQX + VU0463271: 16.67%, 0.00–66.67%; $R_{4AP + CPP + CNQX} = 2.01 \times 10^3$, $R_{4AP + CPP + CNQX + VU0463271} = 2.30 \times 10^3$, $p = 8.54 \times 10^{-17}$, $W = 4.17 \times 10^6$, z = -8.32). As for principal cells, we observed that the proportion of action potentials in the rising phase was significantly lower after the addition of VU0463271 than before (4AP + CPP + CNQX: 0.00%, 0.00–38.46%; 4AP + CPP + CNQX + VU0463271: 0.00%, 0.00–20.00%; $R_{4AP + CPP + CNQX} = 2.84 \times 10^2$, $R_{4AP + CPP + CNQX} = 2.84 \times 10^2$, $R_{4AP + CPP + CNQX} = 2.84 \times 10^2$, $R_{4AP + CPP + CNQX} = 2.84 \times 10^2$, $R_{4AP + CPP + CNQX} = 2.84 \times 10^2$, $R_{4AP + CPP + CNQX} = 2.84 \times 10^2$, $R_{4AP + CPP + CNQX} = 2.84 \times 10^2$, $R_{4AP + CPP + CNQX} = 2.84 \times 10^2$, $R_{4AP + CPP + CNQX} = 2.84 \times 10^2$, $R_{4AP + CPP + CNQX} = 2.84 \times 10^2$, $R_{4AP + CPP + CNQX} = 2.84 \times 10^2$, $R_{4AP + CPP + CNQX} = 2.84 \times 10^2$, $R_{4AP + CPP + CNQX} = 2.84 \times 10^2$, $R_{4AP + CPP + CNQX} = 2.84 \times 10^2$, $R_{4AP + CPP + CNQX} = 2.84 \times 10^2$, $R_{4AP + CPP + CNQX} = 2.84 \times 10^2$, $R_{4AP + CPP + CNQX} = 2.84 \times 10^2$, $R_{4AP + CPP + CNQX} = 2.84 \times 10^2$, $R_{4AP + CPP + CNQX} = 2.84 \times 10^2$, $R_{4AP + CPP + C$

As shown in **Figure 4.4B**, during the falling phase of the interictal spikes, the proportion of interneuron action potentials was significantly lower after the addition of VU0463271 than before (4AP + CPP + CNQX: 33.33%, 0.00–66.67%; 4AP + CPP + CNQX + VU0463271: 25.00%, 0.00–60.00%; $R_{4AP + CPP + CNQX} = 2.23 \times 10^3$, $R_{4AP + CPP + CNQX + VU0463271} = 2.11 \times 10^3$, $p = 6.62 \times 10^{-4}$, $W = 4.62 \times 10^6$, z = 3.40). In contrast, the proportion of principal cell action potentials occurring during the falling phase of the interictal spikes was not significantly different between the two pharmacological conditions (4AP + CPP + CNQX: 20.94%, 0.00–57.14%; 4AP + CPP + CNQX + VU0463271: 10.00%, 0.00–66.67%) (**Figure 4.4B**).

4.5. Discussion

The main findings of our study can be summarized as follows: 1) we confirmed that KCC2 antagonism does not alter the interval of occurrence of interictal spikes generated during application of 4AP and ionotropic glutamatergic receptor antagonists but decreased their amplitude and duration; 2) despite the changes in field activity, interictal spikes were still associated to significant increases in interneuron and principal cell action potential densities under KCC2

antagonism; 3) KCC2 antagonism led to an increase in the proportion of interneuron action potentials in the rising phase concomitant to a decrease in the proportion of principal cell action potentials; and 4) during the falling phase, the proportion of interneuron action potentials decreased when VU0463271 was present in the medium, while no change was observed in the proportion of principal cell action potentials.

4.5.1. KCC2 antagonism alters the dynamics of interictal spikes

In line with findings reported by Hamidi and Avoli (2015), we found that the application of VU0463271 to medium containing 4AP and ionotropic glutamatergic receptor antagonists does not alter the interval of occurrence of interictal spikes. The similarity between intervals of occurrence in our pharmacological conditions suggests that interneurons can periodically and synchronously fire action potentials in the absence of ionotropic excitatory synaptic transmission, which was originally reported by Perreault and Avoli (1991, 1992), as well as during reduced KCC2 function. Moreover, our data suggest that these periodic and synchronous interneuron action potentials are capable of generating postsynaptic responses since they were mirrored by field potential events. Interestingly, the increase in firing associated to interictal spikes in absence of ionotropic glutamatergic signalling could also be identified in principal cells. These increases in firing could result from elevations in extracellular [K⁺] that accompany "excessive" activation of postsynaptic GABA_A receptors (Avoli et al., 1996; Smirnov et al., 1999; Viitanen et al., 2010) and HCO₃-mediated depolarizing currents (Lamsa and Kaila, 1997). In addition, depolarizing GABA_A signalling has been reported in hippocampal (Michelson and Wong, 1991; Perreault and Avoli, 1991, 1992) and EC neurons (Lopantsev and Avoli, 1998). Finally, action potential firing may result from gap junction coupling (Yang and Michelson, 2001; Gigout et al., 2006; Fujiwara-Tsukamoto et al., 2010).

Confirming previous data from our laboratory (Hamidi and Avoli, 2015), we found that the duration and amplitude of ionotropic glutamatergic signalling-independent 4AP-induced interictal spikes became lower in the presence of VU0463271. In light of previous experiments showing that extracellular [K⁺] can influence the duration and the amplitude of synchronous field potentials such as epileptiform interictal spikes (Ogata et al., 1976; Hablitz and Lundervold, 1981; Chizhov et al., 2015), we interpret such changes in duration and amplitude as the result of decreased elevations in extracellular [K⁺] that are known to accompany 4AP-induced interictal spikes (Avoli

et al., 1996), which become smaller than control during pharmacological blockade using KCC2 antagonist (Viitanen et al., 2010). Therefore, our findings are in agreement with previous studies that highlighted the role of transient elevations in extracellular [K⁺] in the generation of field interictal spikes (Avoli et al., 1996; Smirnov et al., 1999).

4.5.2. KCC2 antagonism alters the pattern of single-unit activity during interictal spikes

Using tetrodes, we found that interneuron and principal cell averaged action potential densities significantly increased around the onset of interictal spikes generated in the absence of ionotropic glutamatergic receptor signalling, showing that GABAA signalling can recruit single units through the mechanisms discussed in the previous section (e.g. depolarizing GABA_A signalling, gap junctions, etc.). Upon closer examination, we found changes in the proportions of single-unit action potentials during interictal spikes recorded under KCC2 antagonism, suggesting changes to the underlying interplay between single units. Namely, we found that the proportion of interneuron action potentials in the rising phase was higher in the condition of reduced KCC2 function than in the condition of intact KCC2 function; this increase in the proportion of interneuron action potentials in the rising phase may mirror an increase in interneuron excitability, supporting our previous demonstrations of neuronal hyperexcitability during KCC2 blockade in the in vitro 4AP model (Chen et al., 2019). Furthermore, it has been demonstrated in cultured hippocampal neurons that downregulating KCC2 expression increases neuronal excitability by inducing a depolarizing shift in the GABA_A reversal potential (Sivakumaran et al., 2015; Kelley et al., 2018; Moore et al., 2018). Supporting the studies on cultured hippocampal neurons, both in vitro cell cultures expressing mutated SLC12A5 genes and the hippocampal formation of brain slices taken from pilocarpine-treated animal showed reduced KCC2 cell surface expression with depolarized GABA_A reversal potential (Pathak et al., 2007; Puskarjov et al., 2014). Together, these studies indicate that KCC2 downregulation can promote neuronal hyperexcitability by depolarizing the GABA_A reversal potential.

Despite the known neuronal hyperexcitability induced by KCC2 antagonism, we found significant decreases in the proportion of principal cell action potentials in the rising phase – in contrast with conditions of intact ionotropic glutamatergic receptor signalling (Chen et al., 2019) – and in the proportion of interneuron action potentials in the falling phase. Since interictal spikes were recorded in the absence of ionotropic glutamatergic signalling, the proportion of principal

cell action potentials throughout interictal spikes and the proportion of interneuron action potentials in the falling phase likely reflects a disruption in single-unit recruitment during interictal spikes. Our results are therefore in line with the view that increases in extracellular [K⁺] promotes neuronal recruitment (Viitanen et al., 2010; Avoli and de Curtis, 2011). These findings in single-unit activity also support the observations in the field potential activity – namely, the significant decreases in the duration and the amplitude of interictal spikes could be attributed to extracellular [K⁺]. Taken together, our data emphasize the important role played by extracellular [K⁺] in the dynamics of interictal spikes.

4.5.3. Conclusions

Our findings highlight the interaction between KCC2 antagonism and GABA_A signalling during interictal spikes generated by EC neuronal networks *in vitro* during blockade of ionotropic glutamatergic transmission. Specifically, our data show that KCC2 antagonism is not only capable of inducing neuronal hyperexcitability but that it can also disrupt neuronal recruitment during interictal spikes. The dual influence of KCC2 antagonism on neuronal activity altogether could lead to smaller and shorter spikes, suggesting that pathological neuronal activity depends on neuronal excitability as well as synchrony.

4.6. References

- Avoli M, Barbarosie M, Lücke A, Nagao T, Lopantsev V, Köhling R (1996) Synchronous GABA-Mediated Potentials and Epileptiform Discharges in the Rat Limbic System In Vitro. J Neurosci 16:3912–3924.
- Avoli M, de Curtis M (2011) GABAergic synchronization in the limbic system and its role in the generation of epileptiform activity. Prog Neurobiol 95:104–132.
- Avoli M, Panuccio G, Herrington R, D'Antuono M, de Guzman P, Lévesque M (2013) Two different interictal spike patterns anticipate ictal activity in vitro. Neurobiol Dis 52:168–176.
- Chen L-Y, Lévesque M, Avoli M (2019) KCC2 antagonism increases neuronal network excitability but disrupts ictogenesis in vitro. J Neurophysiol.
- Chen L-Y, Lévesque M, Cataldi M, Avoli M (2018) Single-unit Activity in the in vitro Entorhinal Cortex During Carbachol-induced Field Oscillations. Neuroscience 379:1–12.
- Chizhov AV, Sanchez-Aguilera A, Rodrigues S, de la Prida LM (2015) Simplest relationship between local field potential and intracellular signals in layered neural tissue. Phys Rev E 92:062704.
- Coutin-Churchman PE, Wu JY, Chen LLK, Shattuck K, Dewar S, Nuwer MR (2012) Quantification and localization of EEG interictal spike activity in patients with surgically removed epileptogenic foci. Clin Neurophysiol 123:471–485.
- Csicsvari J, Hirase H, Czurko A, Buzsáki G (1998) Reliability and State Dependence of Pyramidal Cell–Interneuron Synapses in the Hippocampus. Neuron 21:179–189.
- de Curtis M, Avoli M (2016) GABAergic networks jump-start focal seizures. Epilepsia 57:679–687.
- Delpire E, Baranczak A, Waterson AG, Kim K, Kett N, Morrison RD, Scott Daniels J, David Weaver C, Lindsley CW (2012) Further optimization of the K-Cl cotransporter KCC2 antagonist ML077: Development of a highly selective and more potent in vitro probe. Bioorg Med Chem Lett 22:4532–4535.
- Delpire E, Days E, Lewis LM, Mi D, Kim K, Lindsley CW, Weaver CD (2009) Small-molecule screen identifies inhibitors of the neuronal K-Cl cotransporter KCC2. Proc Natl Acad Sci 106:5383–5388.
- Delpire E, Weaver CD (2016) Challenges of finding novel drugs targeting the K-Cl cotransporter. ACS Chem Neurosci 7:1624–1627.
- Di Cristo G, Awad PN, Hamidi S, Avoli M (2018) KCC2, epileptiform synchronization, and epileptic disorders. Prog Neurobiol 162:1–16.

- Dworetzky BA, Reinsberger C (2011) The role of the interictal EEG in selecting candidates for resective epilepsy surgery. Epilepsy Behav 20:167–171.
- Farrant M, Kaila K (2007) The cellular, molecular and ionic basis of GABAA receptor signalling. In: Progress in Brain Research (Tepper JM, Abercrombie ED, Bolam JP, eds), pp 59–87 Gaba and the Basal Ganglia. Elsevier. Available at: http://www.sciencedirect.com/science/article/pii/S0079612306600058 [Accessed July 12, 2018].
- Fisher RS, Cross JH, French JA, Higurashi N, Hirsch E, Jansen FE, Lagae L, Moshé SL, Peltola J, Roulet Perez E, Scheffer IE, Zuberi SM (2017) Operational classification of seizure types by the International League Against Epilepsy: Position Paper of the ILAE Commission for Classification and Terminology. Epilepsia 58:522–530.
- Freund T f., Buzsáki G (1996) Interneurons of the hippocampus. Hippocampus 6:347–470.
- Fujiwara-Tsukamoto Y, Isomura Y, Imanishi M, Ninomiya T, Tsukada M, Yanagawa Y, Fukai T, Takada M (2010) Prototypic Seizure Activity Driven by Mature Hippocampal Fast-Spiking Interneurons. J Neurosci 30:13679–13689.
- Gigout S, Louvel J, Kawasaki H, D'Antuono M, Armand V, Kurcewicz I, Olivier A, Laschet J, Turak B, Devaux B, Pumain R, Avoli M (2006) Effects of gap junction blockers on human neocortical synchronization. Neurobiol Dis 22:496–508.
- González OC, Shiri Z, Krishnan GP, Myers TL, Williams S, Avoli M, Bazhenov M (2018) Role of KCC2-dependent potassium efflux in 4-Aminopyridine-induced Epileptiform synchronization. Neurobiol Dis 109:137–147.
- Hablitz JJ, Lundervold A (1981) Hippocampal excitability and changes in extracellular potassium. Exp Neurol 71:410–420.
- Hamidi S, Avoli M (2015) KCC2 function modulates in vitro ictogenesis. Neurobiol Dis 79:51–58.
- Jacobs J, Kobayashi K, Gotman J (2011) High-frequency changes during interictal spikes detected by time-frequency analysis. Clin Neurophysiol Off J Int Fed Clin Neurophysiol 122:32–42.
- Kaila K, Price TJ, Payne JA, Puskarjov M, Voipio J (2014) Cation-chloride cotransporters in neuronal development, plasticity and disease. Nat Rev Neurosci 15:637–654.
- Kelley MR, Cardarelli RA, Smalley JL, Ollerhead TA, Andrew PM, Brandon NJ, Deeb TZ, Moss SJ (2018) Locally Reducing KCC2 Activity in the Hippocampus is Sufficient to Induce Temporal Lobe Epilepsy. EBioMedicine 32:62–71.
- Kelley MR, Deeb TZ, Brandon NJ, Dunlop J, Davies PA, Moss SJ (2016) Compromising KCC2 transporter activity enhances the development of continuous seizure activity. Neuropharmacology 108:103–110.

- Lamsa K, Kaila K (1997) Ionic Mechanisms of Spontaneous GABAergic Events in Rat Hippocampal Slices Exposed to 4-Aminopyridine. J Neurophysiol 78:2582–2591.
- Lebon F, Pégurier C, Ledecq M, Mathieu B, Bosman N, Frycia A, Lengelé S, Dhurke K, Kanduluru AK, Meunier S, Wagner A, Wolff C, Provins L (2012) Towards a KCC2 blocker pharmacophore model. Bioorg Med Chem Lett 22:3978–3982.
- Lévesque M, Chen L-Y, Hamidi S, Avoli M (2018) Dynamic interneuron-principal cell interplay leads to a specific pattern of in vitro ictogenesis. Neurobiol Dis 115:92–100.
- Lévesque M, Herrington R, Hamidi S, Avoli M (2016) Interneurons spark seizure-like activity in the entorhinal cortex. Neurobiol Dis 87:91–101.
- Librizzi L, Losi G, Marcon I, Sessolo M, Scalmani P, Carmignoto G, Curtis M de (2017) Interneuronal Network Activity at the Onset of Seizure-Like Events in Entorhinal Cortex Slices. J Neurosci 37:10398–10407.
- Lopantsev V, Avoli M (1998) Participation of GABAA-Mediated Inhibition in Ictallike Discharges in the Rat Entorhinal Cortex. J Neurophysiol 79:352–360.
- Mehvari Habibabadi J, Zare M, Tabrizi N (2019) The Role of Interictal Epileptiform Discharges in Epilepsy Surgery Outcome. Int J Prev Med 10:101.
- Michelson HB, Wong RK (1991) Excitatory synaptic responses mediated by GABAA receptors in the hippocampus. Science 253:1420–1423.
- Moore YE, Deeb TZ, Chadchankar H, Brandon NJ, Moss SJ (2018) Potentiating KCC2 activity is sufficient to limit the onset and severity of seizures. Proc Natl Acad Sci:201810134.
- Ogata N, Hori N, Katsuda N (1976) The correlation between extracellular potassium concentration and hippocampal epileptic activity in vitro. Brain Res 110:371–375.
- Panuccio G, D'Antuono M, de Guzman P, De Lannoy L, Biagini G, Avoli M (2010) In vitro ictogenesis and parahippocampal networks in a rodent model of temporal lobe epilepsy. Neurobiol Dis 39:372–380.
- Pathak HR, Weissinger F, Terunuma M, Carlson GC, Hsu F-C, Moss SJ, Coulter DA (2007) Disrupted Dentate Granule Cell Chloride Regulation Enhances Synaptic Excitability during Development of Temporal Lobe Epilepsy. J Neurosci 27:14012–14022.
- Perreault P, Avoli M (1991) Physiology and pharmacology of epileptiform activity induced by 4-aminopyridine in rat hippocampal slices. J Neurophysiol 65:771–785.
- Perreault P, Avoli M (1992) 4-aminopyridine-induced epileptiform activity and a GABA-mediated long- lasting depolarization in the rat hippocampus. J Neurosci 12:104–115.
- Puskarjov M, Seja P, Heron SE, Williams TC, Ahmad F, Iona X, Oliver KL, Grinton BE, Vutskits L, Scheffer IE, Petrou S, Blaesse P, Dibbens LM, Berkovic SF, Kaila K (2014) A variant

- of KCC2 from patients with febrile seizures impairs neuronal Cl– extrusion and dendritic spine formation. EMBO Rep 15:723–729.
- Quiroga RQ, Nadasdy Z, Ben-Shaul Y (2004) Unsupervised spike detection and sorting with wavelets and superparamagnetic clustering. Neural Comput 16:1661–1687.
- Rosati A, Aghakhani Y, Bernasconi A, Olivier A, Andermann F, Gotman J, Dubeau F (2003) Intractable temporal lobe epilepsy with rare spikes is less severe than with frequent spikes. Neurology 60:1290.
- Sakata S, Harris KD (2009) Laminar Structure of Spontaneous and Sensory-Evoked Population Activity in Auditory Cortex. Neuron 64:404–418.
- Sirota A, Montgomery S, Fujisawa S, Isomura Y, Zugaro M, Buzsáki G (2008) Entrainment of neocortical neurons and gamma oscillations by the hippocampal theta rhythm. Neuron 60:683–697.
- Sivakumaran S, Cardarelli RA, Maguire J, Kelley MR, Silayeva L, Morrow DH, Mukherjee J, Moore YE, Mather RJ, Duggan ME, Brandon NJ, Dunlop J, Zicha S, Moss SJ, Deeb TZ (2015) Selective Inhibition of KCC2 Leads to Hyperexcitability and Epileptiform Discharges in Hippocampal Slices and In Vivo. J Neurosci 35:8291–8296.
- Smirnov S, Paalasmaa P, Uusisaari M, Voipio J, Kaila K (1999) Pharmacological Isolation of the Synaptic and Nonsynaptic Components of the GABA-Mediated Biphasic Response in Rat CA1 Hippocampal Pyramidal Cells. J Neurosci 19:9252.
- Spoljaric I, Spoljaric A, Mavrovic M, Seja P, Puskarjov M, Kaila K (2019) KCC2-Mediated Cl–Extrusion Modulates Spontaneous Hippocampal Network Events in Perinatal Rats and Mice. Cell Rep 26:1073-1081.e3.
- Sudbury JR, Avoli M (2007) Epileptiform synchronization in the rat insular and perirhinal cortices in vitro. Eur J Neurosci 26:3571–3582.
- Tatum WO, Rubboli G, Kaplan PW, Mirsatari SM, Radhakrishnan K, Gloss D, Caboclo LO, Drislane FW, Koutroumanidis M, Schomer DL, Kasteleijn-Nolst Trenite D, Cook M, Beniczky S (2018) Clinical utility of EEG in diagnosing and monitoring epilepsy in adults. Clin Neurophysiol Off J Int Fed Clin Neurophysiol 129:1056–1082.
- Viitanen T, Ruusuvuori E, Kaila K, Voipio J (2010) The K+–Cl– cotransporter KCC2 promotes GABAergic excitation in the mature rat hippocampus. J Physiol 588:1527–1540.
- Yang Q, Michelson HB (2001) Gap junctions synchronize the firing of inhibitory interneurons in guinea pig hippocampus. Brain Res 907:139–143.

4.7. Figures

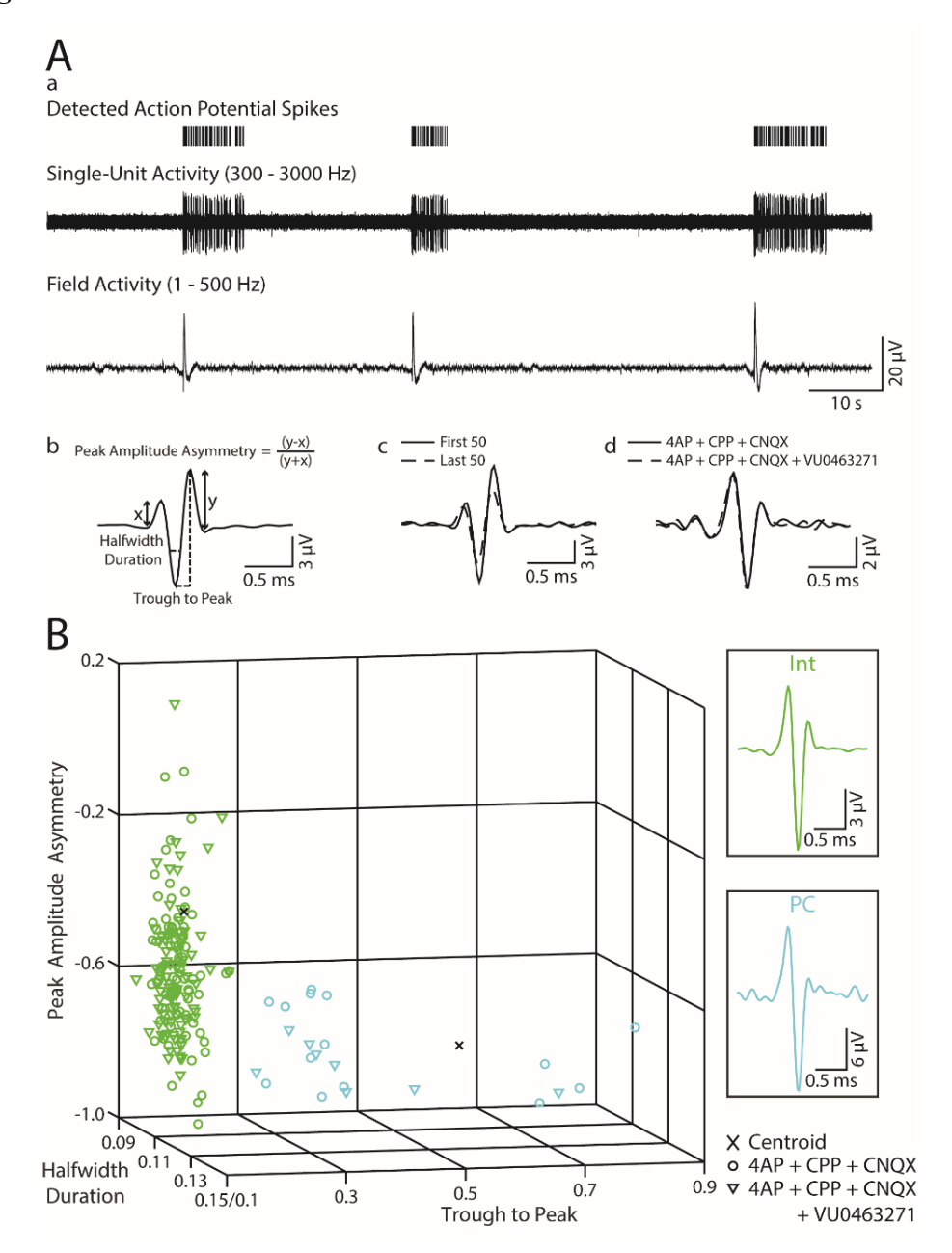


Figure 4.1. Single-unit classification. **A:** Tetrode wire recording of single-unit and field potential activity in the rat EC. **B:** (a) Averaged waveform shapes of the first (solid) and last (dashed) 50 action potentials of a single unit recorded for 10 min. (b) Averaged waveform shape of the action potentials under 4AP + CPP + CNQX (solid line, n = 96) and after the addition of VU0463271 (dashed line, n = 1645). **C:** The waveform shape of action potentials was quantified using three variables: trough to peak, peak amplitude asymmetry, and halfwidth duration. **D:** Clusters of presumptive interneurons (Int, green) and principal cells (PC, blue) under 4AP + CPP + CNQX (circles) and 4AP + CPP + CNQX + VU0463271 (triangles). The centroids of the clusters are marked with x.

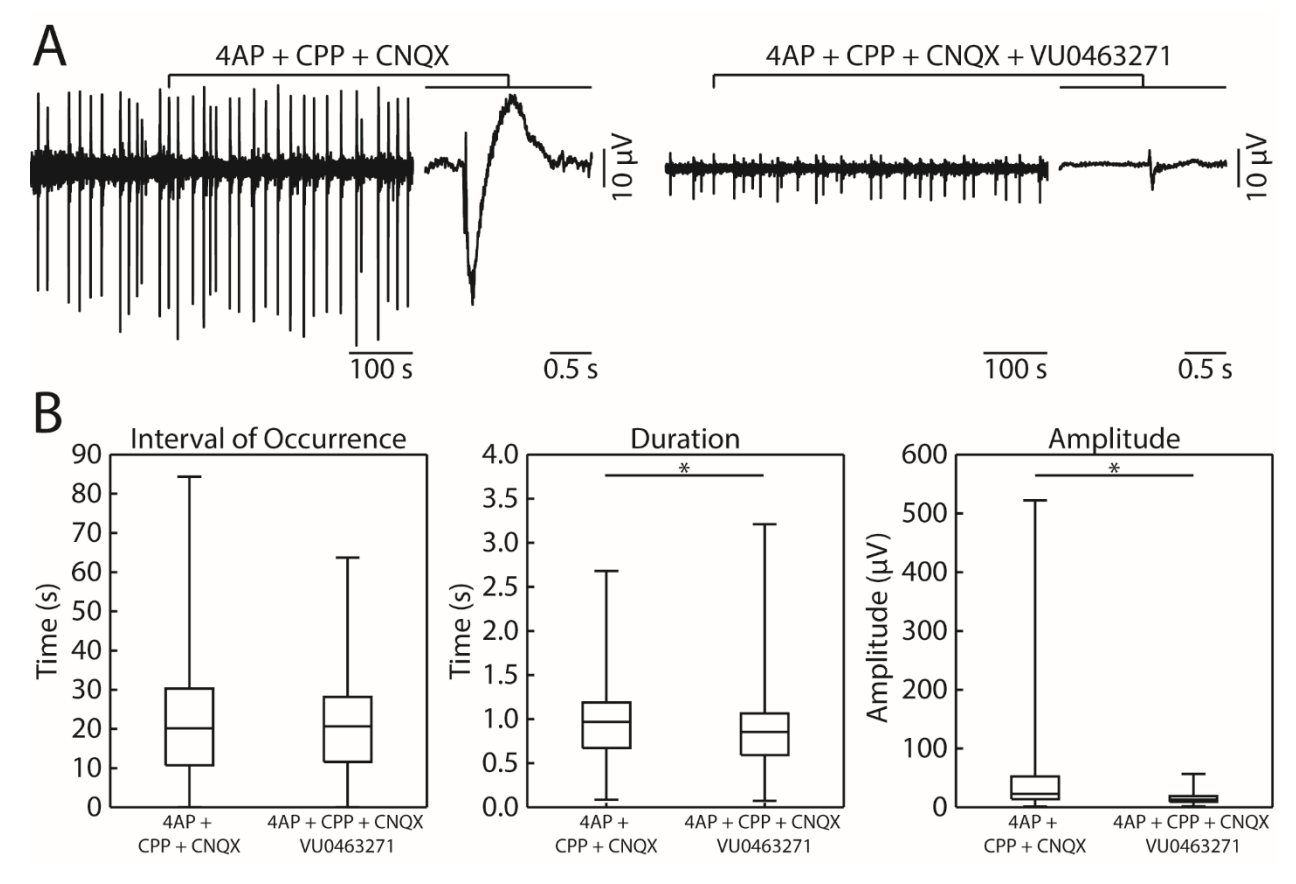


Figure 4.2. Field potential activity recorded from the EC in the presence and absence of VU0463271. **A:** Interictal spikes persisted in the field potential recordings upon the addition of VU0463271 to 4AP + CPP + CNQX condition. **B:** Quantification of the interval of occurrence, duration, and amplitude of interictal spikes recorded under 4AP + CPP + CNQX and 4AP + CPP + CNQX + VU0463271 conditions. Wilcoxon Rank-Sum Test was used to established statistical significance, *p < 0.05.

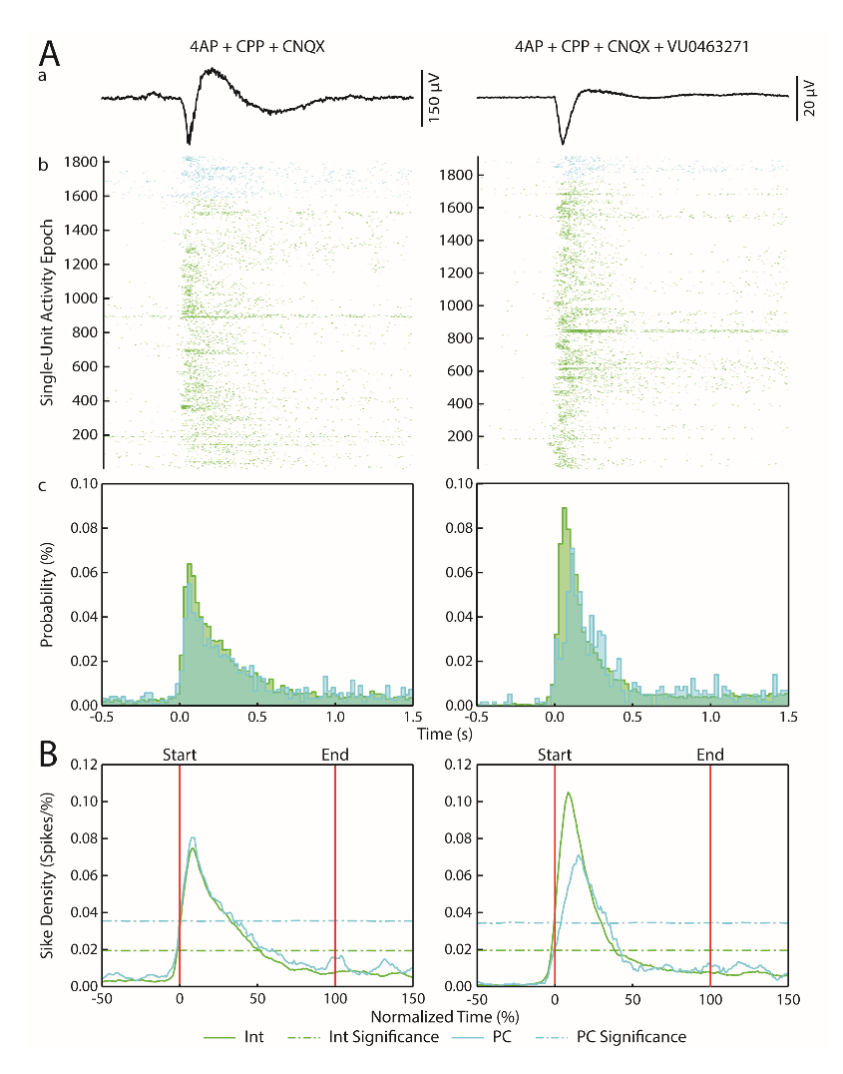


Figure 4.3. Single-unit activity around the onset of interictal spikes. **A**: Single-unit activity around the onset of interictal spikes in the 4AP + CPP + CNQX and 4AP + CPP + CNQX + VU0463271 conditions. Interictal spikes (**a**) along with corresponding raster plots (**b**) and real-time peri-event histograms (25-ms bins) (**c**) are illustrated. In the real-time peri-event histogram, peaks of interneuron and principal cell action potential densities in the 4AP + CPP + CNQX condition were both identified at 0.06 s after the onset of interictal spikes. In the 4AP + CPP + CNQX + VU0463271 condition, peaks of interneuron and principal cell action potential densities were identified at 0.06 s and 0.11 s, respectively, after the onset of interictal spikes. **B**: Normalized peri-event histograms with *time* 0 representing the onset of interictal spikes. Note that in the 4AP + CPP + CNQX condition, the peak of interneuron action potential density during interictal spikes (n = 1588) occurred at 8.50% of the normalized duration, while the peak of principal cell action potential density during interictal spikes (n = 1764) occurred at 8.50%, whereas the peak of principal cell action potential density during interictal spikes (n = 1764) occurred at 8.50%. Dashed lines indicate significance thresholds.

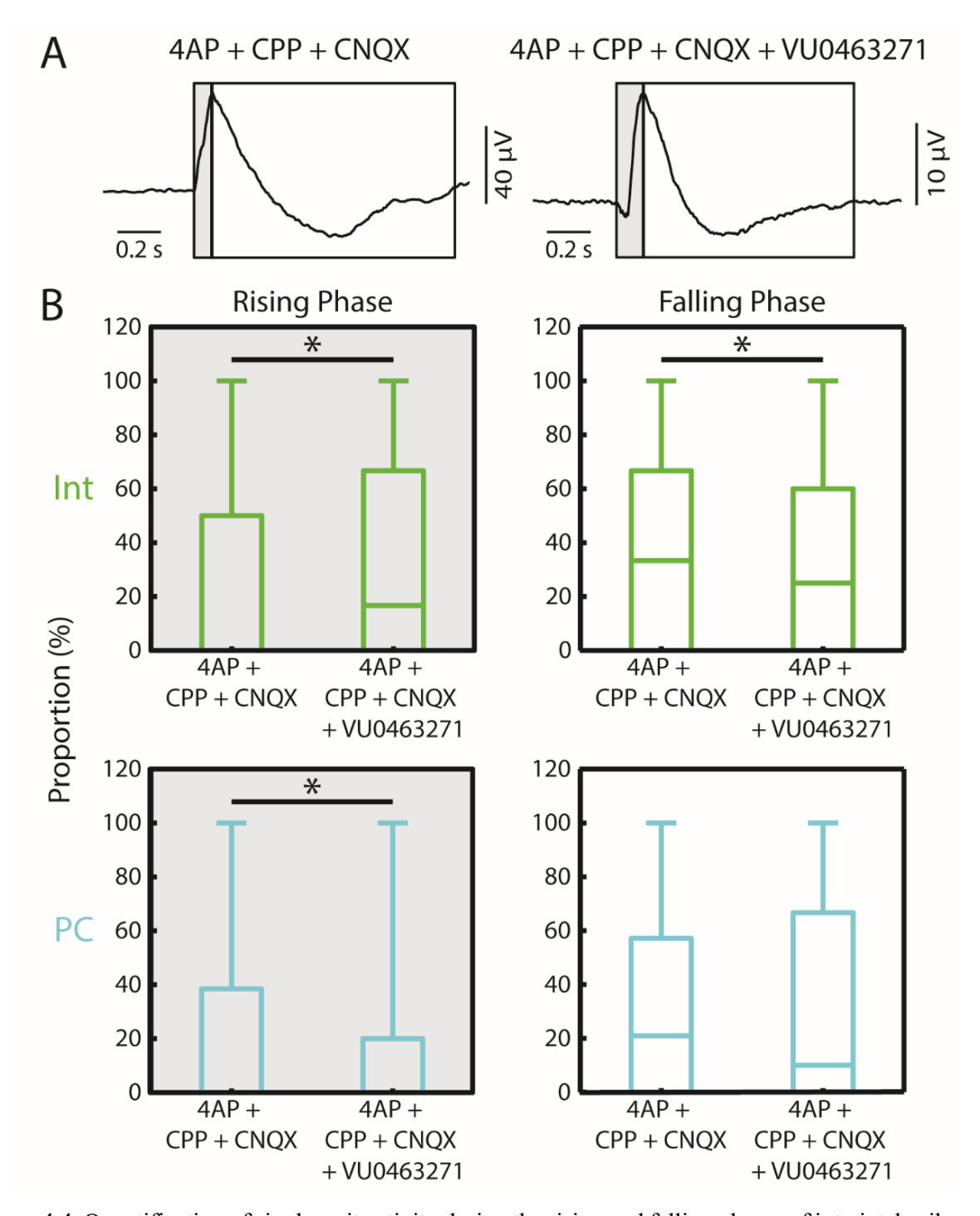


Figure 4.4. Quantification of single-unit activity during the rising and falling phases of interictal spikes. **A**: Examples of interictal spikes recorded in the 4AP + CPP + CNQX and 4AP + CPP + CNQX + VU0463271 conditions. The grey box outlines the rising phase of the interictal spike, while the white box outlines the falling phase of the interictal spike. **B**: Quantification of the proportion of interneuron and principal cell action potentials in the rising and falling phases across pharmacological conditions. Wilcoxon Rank-Sum Test was used to established statistical significance, *p < 0.05.

Chapter 5: Single-Unit Activity in the *In Vitro* Entorhinal Cortex During Carbachol-Induced Field Oscillations

An understanding of ictogenesis has profound clinical implications. Recently, changes in theta rhythm prior to seizure onset were identified. However, the interplay between inhibitory and excitatory mechanisms – especially with respect to the neuronal activity – during this described pre-ictal theta rhythm remained elusive. Therefore, I studied the neuronal activity underlying the *in vitro* model of carbachol (CCh)-induced theta oscillations in the rat entorhinal cortex (EC) using tetrodes. This work was published in 2018 in the *Neuroscience* as a manuscript titled "Single-Unit Activity in the *In Vitro* Entorhinal Cortex During Carbachol-induced Field Oscillations."

Chen L-Y, Lévesque M, Cataldi M, Avoli M (2018) Single-unit Activity in the in vitro Entorhinal Cortex During Carbachol-induced Field Oscillations. Neuroscience 379:1–12.

5.1. Abstract

The muscarinic receptor agonist carbachol (CCh) can induce activity in the theta range (4–15 Hz) in the entorhinal cortex (EC), but the underlying network mechanisms remain unclear. Here, we investigated the interplay between interneurons and principal cells in the EC during CCh-induced theta-like field oscillations in an in vitro brain slice preparation using tetrodes. Field oscillations at 10.1 Hz (IQR = 9.5–10.9 Hz) occurred during bath application of CCh (100 μ M; n = 32experiments) and were associated with single-unit (n = 189) firing. Interneuron activity increased before principal cell activity at the onset of the oscillations, and both interneurons and principal cells fired at specific oscillation phases with interneurons preceding principal cells, suggesting that interneurons modulate principal cell activity during such oscillations. The regularity of occurrence of CCh-induced oscillations was abolished by applying the GABA_A receptor antagonist picrotoxin (100 μ M; n = 13). These effects were accompanied by changes in firing with principal cells discharging action potentials before interneurons, along with a loss of preferred firing phase for principal cells in relation to the oscillation peaks. Blocking ionotropic glutamatergic transmission abolished CCh-induced field oscillations (n = 6), suggesting that ionotropic glutamatergic receptor signalling is necessary for their generation. Our results show that neuronal network interactions leading to CCh-induced theta-like field oscillations rest on the close interplay between interneurons and principal cells and that interneurons modulate principal cell activity during such oscillatory activity. Moreover, they underscore the role of ionotropic glutamatergic transmission in this type of oscillations.

5.2. Introduction

Oscillations of neuronal networks are fundamental in brain functions (Buzsáki, 2015). During development, they are observed as giant depolarizing events that synchronize neuronal activity to assemble and to shape synapse and network formation (Griguoli and Cherubini, 2017). In the adult brain, oscillations have been most often studied in limbic networks, particularly in the hippocampus and in the entorhinal cortex (EC). These brain regions generate theta oscillations (4–12 Hz) during sensorimotor integration, spatial navigation, memory, and learning (Düzel et al., 2010; Buzsáki and Moser, 2013; Hasselmo and Stern, 2014; Colgin, 2016) and could shape synaptic plasticity that underlies these tasks (Pavlides et al., 1988). These oscillations appear to be shaped by interneuron activity that synchronizes principal cells during these oscillatory patterns (Cobb et al., 1995).

The limbic system includes brain structures that have unique circuitries (Bland, 1986; Bland and Oddie, 2001). Among them, the EC plays a fundamental role in regulating the transfer of information between the hippocampal formation and other brain structures (Montoya and Sainsbury, 1985; van Strien et al., 2009; Deshmukh et al., 2010). The EC is known to receive cholinergic inputs from the medial septum, the diagonal band of Broca, and the basal forebrain (Beckstead, 1978; Alonso and Köhler, 1984; Insausti et al., 1987; Gaykema et al., 1990; Heys et al., 2012). These cholinergic inputs can influence memory, spatial navigation, and synaptic plasticity (Yun et al., 2000; McGaughy et al., 2005; Tanninen et al., 2015), as well as EC oscillatory activities (Pilly and Grossberg, 2013; Vandecasteele et al., 2014). Therefore, understanding how cholinergic signalling modifies the interplay between excitation and inhibition in the EC should help us to understand how rhythmic activities occur in this limbic area.

The cholinergic receptor agonist carbachol (CCh) induces oscillations in the theta frequency range when applied *in vitro* to different structures of the limbic system. Konopacki *et al.* (1992) were the first to report *in vitro* theta-like oscillation in the EC during bath application of CCh. These CCh-induced oscillations have been shown to depend on the activation of cholinergic M1 receptors (Cataldi et al., 2011; Kowalczyk et al., 2013). In addition, the generators of these CCh-induced oscillations are not only found in different limbic structures but also self-sustaining and independent of external inputs (D'Antuono et al., 2001; Lévesque et al., 2017).

While some investigators have later found that CCh can also induce oscillations in the gamma frequency range in the EC (Dickson et al., 2000, 2003; Dickson and de Curtis, 2002), CCh-

induced oscillations continue to be used as an *in vitro* model of the theta rhythm that occurs *in vivo* (Kowalczyk et al., 2013). However, it cannot be overlooked that *in vivo* theta oscillations occurring in awake, freely moving animals are atropine-resistant and perhaps less dependent on cholinergic inputs and on interneuron activity (Petsche et al., 1962; Kramis et al., 1975; Williams and Kauer, 1997; Buzsáki, 2002). In the present study, we employed tetrode recordings in the EC to (i) characterize the participation of putative interneurons and principal cells CCh-induced field oscillations, (ii) identify the changes induced by γ -aminobutyric acid type A (GABA_A) receptor antagonism on this oscillatory pattern, and (iii) establish the role played by ionotropic glutamatergic transmission.

5.3. Materials and methods

5.3.1. Brain slice preparation, maintenance, and treatment

All procedures were conducted in compliance with the guidelines of the Canadian Council on Animal Care and the McGill Animal Care Committee. Brains were extracted from male Sprague-Dawley rats (250–275 g; n = 17, Charles River Laboratories, Saint Constant, Quebec, Canada) under isoflurane-induced anesthesia then chilled for 3 min in ice-cold artificial cerebrospinal fluid (ACSF) continuously bubbled with O_2/CO_2 (95%/5%) gas. The ACSF had the following composition (mM): 124 NaCl, 2 KCl, 2 CaCl₂, 2 MgSO₄, 1.25 KH₂PO₄, 26 NaHCO₃, and 10 D-glucose. Horizontal brain slices (thickness = 450 μ m, n = 32) were obtained with a vibratome (VT1000S; Leica, Concord, Ontario, Canada) and were placed in an interface chamber between warm ACSF (31–33 °C; pH 7.4; 305 mOSM/kg) and humidified gas O_2/CO_2 (95%/5%). Brain slices were allowed to recover for 1 h before starting the continuous bath application of CCh (100 μ M) at a flow rate of 2 ml/min.

To investigate the contributions of ionotropic GABAergic and glutamatergic signalling, additional pharmacological agents were applied after stable CCh-induced oscillations were observed. In 13 slices, picrotoxin (PTX; 100 μ M; Sigma-Aldrich, Canada) was applied to block ionotropic GABA_A receptors (CCh + PTX condition). In 6 slices, 3-(2-carboxypiperazin-4-yl)-propyl-1-phosphonate (CPP; 10 μ M; Sigma-Aldrich, Canada) and 2,3-dihydroxy-6-nitro-7-sulfamoyl-benzo[f]quinoxaline-2,3-dione (NBQX; 10 μ M; Sigma-Aldrich, Canada) were applied to block ionotropic glutamatergic signalling (CCh + CPP + NBQX condition).

5.3.2. Tetrode recordings

Neuronal activity was acquired with tetrode wires according to Lévesque *et al.* (2016). Briefly, seven tetrodes, each made from twisting four tungsten wires together, were inserted into individual microdrives (NLX-18; Neuralynx, Bozeman, MT, USA). A ground wire was connected to the recording table. A channel of a tetrode was used as a reference for online data visualization. Tetrodes were slowly lowered into the EC to record 10 min of neuronal activity at a sampling rate of 20 kHz with a recording bandwidth between 0.8 to 22,000 Hz using the Neuroware (2.1) software from Triangle Biosystems (Durham, NC, USA). Off-line data analysis was performed with MATLAB (Mathworks, Natick, MA, USA).

5.3.3. Raw data processing for single-unit activity

Single-unit analyses were adapted from Lévesque *et al.* (2016). Briefly, raw data filtered between 300 and 3,000 Hz were analyzed with WaveClus (Quiroga et al., 2004), which considered action potentials that were five standard deviations (SDs) above the threshold as putative discharges from single units and clustered action potentials according to selected sets of wavelet coefficients. Then the experimenter verified that (i) the putative single-unit clusters were distinct from the noise clusters, (ii) the action potentials had to be visible on at least two out of four channels on a tetrode, (iii) the action potentials on different channels had to differ in amplitude, and (iv) less than 2% of the total number of action potentials of a single-unit cluster could occur during the refractory period (<3 ms) (Csicsvari et al., 1998; Lévesque et al., 2016).

The classification of putative single units as interneurons or principal cells were based on previously published studies (Freund and Buzsáki, 1996; Csicsvari et al., 1998; Sirota et al., 2008; Sakata and Harris, 2009; Lévesque et al., 2016). Briefly, three variables were calculated from the average waveform of action potentials taken from the channel that recorded the largest action potential amplitude: (i) the amplitude from the trough to the peak, (ii) the peak amplitude asymmetry, and (iii) the action potential width at 50% of amplitude (**Figure 5.1Ba** and **5.1Ca**). Average waveforms of the first and last 50 action potentials recorded were plotted together to demonstrate the stability of our recording (**Figure 5.1Bb** and **5.1Cb**); similarly, pharmacological manipulations with GABA_A and ionotropic glutamatergic receptor antagonists did not alter action potential waveform shape (**Figure 5.1D**). Therefore, a *k*-means clustering analysis was applied to all single units to identify putative interneurons and principal cells (**Figure 5.1E**).

5.3.4. Raw data processing for field potential activity

Custom MATLAB scripts were used to identify CCh-induced oscillations in the field potential recordings. Raw data were filtered between 1 and 500 Hz and down sampled to 2,000 Hz. The four channels of the tetrode were averaged together and normalized against an average of all field potentials recorded from all tetrodes used in the recording session, creating the final processed field potential.

To identify the onset and end times of each CCh-induced oscillation, the processed field potential was high-pass filtered above 3 Hz and band-stop filtered between 55 and 65 Hz. The resulting signal was enhanced by raising it to the 5th power. The noise fluctuations of the processed field potentials were estimated by calculating the moving standard deviations (MVSDs) with 1-s windows. The signal fluctuations were estimated by calculating the MVSDs with 0.0625-s window. The CCh-induced oscillation candidates were identified as signal epochs with (i) signal fluctuations greater than the 75th percentile of the noise fluctuation and (ii) duration greater than 0.0625 s; CCh-induced oscillation candidates that were less than 0.25 s apart were merged together. The end times of CCh-induced oscillation candidates were adjusted by searching after the original end times where signal fluctuations became less than 25th percentile of the noise fluctuations. Finally, the algorithm searched before the onset and after the end of CCh-induced oscillation candidates to identify the closest time points when the signal was 0 μ V, which were respectively labeled as the onset and end of CCh-induced oscillations.

To quantify the frequencies of CCh-induced oscillations, discrete short-time Fourier transform with a 1-s hamming window and 80% overlap was applied to the processed field potential to calculate the power spectral densities (PSDs). The mean of frequencies between 4 and 15 Hz, which is the reported CCh-induced oscillation frequency (Buzsáki, 2002), with PSD above the 95th percentile during CCh-induced oscillations was used to estimate the oscillation frequency.

5.3.5. Classification of single-unit activity types

To classify single-unit activity, we calculated the percentage of oscillations and intervals between oscillations that contained single-unit discharges in order to evaluate the consistency of single-unit firing during recurring CCh-induced oscillations. Furthermore, the difference in the proportions of spikes that occurred during CCh-induced oscillations and intervals between field oscillations was

also calculated to assess single-unit firing preference. Single units were classified in three groups: type A comprised of single units with steady firing during CCh-induced oscillations (**Figure 5.2A**), type B comprised of single units that also fired in between field oscillations (**Figure 5.2B**), and type C comprised of single units with sporadic firing during CCh-induced oscillations (**Figure 5.2C**).

5.3.6. Single-unit activities around CCh-induced oscillations

To examine the relationship between single-unit activity and CCh-induced oscillations, single-unit discharges were extracted around CCh-induced oscillations. Each single-unit activity epoch contained segments before, during, and after the CCh-induced oscillation with the same duration as the oscillation. The durations of the single-unit activity epochs were normalized with 0% and 100% as, respectively, the onset and end of CCh-induced oscillations. The spike density of each single unit was calculated by averaging the number of action potentials that occurred in each 1% bin. Average spike densities of single units of the same neuronal type in the same pharmacological conditions were averaged to produce peri-event histograms.

To assess for significant relationship between single-unit activities and CCh-induced oscillations, the Monte Carlo methods were applied. For each subset of data of the same neuronal type and pharmacological condition, 10,000 single units were randomly sampled with replacement. Their action potential timestamps were randomly shuffled to simulate random single-unit discharge patterns. Average spike densities for simulated random single-unit activities were calculated using the same procedure mentioned above. Average spike densities of the acquired data that were 2.5 SDs above the average spike densities of simulated random activities were considered to be statistically significant changes in single-unit discharge activity.

5.3.7. Single-unit phase firing during CCh-induced oscillations

The Hilbert transform of processed field potential filtered between 6 and 14 Hz was used to define the phase of the CCh-induced oscillations with 0° and 360° representing the peaks of oscillations. The probability that single-unit discharges would fire at distinct phases was plotted in polar plots to examine the phase firing of single units during CCh-induced oscillations. The autocorrelations of single-unit discharge patterns were computed using MATLAB function *xcorr*.

5.3.8. Statistics

The Shapiro-Wilks Test was applied to assess the normality of the data distributions. Normally distributed data were compared using the Two-Sample T-Tests; otherwise, data were compared using the Mann-Whitney U-Test. Throughout the text, results are expressed as median (interquartile range). Circular statistics were performed with CircStat Matlab toolbox (Berens, 2009). The Kuiper's Test was performed to compare single-unit discharge firing phase data to von Mises distributions. The Rayleigh Test for uniformity was performed on circularly normal data; otherwise, the Omnibus Test was performed. If non-uniformity was found in the data, the median of the phase data was calculated and plotted in black arrows and expressed as median throughout the text. Statistical significance was established at p < 0.05.

5.4. Results

5.4.1. Single-unit classification

Using tetrodes, we acquired raw data that were filtered between 300 and 3,000 Hz to detect action potentials of putative neurons and between 1 and 500 Hz to visualize field potential activity (Figure 5.1A). As previously reported (Freund and Buzsáki, 1996; Csicsvari et al., 1998; Sirota et al., 2008; Sakata and Harris, 2009; Lévesque et al., 2016), action potential waveforms generated by putative interneurons (Figure 5.1Ba; green, Int) were narrower and more symmetric than those recorded from the putative principal cells (Figure 5.1Ca; blue, PC). Irrespective of the neuronal type, we could follow both types of single units throughout the recording as revealed by the similarity between the averaged action potential waveform shapes of the first and last 50 action potentials (Figure 5.1Bb and 5.1Cb). In addition, we could follow the same single units during different pharmacological manipulations: from the baseline, CCh only condition, to a treatment condition with the application of either the GABA_A receptor antagonist PTX or the ionotropic glutamatergic blockers CPP and NBQX (Figure 5.1Da and 5.1Db).

When we applied k-means clustering to the three waveform variables extracted from all single units, we could distinguish interneurons from principal cells (**Figure 5.1E**). Overall, from 32 slices obtained from 17 rats, 189 single units were identified. In CCh only condition, 106 single units were classified as interneurons, and 17 single units were classified as principal cells. In the CCh + PTX condition (n = 13 slices), we identified 27 interneurons and 4 principal cells. Finally,

in the CCh + CPP + NBQX condition (n = 6 slices), we identified 30 interneurons and 5 principal cells.

5.4.2. Single-unit activity during CCh-induced oscillations

By filtering the field recordings between 1 and 500 Hz, we identified field oscillations during application of CCh. As previously reported (Dickson and Alonso, 1997; Williams and Kauer, 1997; Cataldi et al., 2011; Kowalczyk et al., 2013; Lévesque et al., 2017), CCh induced regular oscillations (median duration = 0.6 s, IQR = 0.3–1.1 s) in the EC (**Figure 5.2**). Visual inspection of the data revealed a diversity in single-unit discharge patterns. To quantitatively describe the diversity in activity pattern, we calculated: (1) the percentage of oscillations that contained single-unit discharges, (2) the percentage of intervals between oscillations that contained single-unit discharges, and (3) the difference in the ratios of spike discharges that occurred during CCh-induced oscillations and during intervals between the oscillations. Single units with steady and preferential firing during most of CCh-induced oscillations were categorized as type A (**Figure 5.2A**). Type B single units were cells that fired both between and during the CCh-induced oscillations (**Figure 5.2B**). Lastly, single unit that fired sporadically during the recording were categorized as type C (**Figure 5.2C**). As shown in **Figure 5.2D**, we found 42 type A (40%), 13 type B (12%), and 51 type C (48%) interneurons as well as 3 type A (18%), 5 type B (29%), and 9 type C (53%) principal cells.

To better understand the relationship between single-unit activity and CCh-induced oscillations, peri-event histograms of the average spike densities were centered around the onset of CCh-induced oscillations with the duration of the field oscillation normalized to 0–100%. As illustrated in **Figure 5.3**, we found increases in both type A interneuron and principal cell firings that were sustained throughout the field oscillations (**Figure 5.3A**). Upon closer inspection of the average spike densities around the onset of CCh-induced oscillations, type A interneurons appeared to increase their activity before principal cells (**Figure 5.3A**). Despite an increase in type B interneuron during CCh-induced oscillations, the increase was not statistically significant (**Figure 5.3B**). Type B principal cells firing also did not exhibit significant increases during CCh-induced oscillations (**Figure 5.3B**). Type C interneurons only briefly significantly increased their firing near the end of oscillations (**Figure 5.3C**), while type C principal cell firing did not significantly increase during CCh-induced oscillations.

5.4.3. GABAA receptor involvement in CCh-induced oscillations

Next, we investigated the role of GABAA receptor signalling in CCh-induced oscillations and single-unit activity by bath applying PTX in addition to CCh. Upon PTX addition, we observed changes in the dynamics of the field oscillations (Figure 5.4A). Specifically, we found a nonsignificant increase in the average interval of occurrence, which changed from 2.9 s (IQR = 2.5– 3.2 s) in absence of PTX to 3.4 s (IQR = 1.9–4.0 s) in presence of PTX (Figure 5.4B). The average duration of the CCh-induced oscillations significantly increased from 0.6 s (IQR = 0.3-1.1 s) to 1.4 s (IQR = 1.0-2.0 s) during PTX application (Figure 5.4B; Wilcoxon Rank Sum Test, W =3560, z = 5.213, p < 0.05). Coefficient of variation (CV) analyses of the duration also showed a significant increase from 0.3 A.U. (IQR = 0.2–0.5 A.U.) in CCh only condition to 0.8 A.U. (IQR = 0.4–0.9 A.U.) in CCh + PTX condition (Figure 5.4B; Wilcoxon Rank Sum Test, W = 3334, z =4.195, p < 0.05). The average frequency of CCh-induced oscillation also changed significantly from 10.1 Hz (IQR = 9.5-10.9 Hz) in absence of PTX to 9.1 Hz (IQR = 8.7-9.7 Hz) in presence of PTX (Figure 5.4B; Wilcoxon Rank Sum Test, W = 1344, z = -4.767, p < 0.05). Finally, CV analyses of frequency revealed a non-significant change from 0.30 A.U. (IQR = 0.27–0.32 A.U.) in CCh only condition to 0.29 A.U. (IQR = 0.26-0.31 A.U.) (Figure 5.4B). During GABAA receptor blockade, we also observed changes in single-unit discharge patterns (Figure 5.4C). We found that 45% (n = 12) of interneurons exhibited type A firing pattern, 11% (n = 3) exhibited type B firing pattern, and 44% (n = 12) exhibited type C firing pattern. In principal cells, we found 25% (n = 1) of type A and 75% (n = 3) of type C activity patterns (**Figure 5.4D**).

To better understand the relationship between single-unit activity and field oscillations occurring during application of CCh and PTX, we built peri-event histograms of the average spike densities centered around the onset of field oscillations with their duration normalized to 0–100%. As illustrated in **Figure 5.5A**, only type A interneurons and principal cells significantly increased their firing but only transiently; thus, in contrast to what was seen in the CCh only condition, the increases in neuronal activity were not sustained. Notably, during GABAA receptor antagonism, the increase in the activity of type A principal cells was much greater in amplitude and occurred at an earlier time than the increase observed in type A interneuron firing (**Figure 5.5A**). Type B and type C interneurons and principal cells did not exhibit significant increases in firing activity (**Figure 5.5B** and **5.5C**).

Peri-event histograms in **Figures 5.3** and **5.5** suggest that only the activity of type A cells presumably contributed to the generation CCh-induced oscillations. However, they did not reveal the single-unit discharge pattern during CCh-induced oscillations, which can be quantified as the phase of oscillation at which single-unit discharge. Therefore, we assessed the phase firing of type A single-unit discharges using the Hilbert transformation of the field potentials. As shown in the inset of **Figure 5.6**, angles 0° and 360° corresponds to the peaks of the CCh-induced oscillations. We found that during application of CCh, type A interneuron firing phase distribution was non-uniformly distributed (**Figure 5.6**, Omnibus Test, m = 10887, p < 0.05) with a median of 258.4° ; under these experimental conditions, Type A principal cell firing phase distribution also exhibited non-uniformity (**Figure 5.6**, upper right; Rayleigh's Test, z = 11.9, p < 0.05) with a median of 72.0° . As illustrated in **Figure 5.5B**, during bath application of PTX, only type A interneuron firing phase distribution exhibited non-uniformity (Omnibus Test, m = 1175, p < 0.05) with a median firing phase of 314.4° .

5.4.4. Ionotropic glutamatergic receptor involvement in CCh-induced oscillations

To investigate the role of ionotropic glutamatergic signalling in CCh-induced field oscillations, we applied CPP and NBQX while recording single-unit activity generated by interneurons and principal cells. As previously reported (Dickson and Alonso, 1997; Lévesque et al., 2017), CCh-induced oscillations were abolished by this pharmacological procedure (**Figure 5.7A**). However, both interneurons and principal cells continued to fire action potentials under these experimental conditions (**Figure 5.7B**). As illustrated in **Figure 5.7C**, there was a non-significant increase in firing frequency of interneurons from 1.1 Hz (IQR = 0.3–4.4 Hz) in the CCh only condition to 1.2 Hz (IQR = 0.5–1.9 Hz) in the CCh + CPP + NBQX condition. Similarly, the principal cell firing frequency in the CCh only condition (1.1 Hz, IQR = 0.3–4.4 Hz) was also not significantly different when compared with the CCh + CPP + NBQX condition (1.2 Hz, IQR = 0.5–1.9 Hz). Despite the non-significant changes in firing frequency, we observed a change in the rhythmicity of firing as revealed by the autocorrelograms of action potential discharge patterns (**Figure 5.7D**). Namely, interneurons in the CCh only condition exhibited rhythmic firing at approximately 17 Hz, or a peak delay of approximately 0.06 s. In contrast, during application of CPP and NBQX, no rhythmicity in interneuron firing was observed. While principal cells did not exhibit a clear

rhythmic firing pattern under both CCh only and CCh + CPP + NBQX conditions, the autocorrelograms suggested that principal cell firing was more irregular during the latter condition.

5.5. Discussion

In this study, we performed tetrode recordings to examine single-unit activity during field oscillations that were induced by the cholinergic agent CCh in the rat EC maintained *in vitro*. The main findings obtained from our experiments are as follows: (i) during bath application of CCh, approximately half of the recorded single units increased their firing rate in coincidence with CCh-induced oscillations; (ii) around the onset of CCh-induced oscillations, interneuron activity increased before principal cell activity; (iii) blockade of GABA_A-receptor signalling led to a transient increase in neuronal firing during the field oscillations that was not sustained to the end of CCh-induced oscillations; (iv) antagonizing ionotropic glutamatergic signalling abolished the field oscillations but did not change the firing frequency while affecting their rhythmicity.

5.5.1. CCh induced increases in single-unit activity during CCh-induced oscillations

In line with previous *in vitro* studies performed in the hippocampus (Bland et al., 1988; Williams and Kauer, 1997; Konopacki et al., 2006), our findings show that CCh-induced field oscillations are associated with different single-unit activity patterns. Specifically, we found that approximately half of the principal cells and interneurons increased their activity during CCh-induced oscillations. Upon closer examination, we also observed that the increases in interneuron activity preceded that in principal cells at the onset of CCh-induced oscillations. Furthermore, interneurons fired at a preferred phase of 258.4°, which was earlier than the principal cell preferred phase of 72.0°. Together, our data suggest that interneurons could be modulating principal cell activity during CCh-induced oscillations in the EC. Previously, Konopacki *et al.* (2006) have also conducted phase firing analysis and found that unclassified cells firing during CCh-induced oscillations exhibit a mean preferred firing phase of 234.6 \pm 47.29° in the hippocampus, which is similar to what was observed here in EC interneurons. In our study, we further categorized our cells into interneurons and principal cells, and we show a presumptive role that is played by the interneurons in modulating principal cells during CCh-induced oscillations.

Interneurons have been proposed to control the activity of principal cells and to modulate rhythmic activities of the brain (Cobb et al., 1995; Colgin, 2016). *In vivo* optogenetics studies have

also shown that interneurons could modulate the frequencies of *in vivo* hippocampal theta oscillations, gamma rhythm, and ripples (Stark et al., 2013; Lasztóczi and Klausberger, 2014; Amilhon et al., 2015). In addition to physiological brain rhythms, interneurons also play a role in pathological brain oscillations, such as the initiation of epileptiform activities (Sessolo et al., 2015; Yekhlef et al., 2015; Shiri et al., 2016). Therefore, our findings support the view that interneurons can modulate the activity of principal cells during CCh-induced oscillations in the EC.

5.5.2. The role of interneurons and GABAA-receptor during CCh-induced oscillations

By antagonizing GABA_A-receptor signalling with PTX, we found an increase in the duration of CCh-induced oscillations, which may be attributed to a loss of regularity in the pattern of CChinduced oscillations, as demonstrated by a significant increase in the CV after PTX application. These results are in keeping with previous findings (Williams and Kauer, 1997; D'Antuono et al., 2001; Lévesque et al., 2017). Therefore, in light of a previous investigation showing that CCh could induce membrane potential oscillations in the theta frequency range in a subtype of neocortical interneurons (Blatow et al., 2003), we propose that GABA_A-receptor signalling forms a network that modulates CCh-induced oscillations. When we examined single-unit activity, we found that both interneurons and principal cells only fired transiently around the onset of the field oscillations recorded during GABAA-receptor antagonism, in contrast to their sustained firing when GABA_A-receptor signalling was preserved. In addition, during application of medium containing CCh and PTX, principal cells increased their firing activity before interneurons at the onset of the field oscillations. Finally, preferred firing phase analyses showed that, while interneurons still exhibited a preference in their firing at 314.4°, principal cells did not fire at a preferred phase in absence of GABA_A-receptor signalling. This evidence therefore supports the hypothesis that interneurons are involved in synchronizing the activity of principal cells and in modulating the structure and dynamics of CCh-induced oscillations. However, in the absence of GABAergic signalling, CCh-induced oscillations could still be present but with less regularity in their pattern.

5.5.3. Ionotropic glutamatergic signaling is necessary for the generation of CCh-induced oscillations

We also found that CCh-induced oscillations were abolished by antagonizing ionotropic glutamatergic receptors. These data are consistent with what was reported in previous studies (Dickson and Alonso, 1997; Lévesque et al., 2017), and suggest that excitatory ionotropic glutamatergic receptor signalling is necessary for the generation of CCh-induced oscillations. By examining single-unit activity, we could identify a change in the rhythmicity of both interneuron and principal cell firing patterns. Together, our data suggest that ionotropic glutamatergic receptor signalling plays a crucial role in the generation of CCh-induced oscillations.

5.5.4. Epileptiform synchronization and CCh-induced oscillations

Several authors have emphasized that *in vitro* CCh-induced oscillations are similar to the atropine-sensitive *in vivo* theta rhythm that occur under anesthesia (Bland et al., 1988; Kowalczyk et al., 2013). These *in vivo* theta rhythms have been widely studied because they appear to facilitate sensorimotor integration, spatial navigation, memory, and learning (Düzel et al., 2010; Buzsáki and Moser, 2013; Hasselmo and Stern, 2014; Colgin, 2016). These physiological processes are believed to support long-term potentiation (LTP) (Bliss and Collingridge, 1993). In line with this view, *in vivo* hippocampal theta rhythm has been shown to facilitate LTP in anesthetized animals (Pavlides et al., 1988). Similarly, CCh-induced oscillations not only exhibit frequency ranges that overlap with *in vivo* theta rhythm but also have been shown to facilitate synaptic plasticity when applied to hippocampal slices (Huerta and Lisman, 1993).

Therefore, it could be argued that CCh-induced oscillations represent a model of *in vivo* theta rhythm. However, it has been reported that *in vivo* theta oscillations in freely moving animals can be atropine-resistant as well as that they also do not rest upon principal cell involvement as much as CCh-induced oscillations (Buzsáki et al., 1983; Williams and Kauer, 1997; Buzsáki, 2002). We have found here that principal cell activity is indeed necessary for the generation of CCh-induced oscillations *in vitro*, suggesting that they may not fully model the *in vivo* theta rhythm.

The mechanisms underlying CCh-induced oscillations could be related to oscillatory activities that occur during epileptiform discharges. In human depth electrode recordings, it has been documented that some seizure onset patterns are marked by rhythmic activity in the theta

frequency range (Wennberg et al., 2002; Perucca et al., 2014). In the tetanus toxin animal model, spontaneous hippocampal seizures have been shown to occur more frequently during periods of prominent theta rhythm, namely the rapid eye movement sleep and exploratory wake behaviors (Sedigh-Sarvestani et al., 2014). Furthermore, recent studies in the hippocampus of the pilocarpine animal model of epilepsy have noted the appearance of oscillatory activities in the theta frequency range that preceded ictal events (Grasse et al., 2013; Fujita et al., 2014; Toyoda et al., 2015; Karunakaran et al., 2016). Upon closer examination, interneuron firing rate and coherence with field oscillations have been shown to increase during the appearance of this pre-ictal theta rhythm in the CA3 (Grasse et al., 2013; Karunakaran et al., 2016). Since several studies have found that CCh-induced oscillations are generated locally (Dickson and Alonso, 1997; Konopacki et al., 2000; Lévesque et al., 2017), we propose that the pre-ictal theta rhythm, which is observed in the hippocampus of epileptic animals, could be acting through the same network underlying CChinduced oscillations described here. Williams and Kauer (1997) have reported that CCh-induced oscillations were longer in duration and smaller in amplitude when extracellular K+ was elevated from 2.5 mM to 5 mM. These findings could be further explored using tetrode recordings to uncover the contributions of interneurons and principal cells.

5.6. References

- Alonso A, Köhler C (1984) A study of the reciprocal connections between the septum and the entorhinal area using anterograde and retrograde axonal transport methods in the rat brain. J Comp Neurol 225:327–343.
- Amilhon B, Huh CYL, Manseau F, Ducharme G, Nichol H, Adamantidis A, Williams S (2015) Parvalbumin Interneurons of Hippocampus Tune Population Activity at Theta Frequency. Neuron 86:1277–1289.
- Beckstead RM (1978) Afferent connections of the entorhinal area in the rat as demonstrated by retrograde cell-labeling with horseradish peroxidase. Brain Res 152:249–264.
- Berens P (2009) CircStat: A MATLAB Toolbox for Circular Statistics. J Stat Softw 31 Available at: https://www.jstatsoft.org/article/view/v031i10 [Accessed September 14, 2017].
- Bland BH (1986) The physiology and pharmacology of hippocampal formation theta rhythms. Prog Neurobiol 26:1–54.
- Bland BH, Colom LV, Konopacki J, Roth SH (1988) Intracellular records of carbachol-induced theta rhythm in hippocampal slices. Brain Res 447:364–368.
- Bland BH, Oddie SD (2001) Theta band oscillation and synchrony in the hippocampal formation and associated structures: the case for its role in sensorimotor integration. Behav Brain Res 127:119–136.
- Blatow M, Rozov A, Katona I, Hormuzdi SG, Meyer AH, Whittington MA, Caputi A, Monyer H (2003) A Novel Network of Multipolar Bursting Interneurons Generates Theta Frequency Oscillations in Neocortex. Neuron 38:805–817.
- Bliss TVP, Collingridge GL (1993) A synaptic model of memory: long-term potentiation in the hippocampus. Nature 361:31.
- Buzsáki G (2002) Theta oscillations in the hippocampus. Neuron 33:325–340.
- Buzsáki G (2015) Hippocampal sharp wave-ripple: A cognitive biomarker for episodic memory and planning. Hippocampus 25:1073–1188.
- Buzsáki G, Lai-Wo S. L, Vanderwolf CH (1983) Cellular bases of hippocampal EEG in the behaving rat. Brain Res Rev 6:139–171.
- Buzsáki G, Moser EI (2013) Memory, navigation and theta rhythm in the hippocampal-entorhinal system. Nat Neurosci 16:130–138.
- Cataldi M, Panuccio G, Cavaccini A, D'Antuono M, Taglialatela M, Avoli M (2011) Involvement of inward rectifier and M-type currents in carbachol-induced epileptiform synchronization. Neuropharmacology 60:653–661.

- Cobb SR, Buhl EH, Halasy K, Paulsen O, Somogyi P (1995) Synchronization of neuronal activity in hippocampus by individual GABAergic interneurons. Nature 378:75–78.
- Colgin LL (2016) Rhythms of the hippocampal network. Nat Rev Neurosci 17:239–249.
- Csicsvari J, Hirase H, Czurko A, Buzsáki G (1998) Reliability and State Dependence of Pyramidal Cell–Interneuron Synapses in the Hippocampus. Neuron 21:179–189.
- D'Antuono M, Kawasaki H, Palmieri C, Avoli M (2001) Network and intrinsic contributions to carbachol-induced oscillations in the rat subiculum. J Neurophysiol 86:1164–1178.
- Deshmukh SS, Yoganarasimha D, Voicu H, Knierim JJ (2010) Theta Modulation in the Medial and the Lateral Entorhinal Cortices. J Neurophysiol 104:994–1006.
- Dickson CT, Alonso A (1997) Muscarinic Induction of Synchronous Population Activity in the Entorhinal Cortex. J Neurosci 17:6729–6744.
- Dickson CT, Biella G, Curtis M de (2003) Slow Periodic Events and Their Transition to Gamma Oscillations in the Entorhinal Cortex of the Isolated Guinea Pig Brain. J Neurophysiol 90:39–46.
- Dickson CT, de Curtis M (2002) Enhancement of temporal and spatial synchronization of entorhinal gamma activity by phase reset. Hippocampus 12:447–456.
- Dickson CT, Magistretti J, Shalinsky MH, Fransén E, Hasselmo ME, Alonso A (2000) Properties and Role of I h in the Pacing of Subthreshold Oscillations in Entorhinal Cortex Layer II Neurons. J Neurophysiol 83:2562–2579.
- Düzel E, Penny WD, Burgess N (2010) Brain oscillations and memory. Curr Opin Neurobiol 20:143–149.
- Freund T f., Buzsáki G (1996) Interneurons of the hippocampus. Hippocampus 6:347–470.
- Fujita S, Toyoda I, Thamattoor AK, Buckmaster PS (2014) Preictal activity of subicular, CA1, and dentate gyrus principal neurons in the dorsal hippocampus before spontaneous seizures in a rat model of temporal lobe epilepsy. J Neurosci Off J Soc Neurosci 34:16671–16687.
- Gaykema RPA, Luiten PGM, Nyakas C, Traber J (1990) Cortical projection patterns of the medial septum-diagonal band complex. J Comp Neurol 293:103–124.
- Grasse DW, Karunakaran S, Moxon KA (2013) Neuronal synchrony and the transition to spontaneous seizures. Exp Neurol 248:72–84.
- Griguoli M, Cherubini E (2017) Early Correlated Network Activity in the Hippocampus: Its Putative Role in Shaping Neuronal Circuits. Front Cell Neurosci 11 Available at: https://www.frontiersin.org/articles/10.3389/fncel.2017.00255/full [Accessed October 2, 2017].

- Hasselmo ME, Stern CE (2014) Theta rhythm and the encoding and retrieval of space and time. NeuroImage 85 Pt 2:656–666.
- Heys JG, Schultheiss NW, Shay CF, Tsuno Y, Hasselmo ME (2012) Effects of acetylcholine on neuronal properties in entorhinal cortex. Front Behav Neurosci 6 Available at: http://journal.frontiersin.org/article/10.3389/fnbeh.2012.00032/full [Accessed September 18, 2017].
- Huerta PT, Lisman JE (1993) Heightened synaptic plasticity of hippocampal CA1 neurons during a Cholinergically induced rhythmic state. Nature 364:723–725.
- Insausti R, Amaral DG, Cowan WM (1987) The entorhinal cortex of the monkey: III. Subcortical afferents. J Comp Neurol 264:396–408.
- Karunakaran S, Grasse DW, Moxon KA (2016) Role of CA3 theta-modulated interneurons during the transition to spontaneous seizures. Exp Neurol 283:341–352.
- Konopacki J, Eckersdorf B, Kowalczyk T, Gołębiewski H (2006) Firing cell repertoire during carbachol-induced theta rhythm in rat hippocampal formation slices. Eur J Neurosci 23:1811–1818.
- Konopacki J, Gołebiewski H, Eckersdorf B (1992) Carbachol-induced theta-like activity in entorhinal cortex slices. Brain Res 572:76–80.
- Konopacki J, Gołebiewski H, Eckersdorf B, Kowalczyk T, Bocian R (2000) In vitro recorded theta-like activity in the limbic cortex: comparison with spontaneous theta and epileptiform discharges. Acta Neurobiol Exp (Warsz) 60:67–85.
- Kowalczyk T, Bocian R, Konopacki J (2013) The generation of theta rhythm in hippocampal formation maintained in vitro. Eur J Neurosci 37:679–699.
- Kramis R, Vanderwolf CH, Bland BH (1975) Two types of hippocampal rhythmical slow activity in both the rabbit and the rat: Relations to behavior and effects of atropine, diethyl ether, urethane, and pentobarbital. Exp Neurol 49:58–85.
- Lasztóczi B, Klausberger T (2014) Layer-Specific GABAergic Control of Distinct Gamma Oscillations in the CA1 Hippocampus. Neuron 81:1126–1139.
- Lévesque M, Cataldi M, Chen L-Y, Hamidi S, Avoli M (2017) Carbachol-induced network oscillations in an in vitro limbic system brain slice. Neuroscience Available at: http://www.sciencedirect.com/science/article/pii/S0306452217301045.
- Lévesque M, Herrington R, Hamidi S, Avoli M (2016) Interneurons spark seizure-like activity in the entorhinal cortex. Neurobiol Dis 87:91–101.
- McGaughy J, Koene RA, Eichenbaum H, Hasselmo ME (2005) Cholinergic Deafferentation of the Entorhinal Cortex in Rats Impairs Encoding of Novel But Not Familiar Stimuli in a Delayed Nonmatch-to-Sample Task. J Neurosci 25:10273–10281.

- Montoya CP, Sainsbury RS (1985) The effects of entorhinal cortex lesions on type 1 and type 2 theta. Physiol Behav 35:121–126.
- Pavlides C, Greenstein YJ, Grudman M, Winson J (1988) Long-term potentiation in the dentate gyrus is induced preferentially on the positive phase of θ-rhythm. Brain Res 439:383–387.
- Perucca P, Dubeau F, Gotman J (2014) Intracranial electroencephalographic seizure-onset patterns: effect of underlying pathology. Brain 137:183–196.
- Petsche H, Stumpf C, Gogolak G (1962) The significance of the rabbit's septum as a relay station between the midbrain and the hippocampus. I. The control of hippocampus arousal activity by the septum cells. Electroencephalogr Clin Neurophysiol 14:202–211.
- Pilly PK, Grossberg S (2013) How reduction of theta rhythm by medial septum inactivation may covary with disruption of entorhinal grid cell responses due to reduced cholinergic transmission. Front Neural Circuits 7 Available at: https://www.frontiersin.org/articles/10.3389/fncir.2013.00173/full.
- Quiroga RQ, Nadasdy Z, Ben-Shaul Y (2004) Unsupervised spike detection and sorting with wavelets and superparamagnetic clustering. Neural Comput 16:1661–1687.
- Sakata S, Harris KD (2009) Laminar Structure of Spontaneous and Sensory-Evoked Population Activity in Auditory Cortex. Neuron 64:404–418.
- Sedigh-Sarvestani M, Thuku GI, Sunderam S, Parkar A, Weinstein SL, Schiff SJ, Gluckman BJ (2014) Rapid eye movement sleep and hippocampal theta oscillations precede seizure onset in the tetanus toxin model of temporal lobe epilepsy. J Neurosci Off J Soc Neurosci 34:1105–1114.
- Sessolo M, Marcon I, Bovetti S, Losi G, Cammarota M, Ratto GM, Fellin T, Carmignoto G (2015) Parvalbumin-Positive Inhibitory Interneurons Oppose Propagation But Favor Generation of Focal Epileptiform Activity. J Neurosci 35:9544–9557.
- Shiri Z, Manseau F, Lévesque M, Williams S, Avoli M (2016) Activation of specific neuronal networks leads to different seizure onset types. Ann Neurol 79:354–365.
- Sirota A, Montgomery S, Fujisawa S, Isomura Y, Zugaro M, Buzsáki G (2008) Entrainment of neocortical neurons and gamma oscillations by the hippocampal theta rhythm. Neuron 60:683–697.
- Stark E, Eichler R, Roux L, Fujisawa S, Rotstein HG, Buzsaki G (2013) Inhibition-induced theta resonance in cortical circuits. Neuron 80:1263–1276.
- Tanninen SE, Yu X, Giritharan T, Tran L, Bakir R, Volle J, Morrissey MD, Takehara-Nishiuchi K (2015) Cholinergic, but not NMDA, receptors in the lateral entorhinal cortex mediate acquisition in trace eyeblink conditioning. Hippocampus 25:1456–1464.

- Toyoda I, Fujita S, Thamattoor AK, Buckmaster PS (2015) Unit Activity of Hippocampal Interneurons before Spontaneous Seizures in an Animal Model of Temporal Lobe Epilepsy. J Neurosci Off J Soc Neurosci 35:6600–6618.
- van Strien NM, Cappaert NLM, Witter MP (2009) The anatomy of memory: an interactive overview of the parahippocampal-hippocampal network. Nat Rev Neurosci 10:272–282.
- Vandecasteele M, Varga V, Berényi A, Papp E, Barthó P, Venance L, Freund TF, Buzsáki G (2014) Optogenetic activation of septal cholinergic neurons suppresses sharp wave ripples and enhances theta oscillations in the hippocampus. Proc Natl Acad Sci 111:13535–13540.
- Wennberg R, Arruda F, Quesney LF, Olivier A (2002) Preeminence of Extrahippocampal Structures in the Generation of Mesial Temporal Seizures: Evidence from Human Depth Electrode Recordings. Epilepsia 43:716–726.
- Williams JH, Kauer JA (1997) Properties of Carbachol-Induced Oscillatory Activity in Rat Hippocampus. J Neurophysiol 78:2631–2640.
- Yekhlef L, Breschi GL, Lagostena L, Russo G, Taverna S (2015) Selective activation of parvalbumin- or somatostatin-expressing interneurons triggers epileptic seizurelike activity in mouse medial entorhinal cortex. J Neurophysiol 113:1616–1630.
- Yun SH, Cheong MY, Mook-Jung I, Huh K, Lee C-J, Jung MW (2000) Cholinergic modulation of synaptic transmission and plasticity in entorhinal cortex and hippocampus of the rat. Neuroscience 97:671–676.

5.7. Figures

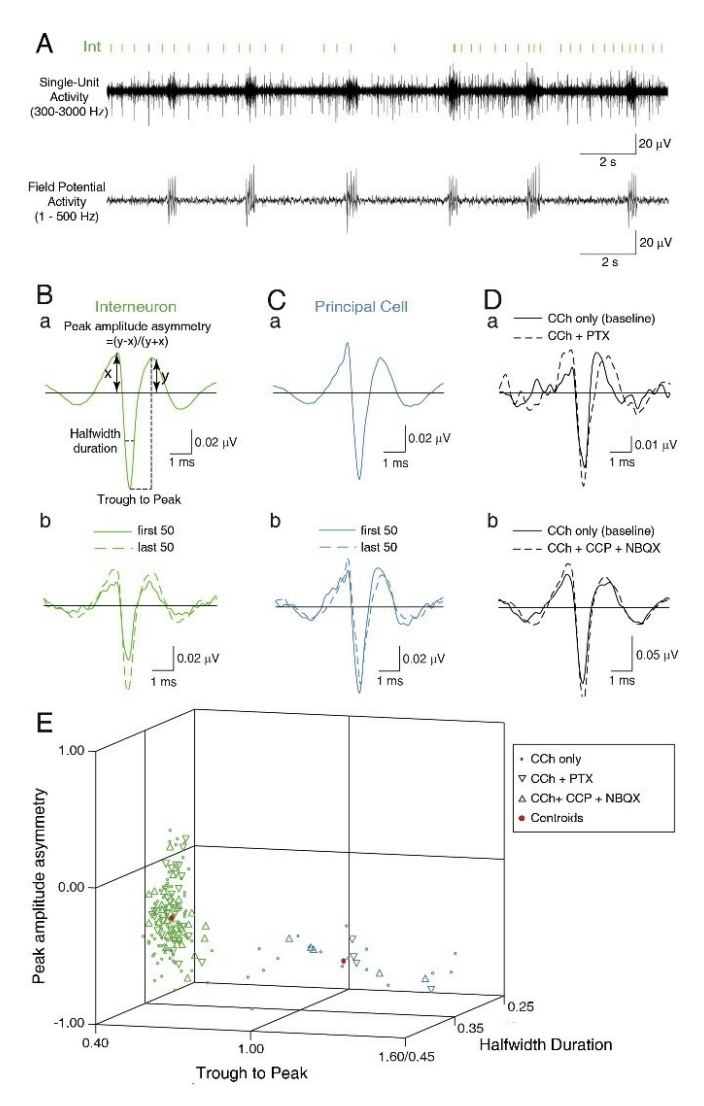


Figure 5.1. Single-unit clustering of interneurons and principal cells. **A**: An example of raw data filtered between 300 and 3,000 Hz to detect action potential discharges (bars) and between 1 and 500 Hz to visualize field potential activity. In this example, the single unit is classified as a putative interneuron. **B**: Representative single unit shown in **A** classified as a putative interneuron (Int) based on the average action potential waveform shape (**a**). Single-unit activity was stable throughout the recording as shown by the similarities between the average action potential waveform shape of the first 50 (solid line) and last 50 (dash line) action potentials during each tetrode recording (**b**). **C**: Representative single unit classified as a putative principal cell (PC). **D**: Average waveform shape of 2 single units that were followed under different pharmacological conditions: first under bath application of only CCh (**a** and **b**, solid line) then under bath application of CCh with the GABAergic antagonist PTX (**a**, dash line) or the glutamatergic antagonists CPP and NBQX (**b**, dash line). **E**: *K*-means clustering to classify putative single units into interneurons (green) and principal cells (blue).

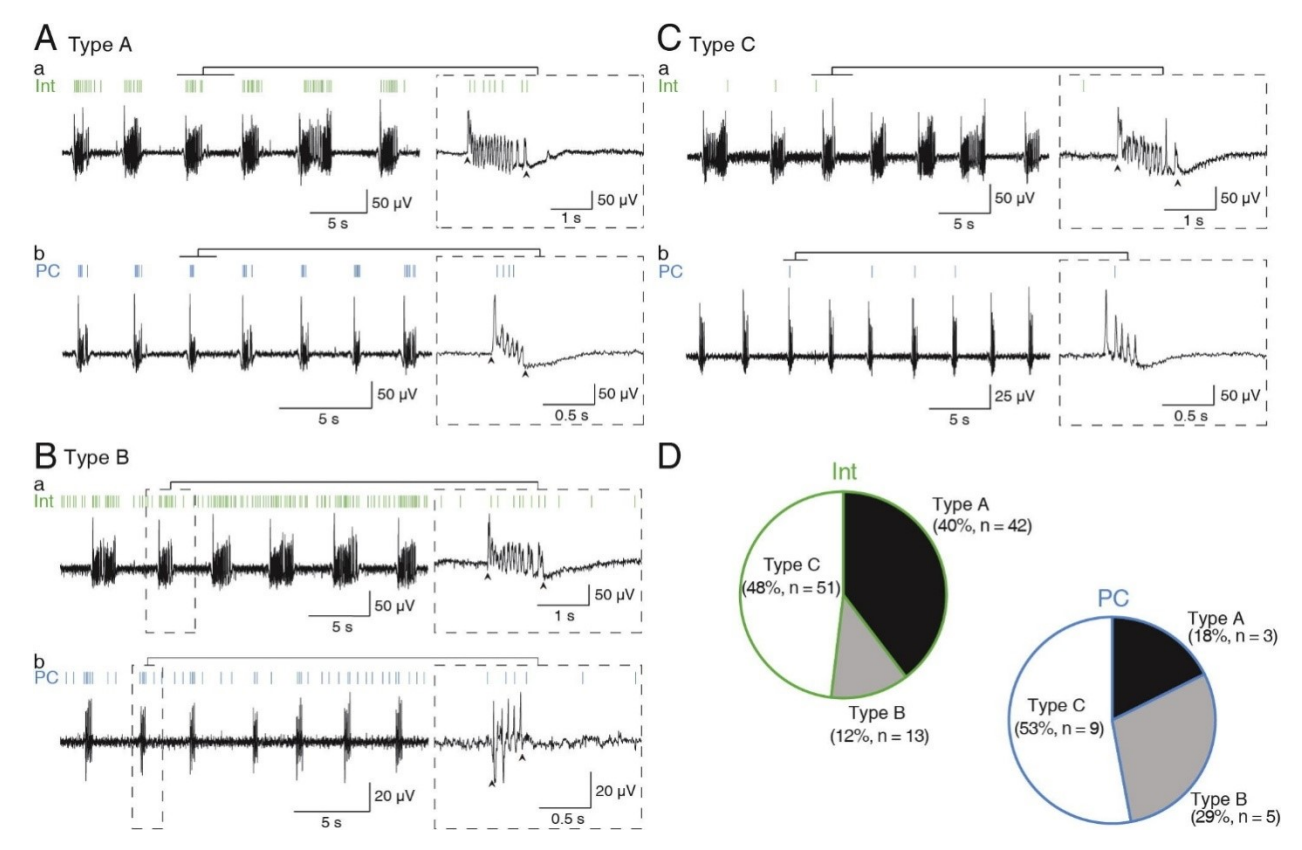


Figure 5.2. Examples of single-unit activity during CCh-induced field oscillations. A: Representative recordings of type A interneuron (a, green) and a putative principal cell (b, blue). The field potential was high-pass filtered with cutoff frequency of 3 Hz for visual clarity. A selected oscillation was expanded in the inset showing the oscillation without additional high-pass filtering with black arrowheads marking the computer-identified onset and termination of the oscillation. B: Same as A for type B interneurons (a, green) and principal cells (b, blue). C: Same as A for type C interneurons (a, green) and principal cells (b, blue). D: Pie charts summarizing the proportion of type A, B, and C interneurons and principal cells identified in CCh only condition.

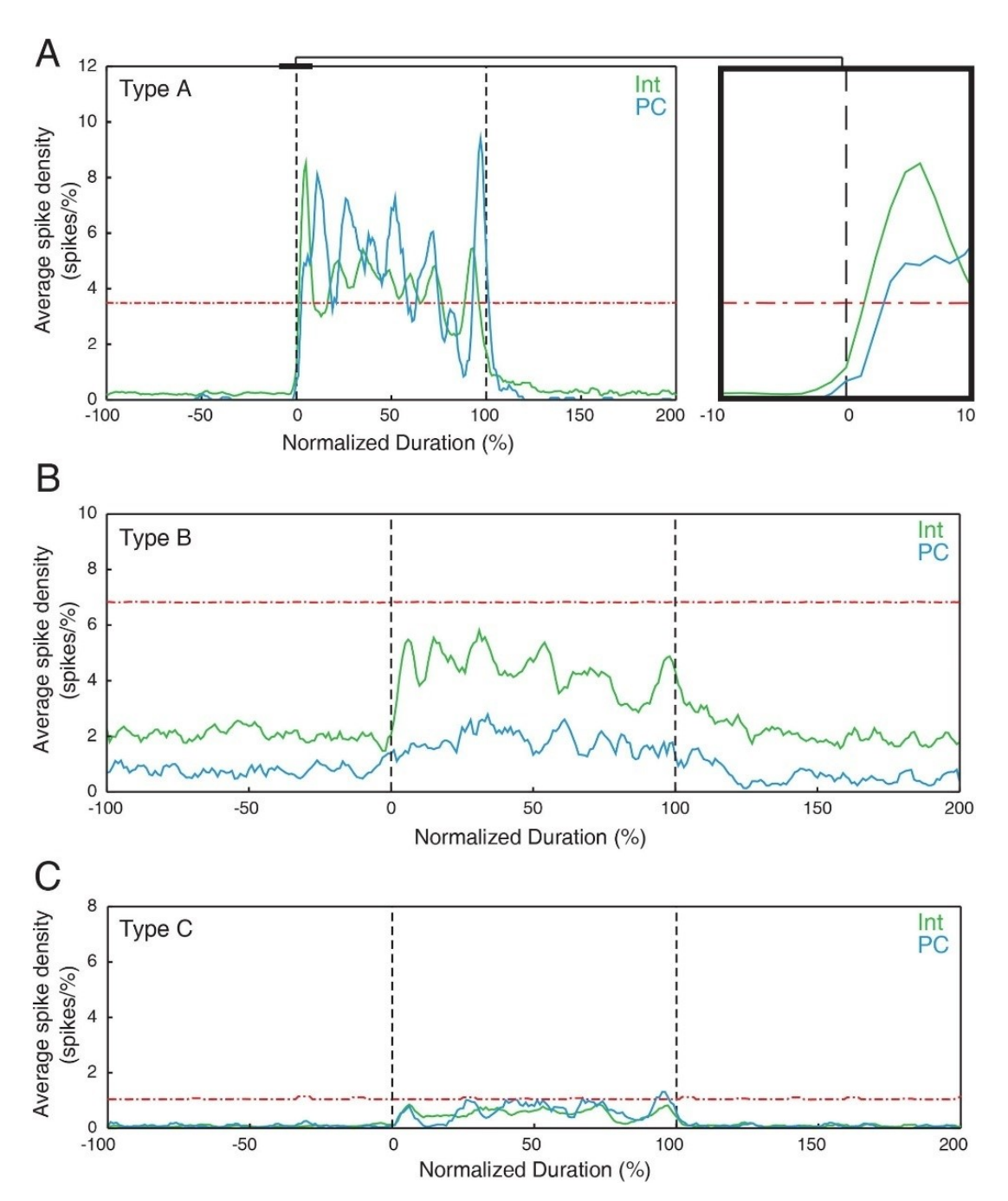


Figure 5.3. Average spike densities of interneuron and principal cell activity during CCh-induced field oscillations. **A**: A peri-event histogram of the average spike densities of type A interneuron (green) and principal cell (blue) around the onset of CCh-induced oscillations. The dashed line shows the significance threshold (2.5 SDs above the simulated random neuronal activities). **B**: Same as **A** for type B interneuron (green) and principal cell (blue) activity around the onset of CCh-induced oscillations. **C**: Same as **A** for type C interneuron (green) and principal cell (blue) activity around the onset of CCh-induced oscillations.

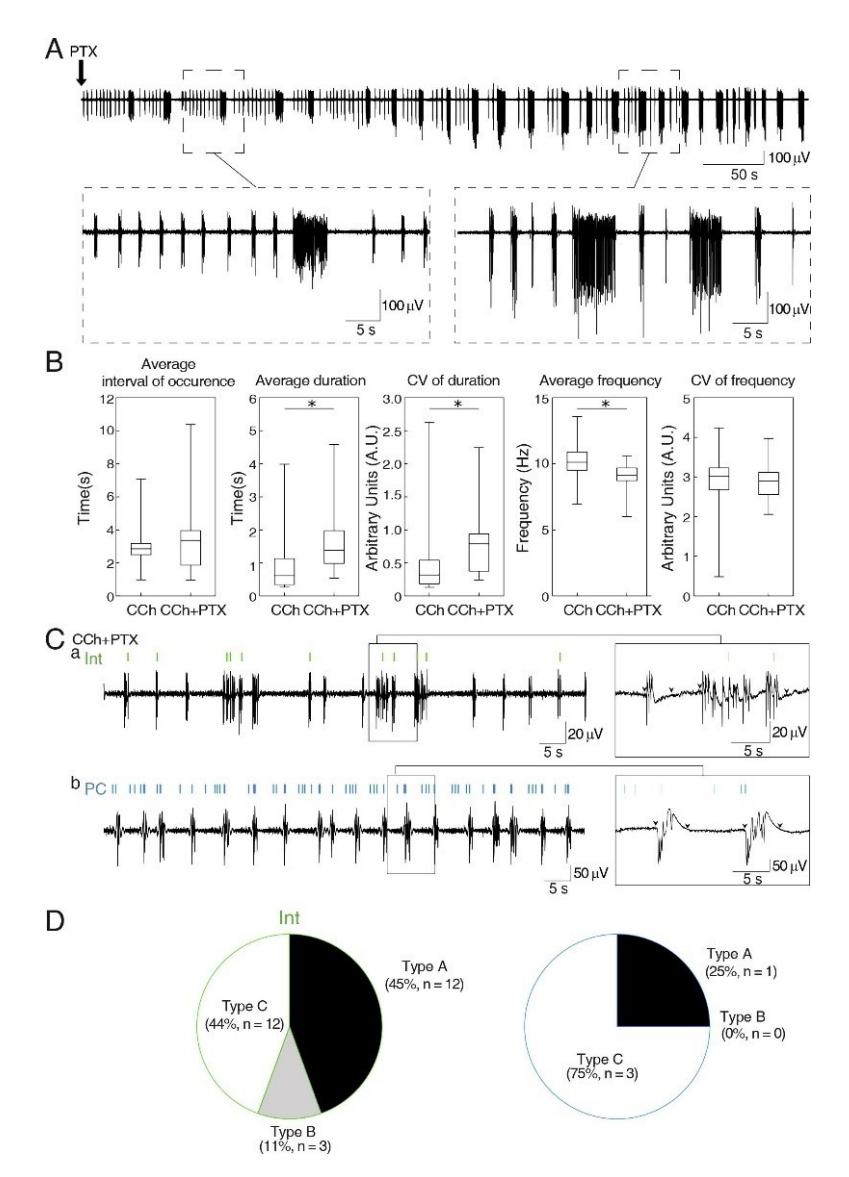


Figure 5.4. CCh-induced field oscillations under GABA_A-receptor antagonism. **A**: A representative recording showing the change in dynamics of CCh-induced oscillations upon the addition of PTX. **B**: Boxplots summarizing the distribution of the average interval of occurrence (left), average duration (center, left), coefficient of variation (CV) of duration (center), average oscillation frequency (center, right), and CV of oscillation frequency (right) of CCh-induced field oscillations of the single units in CCh only and CCh + PTX conditions. The Shapiro-Wilks Test was performed to test for data normality. The Wilcoxon Rank-Sum Test was performed to test for significant alteration of CCh-induced field oscillations under GABA_A-receptor antagonism if data are not normally distributed. Otherwise, the Two-Sample *T*-Test was used for normally distributed data. *p < 0.05. **C**: Two representative recordings showing an interneuron discharge pattern (**a**) with CCh-induced oscillations and a principal cell discharge pattern (**b**) with CCh-induced oscillations. **D**: Pie charts summarizing the proportion of type A, B, and C interneurons (green) and principal cells (blue) identified in CCh + PTX only condition.

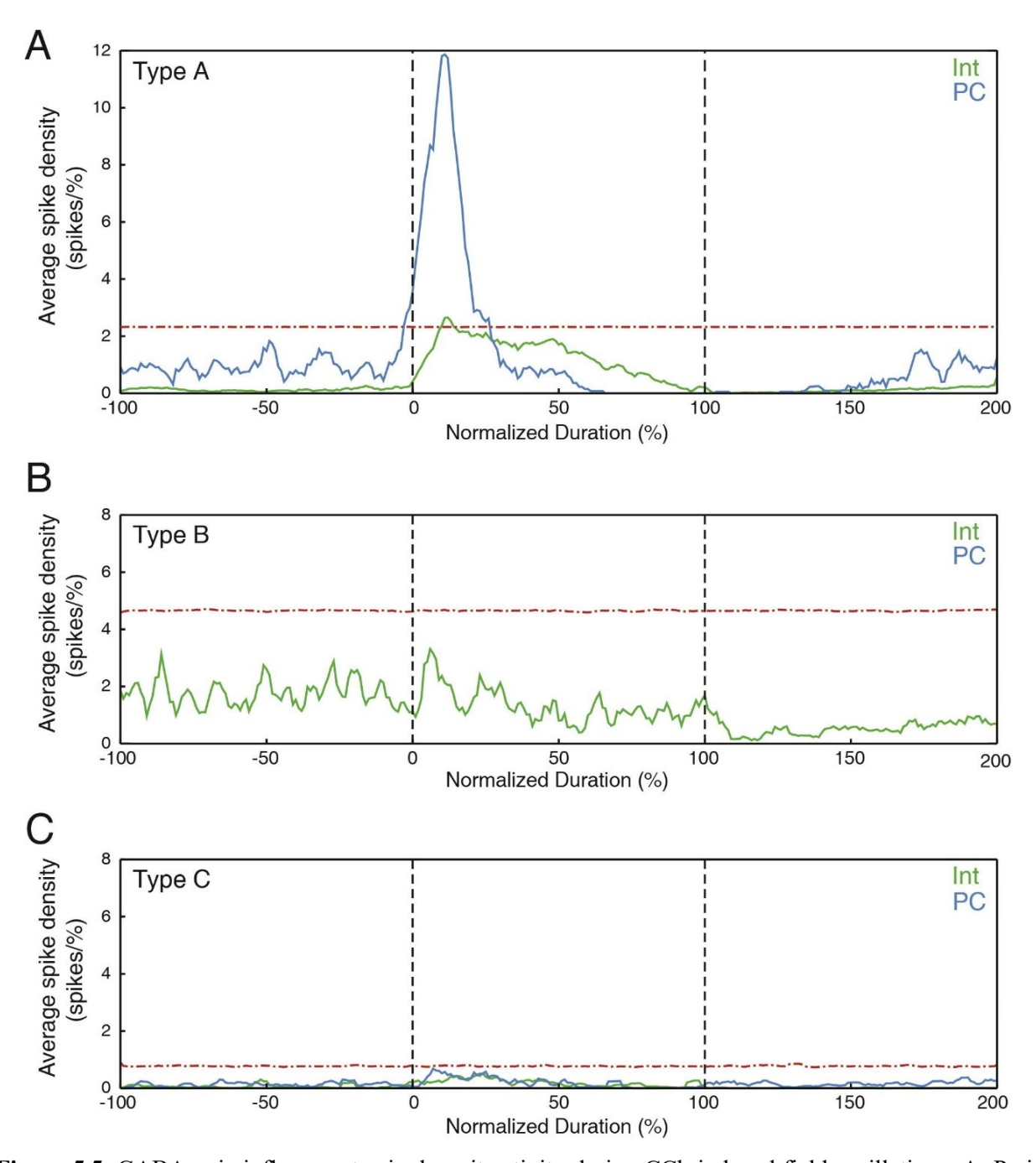


Figure 5.5. GABAergic influences to single-unit activity during CCh-induced field oscillations. **A**: Perievent histogram of average spike densities showing type A interneuron (green) and principal cell (blue) activities around the onset of CCh-induced oscillations under GABA_A-receptor antagonism. The dashed line shows the significance threshold (2.5 SDs above the simulated random neuronal activities). **B**: Same as **A** for type B interneuron (green) and principal cell (blue) activity around the onset of CCh-induced oscillations under bath application of PTX. **C**: Same as **A** for type C interneuron (green) and principal cell (blue) activity around the onset of CCh-induced oscillations with the addition of PTX.

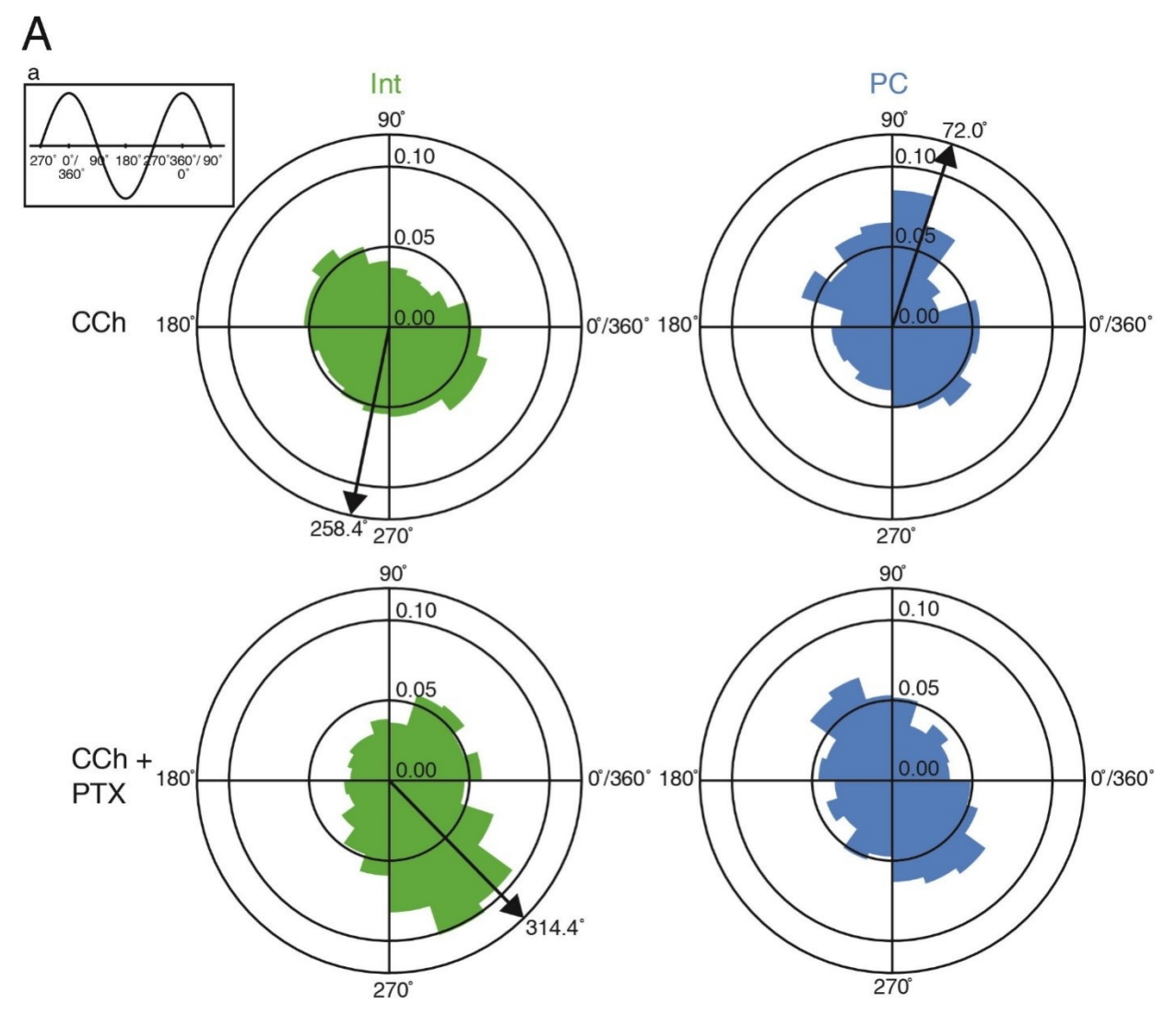
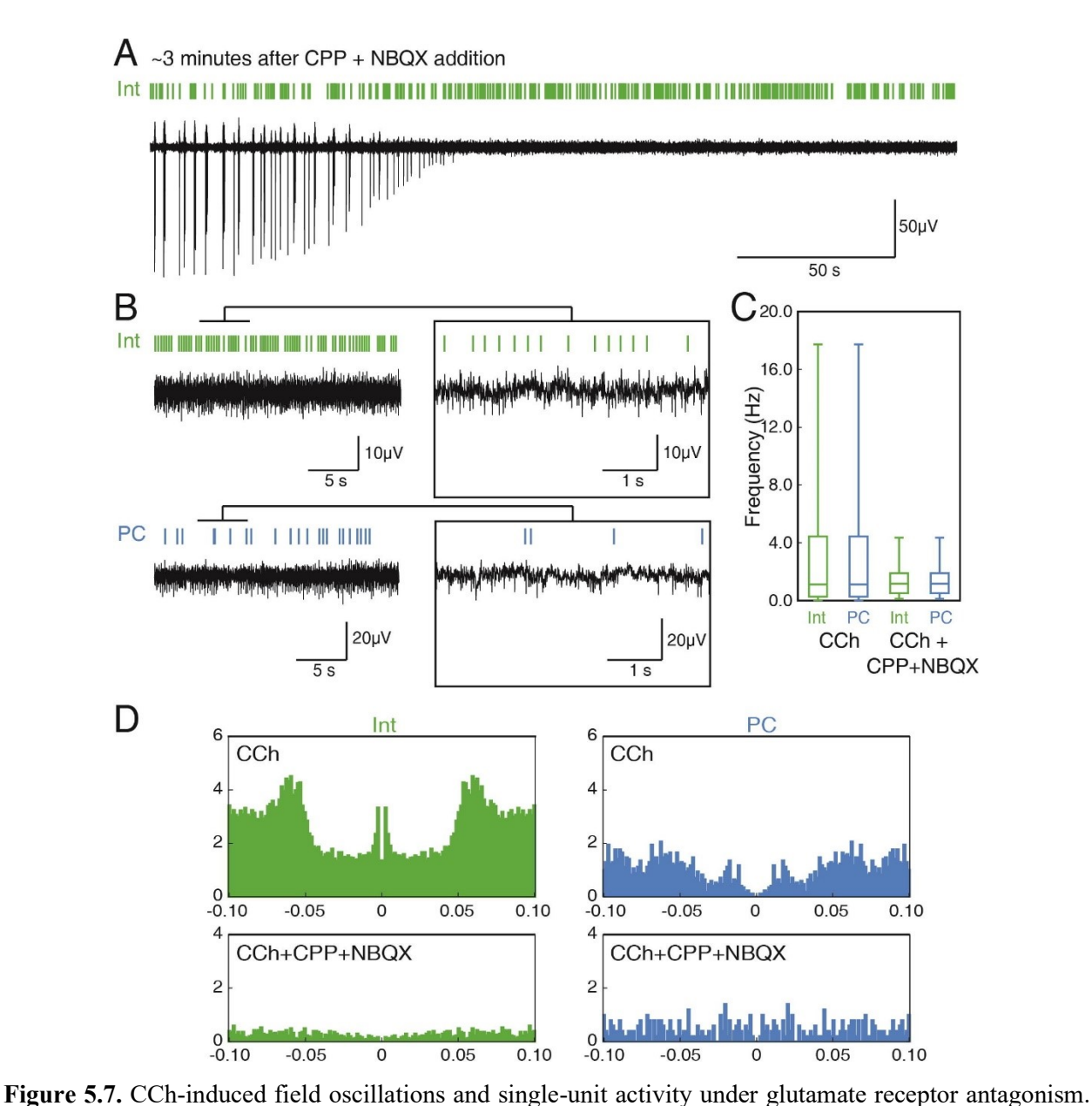


Figure 5.6. Phase Firing of type A single units in CCh only and CCh + PTX conditions. A: Polar histogram plotting the probability of type A interneurons (green) and principal cells (blue) firing at different phases, or angles, of CCh-induced field oscillations in absence and presence of the GABA_A-receptor antagonist. Angles 0° and 360° correspond to the peaks of a cycle in an oscillation, while angle 180° corresponds to the trough of a cycle in an oscillation (a). The Kuiper's Test was performed to compare single-unit phase firing data distribution to the von Mises distribution. The Rayleigh's Test for uniformity was performed for circularly normal data; otherwise, the Omnibus Test was performed. *p < 0.05. For data with significant non-uniformity, the median angle is plotted in black arrow.



A: A representative recording showing the abolishment of CCh-induced field oscillations upon the application of glutamate receptor antagonists CPP and NBQX with preserved single-unit activity. The activity of an interneuron (green) is shown. **B**: Examples of interneuron (green) and principal cell (blue) activities under the bath application of CCh with CPP and NBQX. **C**: Boxplots summarizing the median firing frequencies of interneurons (green) and principal cells (blue) in the absence and presence of glutamatergic blockers. The Shapiro-Wilks Test was performed to test for data normality; the Two-Sample T-Test was used for normally distributed data, while the Wilcoxon Rank-Sum Test was performed to test for significant difference if data are not normally distributed. *p < 0.05. **D**: Auto-correlograms of interneuron and principal action potential discharge patterns.

Chapter 6: General Discussion

In this last chapter of my thesis, I discuss the significance of the findings obtained from my experiments. The chapter begins with a summary of the major findings that is followed by an examination the relevance of my findings to our understanding of the basic mechanisms of epilepsy. Finally, possible future directions that will extend the work described in this thesis are considered.

6.1. Summary of findings

Despite our appreciation of the fundamental relationship between neuronal action potentials and the resulting local field potential (LFP) activity, our knowledge of the neuronal activity underlying epileptiform activity is limited. To date, the changes in neuronal activity in association to epileptiform activity were largely described as diverse and heterogenous – which is, in other words, uncharacterized. Recently, emerging literature demonstrated that heterogenous changes in neuronal activity during epileptiform activity could be characterized based on the type of neuronal activity and the seizure onset pattern. Extending these research efforts to advance our understanding of the basic mechanisms of epilepsy, I studied simultaneously recorded neuronal and epileptiform or physiological activities in the rat entorhinal cortex (EC) using *in vitro* tetrode recordings.

In Chapter 2, my colleagues and I characterized the changes in neuronal activity during *in vitro* 4-aminopyridine (4AP)-induced ictal events presented with the sudden onset seizure pattern. We found that, around the onsets of 4AP-induced sudden onset ictal events, the firing rate of principal cells increased before that of interneurons. Immediately after ictal onsets, further increases in principal cell and interneuron firing rates were observed; notably, similar to the pre-ictal firing rate increase, this increase in principal cell firing rate preceded the increase in interneuron firing rate. Therefore, 4AP-induced sudden onset ictal events are characterized by principal cell activity increasing before interneuron activity – which is in stark contrast to the 4AP-induced low-voltage fast (LVF) onset ictal events that are characterized by interneuron activity increasing before principal cell activity.

In **Chapter 3** and **4**, I studied the influence of K⁺-Cl⁻ cotransporter 2 (KCC2) activity on neuronal and epileptiform activity by antagonizing KCC2 using VU0463271 in the *in vitro* 4AP model of epileptiform activity. By analyzing neuronal activity using single-unit recordings, I established that LVF onset ictal events were indeed abolished upon the application of VU0463271 and were replaced by continuous interictal spikes. These 4AP-induced interictal events occurring in the absence of KCC2 activity were associated with significant increases in interneuron and principal cell firing. When I further dissected the influence of KCC2 on neuronal activity during 4AP-induced epileptiform activity by antagonizing ionotropic glutamatergic signalling, I found that KCC2 antagonism shifted the occurrence of interneuron action potentials from the falling to

the rising phase of interictal events. Altogether, these findings suggest that KCC2 antagonism promotes neuronal hyperexcitability, particularly in interneurons.

In **Chapter 5**, I examined the interplay between inhibitory and excitatory mechanisms during theta oscillations induced *in vitro* by carbachol (CCh). I found that, around the onset of CCh-induced theta oscillations, the increase in interneuron activity preceded the increase in principal cell activity; furthermore, both increases were sustained throughout the theta oscillations. Upon GABA_A signalling antagonism, the sustained increases in interneuron and principal cell activities became transient, while the duration of the ongoing theta oscillations became more variable. Lastly, antagonizing ionotropic glutamatergic signalling abolished the theta oscillations and disrupted neuronal rhythmicity but did not change the neuronal firing rate. Therefore, the dynamics of theta oscillations are largely regulated by inhibitory mechanisms.

6.2. Seizure onset patterns and changes in neuronal activity

In light of existing experimental data, the work outlined in Chapter 2 of my thesis demonstrates that different seizure onset patterns are associated to distinct neuronal activity patterns. Previous experiments established that the increase in interneuron activity preceded the increase in principal cell activity around the onsets of LVF onset ictal events in the *in vitro* 4AP model of epileptiform activity (Lévesque et al., 2016b) and in human epileptic patients (Elahian et al., 2018). By demonstrating that principal cell activity increased before interneuron activity around the onsets of 4AP-induced sudden onset ictal events, I establish the relevance of ictal onset patterns to the characterization of changes in neuronal activity around ictal events.

Notably, a causal relationship exists between the specific types of neuronal activity and the observed ictal onset patterns. Using optogenetic techniques, activation of parvalbumin- and somatostatin-expressing interneurons – but not of calmodulin-dependent protein kinase-positive principal cells – induced LVF onset ictal events in the *in vitro* 4AP model (Shiri et al., 2016). Altogether, seizure onset patterns are associated to specific, and perhaps distinct, patterns of neuronal activity.

6.3. KCC2 antagonism and dynamics of neuronal activity

In Chapter 3, I found that 4AP-induced LVF onset ictal events – which involved interneuron activity around their seizure onsets as previously discussed – were abolished upon KCC2

antagonism. In the literature, KCC2 antagonisms were found to induce increases in intracellular [Cl⁻] (Sivakumaran et al., 2015; Kelley et al., 2018; Moore et al., 2018) but not in extracellular [K⁺] (Viitanen et al., 2010). With respect to ictogenesis, increases in intracellular [Cl⁻] and extracellular [K⁺] were found around seizure onset and thus proposed to facilitate ictogenesis (Lillis et al., 2012; Librizzi et al., 2017) through KCC2-mediated increases in neuronal excitability (Viitanen et al., 2010; Sivakumaran et al., 2015; Kelley et al., 2018; Moore et al., 2018). Therefore, my finding – namely, KCC2 antagonism abolished ictal events – underscores the ictogenic role of extracellular increases in [K⁺]. Furthermore, since extracellular [K⁺] were proposed to facilitate ictogenesis by synchronously increasing excitability of populations of neurons in close proximity (de Curtis and Avoli, 2016; de Curtis et al., 2018), my findings suggest that KCC2 antagonism could be opposing the ictogenesis of LVF onset ictal by preventing neuronal hypersynchrony in local populations of neurons.

With consideration to the existing data in literature, my investigations of the effects of KCC2 antagonism on 4AP-induced epileptiform activity in Chapter 3 and 4 provide further evidence emphasizing the role of KCC2 activity in neuronal excitability. Specifically, in 4AP-induced interictal events that continued to occur in the absence of KCC2 activity, I identified increases in interneuron and principal cell firing. Such increases in neuronal firing supported the presence of neuronal hyperexcitability, which was previously associated with the intracellular increase in [Cl⁻] after KCC2 antagonism (Sivakumaran et al., 2015; Kelley et al., 2018; Moore et al., 2018). Neuronal hyperexcitability was further demonstrated when interneuron action potentials were redistributed to the rising phase of 4AP-induced, ionotropic glutamatergic signalling-independent interictal events after KCC2 antagonism. Therefore, my experiments demonstrated that KCC2 antagonism induces neuronal excitability, presumably caused by intracellular [Cl⁻] increases, during epileptiform activity. Altogether, the experiments outlined in Chapter 3 and 4 demonstrate that KCC2 activity inversely modulates neuronal excitability and synchrony.

6.4. Interneurons in epilepsy

In the work highlighted in this thesis, changes in interneuron activity underlie several changes observed in the LFP activity. More specifically, significant increases in interneuron activity preceded that in principal cell activity around interictal events occurring with the 4AP-induced sudden onset ictal events. Furthermore, KCC2 antagonism enhanced interneuron firing rate during

4AP-induced interictal events. For 4AP-induced interictal events that occurred in the absence of ionotropic glutamatergic signalling, KCC2 antagonism altered the underlying interneuron firing pattern. Finally, antagonizing GABA_A signalling disrupted the interneuron activity and the rhythmicity of CCh-induced theta oscillations. Taken together, a recurrent theme throughout my investigations of neuronal activity underlying epileptiform activity is that interneuron activity contributes to epileptiform synchronization.

The work outlined in this thesis thus echoes one of the fundamental concepts in our current understanding of the basic mechanisms of epilepsy – interneurons actively contribute to the generation of epileptiform synchronization (de Curtis and Avoli, 2016). Investigations of ionic gradient attributed increases in intracellular [Cl] as well as extracellular [K⁺] that were identified around ictal onset to increases in interneuron activity (Lillis et al., 2012; Librizzi et al., 2017). Furthermore, analyses of neuronal firings associated increases in interneuron firing (Butuzova and Kitchigina, 2008; Grasse et al., 2013; Lévesque et al., 2016b; Wenzel et al., 2019) as well as interneuron synchrony with LFP (Grasse et al., 2013; Neumann et al., 2017) with ictal events. Similarly, interneuron activity was reported to increase before principal cell activity in human epilepsy (Elahian et al., 2018; Kandrács et al., 2019). In addition, examinations of pre-ictal theta rhythm reported increases in theta rhythm power and synchrony with underlying interneuron activity (Butuzova and Kitchigina, 2008; Grasse et al., 2013; Karunakaran et al., 2016). With optogenetic technology, researchers were able to establish a causal relationship between interneurons and ictal onsets – namely, optogenetic activation of interneurons initiates ictal events (Sessolo et al., 2015; Shiri et al., 2015, 2016; Yekhlef et al., 2015; Assaf and Schiller, 2016; Chang et al., 2018; Lévesque et al., 2019). Altogether, the experiments outlined in this thesis corroborate the literature and emphasize interneuron activity as an underlying mechanism of ictogenesis.

6.5. Future perspective and concluding remarks

The goal of my graduate studies is to advance therapeutic strategies for epilepsy. Given that many epileptic abnormalities could be captured by recording the LFP activity – which reflects the neuronal population activity – of the brain, understanding the neuronal activity during epileptic LFP activity could reveal mechanistic insights into the generation of epileptiform abnormalities. Accordingly, I utilized tetrodes – a technique that allowed me to simultaneously record neuronal and LFP activities – in *in vitro* models of epileptiform synchronization. A recurring revelation

throughout the experiments outlined in this thesis is that epileptic changes in LFP activity can be associated to distinct and specific changes in neuronal activity.

In Chapter 2, my colleagues and I characterized the neuronal activity during 4AP-induced sudden onset ictal and interictal events. By demonstrating that neuronal dynamics around the initiation of 4AP-induced sudden onset ictal events differs from that around the initiation of 4AP-induced LVF onset ictal events (Lévesque et al., 2016b) — it is evident that seizures are heterogenous and could to be sub-classified based on the LFP pattern. In addition, the experiments revealed that the neuronal dynamics underlying 4AP-induced sudden onset ictal events also differ from that underlying the accompanying interictal events, which raised the question about the mechanisms underlying the switch in neuronal dynamics between ictal and interictal events for future work. Altogether, the work outlined in Chapter 2 demonstrates that the epileptic LFP patterns could be associated to distinct neuronal dynamics.

In Chapter 3 and 4, I characterized the effects of KCC2 antagonism on the 4AP-induced neuronal and LFP activities. These experiments focused on 4AP-induced LVF onset ictal events, interictal events accompanying 4AP-induced LVF onset ictal events, and 4AP-induced interictal events that persist after ionotropic glutamatergic antagonism. As highlighted previously in the field, KCC2 involvement in epilepsy is highly dependent on the pathophysiological contexts that are under examination (Di Cristo et al., 2018). In other words, the effects of KCC2 antagonism must be examined in other models of epileptiform synchronization in order to increase the generalizability of the findings presented in these chapters.

In Chapter 5, I examined the inhibitory-excitatory interplay during CCh-induced theta oscillations. My experiments implicated inhibitory mechanisms in the control of theta rhythm dynamics, which were found to be altered prior to seizure onset (Butuzova and Kitchigina, 2008; Grasse et al., 2013; Fujita et al., 2014; Sedigh-Sarvestani et al., 2014; Toyoda et al., 2015; Karunakaran et al., 2016). Hence, my findings in this chapter corroborate previous work pointing to inhibitory mechanisms as the source of pre-ictal changes in theta oscillations (Butuzova and Kitchigina, 2008; Grasse et al., 2013; Toyoda et al., 2015; Karunakaran et al., 2016). In other words, epileptic changes in the theta rhythm of LFP activity could be an indication of changes in the underlying inhibitory mechanisms.

Altogether, the experiments outlined in this thesis associated epileptic changes in LFP activity with specific changes in the underlying neuronal activity. Future work could build on these

findings by characterizing the specific neuronal dynamics in other epileptic changes in LFP activity and establishing the reliability of epileptic changes in LFP activity as markers of neuronal activity changes in the epileptic pathophysiology. Together, these investigations would explore the potentials of epileptic changes in LFP activity as epileptic biomarkers, which would help advance epileptic therapeutic strategies in the clinic (Engel and Pitkänen, 2019; Pitkänen et al., 2019). While the work outlined in this thesis is not clinical in nature, it is part of the fundamental knowledge necessary for developing future clinical research that could advance therapeutic strategies available to people living with epilepsy.

In conclusion, the aim of my PhD study is to expand our understanding of neuronal activity underlying epileptiform activity – in particular, to decipher the reported heterogeneity in neuronal activities associated with epileptiform activity. While the findings presented in this thesis are not immediately translatable into the clinics, I believe that they are making critical contributions to our understanding of the basic mechanisms of epilepsy.

Reference List

- Aeed F, Shnitzer T, Talmon R, Schiller Y (2020) Layer- and Cell-Specific Recruitment Dynamics during Epileptic Seizures In Vivo. Annals of Neurology 87:97–115.
- Altafullah I, Halgren E, Stapleton JM, Crandall PH (1986) Interictal spike-wave complexes in the human medial temporal lobe: typical topography and comparisons with cognitive potentials. Electroencephalography and Clinical Neurophysiology 63:503–516.
- Alvarado-Rojas C, Lehongre K, Bagdasaryan J, Bragin A, Staba R, Engel JJ, Navarro V, Le Van Quyen M (2013) Single-unit activities during epileptic discharges in the human hippocampal formation. Front Comput Neurosci 7 Available at: https://www.frontiersin.org/articles/10.3389/fncom.2013.00140/full [Accessed January 24, 2020].
- Assaf F, Schiller Y (2016) The antiepileptic and ictogenic effects of optogenetic neurostimulation of PV-expressing interneurons. Journal of Neurophysiology 116:1694–1704.
- Avoli M, de Curtis M, Gnatkovsky V, Gotman J, Köhling R, Lévesque M, Manseau F, Shiri Z, Williams S (2016) Specific imbalance of excitatory/inhibitory signaling establishes seizure onset pattern in temporal lobe epilepsy. Journal of Neurophysiology 115:3229–3237.
- Avoli M, Jefferys JGR (2016) Models of drug-induced epileptiform synchronization in vitro. Journal of Neuroscience Methods 260:26–32.
- Avoli M, Panuccio G, Herrington R, D'Antuono M, de Guzman P, Lévesque M (2013) Two different interictal spike patterns anticipate ictal activity in vitro. Neurobiology of Disease 52:168–176.
- Babb TL, Crandall PH (1976) Epileptogenesis of human limbic neurons in psychomotor epileptics. Electroencephalography and Clinical Neurophysiology 40:225–243.
- Babb TL, Wilson CL, Isokawa-Akesson M (1987) Firing patterns of human limbic neurons during stereoencephalography (SEEG) and clinical temporal lobe seizures. Electroencephalography and Clinical Neurophysiology 66:467–482.
- Behr C, D'Antuono M, Hamidi S, Herrington R, Lévesque M, Salami P, Shiri Z, Köhling R, Avoli M (2014) Limbic networks and epileptiform synchronization: the view from the experimental side. Int Rev Neurobiol 114:63–87.
- Bikson M, Fox JE, Jefferys JGR (2003) Neuronal Aggregate Formation Underlies Spatiotemporal Dynamics of Nonsynaptic Seizure Initiation. Journal of Neurophysiology 89:2330–2333.
- Bower MR, Buckmaster PS (2008) Changes in Granule Cell Firing Rates Precede Locally Recorded Spontaneous Seizures by Minutes in an Animal Model of Temporal Lobe Epilepsy. Journal of Neurophysiology 99:2431–2442.
- Bower MR, Stead M, Meyer FB, Marsh WR, Worrell GA (2012) Spatiotemporal neuronal correlates of seizure generation in focal epilepsy. Epilepsia 53:807–816.

- Brodie MJ, Kelly K, Stephen LJ (2014) Prospective audits with newer antiepileptic drugs in focal epilepsy: Insights into population responses? Epilepsy & Behavior 31:73–76.
- Butuzova MV, Kitchigina VF (2008) Repeated blockade of GABAA receptors in the medial septal region induces epileptiform activity in the hippocampus. Neuroscience Letters 434:133–138.
- Buzsáki G (2002) Theta Oscillations in the Hippocampus. Neuron 33:325–340.
- Buzsáki G, Anastassiou CA, Koch C (2012) The origin of extracellular fields and currents EEG, ECoG, LFP and spikes. Nature Reviews Neuroscience 13:407–420.
- Calvin WH, Ojemann GA, Ward AA (1973) Human cortical neurons in epileptogenic foci: Comparison of inter-ictal firing patterns to those of "epileptic" neurons in animals. Electroencephalography and Clinical Neurophysiology 34:337–351.
- Chang M, Dian JA, Dufour S, Wang L, Moradi Chameh H, Ramani M, Zhang L, Carlen PL, Womelsdorf T, Valiante TA (2018) Brief activation of GABAergic interneurons initiates the transition to ictal events through post-inhibitory rebound excitation. Neurobiology of Disease 109:102–116.
- Chatrian GE, Bergamini, L, Dondey M, Klass DW, Lennox-Buchthal M, Petersén I (1974) A glossary of terms most commonly used by clinical electroencephalographers. Electroencephalography and Clinical Neurophysiology 37:538–548.
- Chen Z, Brodie MJ, Liew D, Kwan P (2018) Treatment Outcomes in Patients With Newly Diagnosed Epilepsy Treated With Established and New Antiepileptic Drugs: A 30-Year Longitudinal Cohort Study. JAMA Neurol 75:279–286.
- Choi H, Hayat MJ, Zhang R, Hirsch LJ, Bazil CW, Mendiratta A, Kato K, Javed A, Legge AW, Buchsbaum R, Resor S, Heiman GA (2016) Drug-resistant epilepsy in adults: Outcome trajectories after failure of two medications. Epilepsia 57:1152–1160.
- Cohen I, Huberfeld G, Miles R (2006) Emergence of disinhibition-induced synchrony in the CA3 region of the guinea pig hippocampus in vitro. The Journal of Physiology 570:583–594.
- Colgin LL (2016) Rhythms of the hippocampal network. Nat Rev Neurosci 17:239–249.
- Cymerblit-Sabba A, Schiller Y (2010) Network Dynamics during Development of Pharmacologically Induced Epileptic Seizures in Rats In Vivo. J Neurosci 30:1619–1630.
- de Curtis M, Avoli M (2016) GABAergic networks jump-start focal seizures. Epilepsia 57:679–687.
- de Curtis M, Uva L, Gnatkovsky V, Librizzi L (2018) Potassium dynamics and seizures: Why is potassium ictogenic? Epilepsy research 143:50–59.

- Delpire E, Baranczak A, Waterson AG, Kim K, Kett N, Morrison RD, Scott Daniels J, David Weaver C, Lindsley CW (2012) Further optimization of the K-Cl cotransporter KCC2 antagonist ML077: Development of a highly selective and more potent in vitro probe. Bioorganic & Medicinal Chemistry Letters 22:4532–4535.
- Di Cristo G, Awad PN, Hamidi S, Avoli M (2018) KCC2, epileptiform synchronization, and epileptic disorders. Progress in Neurobiology 162:1–16.
- Dichter M, Herman C, Selzer M (1973) Extracellular unit analysis of the hippocampal penicillin focus. Electroencephalography and Clinical Neurophysiology 34:619–629.
- Elahian B, Lado NE, Mankin E, Vangala S, Misra A, Moxon K, Fried I, Sharan A, Yeasin M, Staba R, Bragin A, Avoli M, Sperling MR, Engel J, Weiss SA (2018) Low-Voltage Fast Seizures in Humans Begin With Increased Interneuron Firing. Annals of Neurology 0 Available at: https://onlinelibrary.wiley.com/doi/abs/10.1002/ana.25325 [Accessed September 26, 2018].
- Engel J (2018) The current place of epilepsy surgery. Current Opinion in Neurology 31:192–197.
- Engel J, McDermott MP, Wiebe S, Langfitt JT, Stern JM, Dewar S, Sperling MR, Gardiner I, Erba G, Fried I, Jacobs M, Vinters HV, Mintzer S, Kieburtz K, for the Early Randomized Surgical Epilepsy Trial (ERSET) Study Group (2012) Early Surgical Therapy for Drug-Resistant Temporal Lobe Epilepsy: A Randomized Trial. JAMA 307:922–930.
- Engel J, Pitkänen A (2019) Biomarkers for epileptogenesis and its treatment. Neuropharmacology:107735.
- Engel JJr (2013) Seizures and epilepsy, Second edition. New York: Oxford University Press.
- Enomoto TF, Ajmone-Marsan C (1959) Epileptic activation of single cortical neurons and their relationship with electroencephalographic discharges. Electroencephalography and Clinical Neurophysiology 11:199–218.
- Ewell LA, Liang L, Armstrong C, Soltész I, Leutgeb S, Leutgeb JK (2015) Brain State Is a Major Factor in Preseizure Hippocampal Network Activity and Influences Success of Seizure Intervention. J Neurosci 35:15635–15648.
- Fiest KM, Sauro KM, Wiebe S, Patten SB, Kwon C-S, Dykeman J, Pringsheim T, Lorenzetti DL, Jetté N (2017) Prevalence and incidence of epilepsy: A systematic review and meta-analysis of international studies. Neurology 88:296–303.
- Fisher RS, Acevedo C, Arzimanoglou A, Bogacz A, Cross JH, Elger CE, Engel J, Forsgren L, French JA, Glynn M, Hesdorffer DC, Lee BI, Mathern GW, Moshé SL, Perucca E, Scheffer IE, Tomson T, Watanabe M, Wiebe S (2014) ILAE Official Report: A practical clinical definition of epilepsy. Epilepsia 55:475–482.

- Fisher RS, Boas W van E, Blume W, Elger C, Genton P, Lee P, Engel J (2005) Epileptic Seizures and Epilepsy: Definitions Proposed by the International League Against Epilepsy (ILAE) and the International Bureau for Epilepsy (IBE). Epilepsia 46:470–472.
- Fujita S, Toyoda I, Thamattoor AK, Buckmaster PS (2014) Preictal activity of subicular, CA1, and dentate gyrus principal neurons in the dorsal hippocampus before spontaneous seizures in a rat model of temporal lobe epilepsy. J Neurosci 34:16671–16687.
- Gibbs FA, Davis H, Lennox WG (1935) THE ELECTRO-ENCEPHALOGRAM IN EPILEPSY AND IN CONDITIONS OF IMPAIRED CONSCIOUSNESS. Arch NeurPsych 34:1133–1148.
- Gilioli I, Vignoli A, Visani E, Casazza M, Canafoglia L, Chiesa V, Gardella E, Briola FL, Panzica F, Avanzini G, Canevini MP, Franceschetti S, Binelli S (2012) Focal epilepsies in adult patients attending two epilepsy centers: Classification of drug-resistance, assessment of risk factors, and usefulness of "new" antiepileptic drugs. Epilepsia 53:733–740.
- Gilmour H, Ramage-Morin P, Wong SL (2016) Epilepsy in Canada: Prevalence and impact. Health Reports 27:24–30.
- Grasse DW, Karunakaran S, Moxon KA (2013) Neuronal synchrony and the transition to spontaneous seizures. Exp Neurol 248:72–84.
- Gulyás AI, Sík A, Payne JA, Kaila K, Freund TF (2001) The KCl cotransporter, KCC2, is highly expressed in the vicinity of excitatory synapses in the rat hippocampus. European Journal of Neuroscience 13:2205–2217.
- Ishijima B (1972) Unitary Analysis of Epileptic Activity in Acute and Chronic Foci and Related Cortex of Cat and Monkey. Epilepsia 13:561–581.
- Ishijima B, Hori T, Yoshimasa N, Fukushima T, Hirakawa K, Sekino H (1975) Neuronal activities in human epileptic foci and surrounding areas. Electroencephalography and Clinical Neurophysiology 39:643–650.
- Jobst BC, Cascino GD (2015) Resective Epilepsy Surgery for Drug-Resistant Focal Epilepsy: A Review. JAMA 313:285–293.
- Kahle KT et al. (2014) Genetically encoded impairment of neuronal KCC2 cotransporter function in human idiopathic generalized epilepsy. EMBO reports 15:766–774.
- Kaila K, Price TJ, Payne JA, Puskarjov M, Voipio J (2014) Cation-chloride cotransporters in neuronal development, plasticity and disease. Nature Reviews Neuroscience 15:637–654.
- Kandel ER, Schwartz JH, Jessell TM, Siegelbaum SA, Hudspeth AJ (2013) Principles of neural science, 5th ed. New York: McGraw-Hill. Available at: http://books.google.com/books?vid=isbn9780071390118.

- Kandrács Á, Hofer KT, Tóth K, Tóth EZ, Entz L, Bagó AG, Erőss L, Jordán Z, Nagy G, Fabó D, Ulbert I, Wittner L (2019) Presence of synchrony-generating hubs in the human epileptic neocortex. The Journal of Physiology 597:5639–5670.
- Karlócai MR, Kohus Z, Káli S, Ulbert I, Szabó G, Máté Z, Freund TF, Gulyás AI (2014) Physiological sharp wave-ripples and interictal events in vitro: what's the difference? Brain 137:463–485.
- Karunakaran S, Grasse DW, Moxon KA (2016) Role of CA3 theta-modulated interneurons during the transition to spontaneous seizures. Exp Neurol 283:341–352.
- Keller CJ, Truccolo W, Gale JT, Eskandar E, Thesen T, Carlson C, Devinsky O, Kuzniecky R, Doyle WK, Madsen JR, Schomer DL, Mehta AD, Brown EN, Hochberg LR, Ulbert I, Halgren E, Cash SS (2010) Heterogeneous neuronal firing patterns during interictal epileptiform discharges in the human cortex. Brain 133:1668–1681.
- Kelley MR, Cardarelli RA, Smalley JL, Ollerhead TA, Andrew PM, Brandon NJ, Deeb TZ, Moss SJ (2018) Locally Reducing KCC2 Activity in the Hippocampus is Sufficient to Induce Temporal Lobe Epilepsy. EBioMedicine 32:62–71.
- Kowalczyk T, Bocian R, Konopacki J (2013) The generation of theta rhythm in hippocampal formation maintained in vitro. Eur J Neurosci 37:679–699.
- Kwan P, Arzimanoglou A, Berg AT, Brodie MJ, Hauser WA, Mathern G, Moshé SL, Perucca E, Wiebe S, French J (2010) Definition of drug resistant epilepsy: Consensus proposal by the ad hoc Task Force of the ILAE Commission on Therapeutic Strategies. Epilepsia 51:1069–1077.
- Lambrecq V, Lehongre K, Adam C, Frazzini V, Mathon B, Clemenceau S, Hasboun D, Charpier S, Baulac M, Navarro V, Quyen MLV (2017) Single-unit activities during the transition to seizures in deep mesial structures. Annals of Neurology 82:1022–1028.
- Lévesque M, Avoli M (2018) Carbachol-Induced theta-like oscillations in the rodent brain limbic system: Underlying mechanisms and significance. Neuroscience & Biobehavioral Reviews 95:406–420.
- Lévesque M, Avoli M, Bernard C (2016a) Animal models of temporal lobe epilepsy following systemic chemoconvulsant administration. Journal of Neuroscience Methods 260:45–52.
- Lévesque M, Chen L-Y, Etter G, Shiri Z, Wang S, Williams S, Avoli M (2019) Paradoxical effects of optogenetic stimulation in mesial temporal lobe epilepsy. Ann Neurol.
- Lévesque M, Herrington R, Hamidi S, Avoli M (2016b) Interneurons spark seizure-like activity in the entorhinal cortex. Neurobiology of Disease 87:91–101.
- Librizzi L, Losi G, Marcon I, Sessolo M, Scalmani P, Carmignoto G, Curtis M de (2017) Interneuronal Network Activity at the Onset of Seizure-Like Events in Entorhinal Cortex Slices. J Neurosci 37:10398–10407.

- Lillis KP, Kramer MA, Mertz J, Staley KJ, White JA (2012) Pyramidal cells accumulate chloride at seizure onset. Neurobiology of Disease 47:358–366.
- Löscher W, Schmidt D (2011) Modern antiepileptic drug development has failed to deliver: Ways out of the current dilemma. Epilepsia 52:657–678.
- Misra A, Long X, Sperling MR, Sharan AD, Moxon KA (2018) Increased neuronal synchrony prepares mesial temporal networks for seizures of neocortical origin. Epilepsia 59:636–649.
- Moore YE, Deeb TZ, Chadchankar H, Brandon NJ, Moss SJ (2018) Potentiating KCC2 activity is sufficient to limit the onset and severity of seizures. PNAS:201810134.
- Muldoon SF, Villette V, Tressard T, Malvache A, Reichinnek S, Bartolomei F, Cossart R (2015) GABAergic inhibition shapes interictal dynamics in awake epileptic mice. Brain 138:2875–2890.
- Naftulin JS, Ahmed OJ, Piantoni G, Eichenlaub J-B, Martinet L-E, Kramer MA, Cash SS (2018) Ictal and preictal power changes outside of the seizure focus correlate with seizure generalization. Epilepsia 59:1398–1409.
- Neumann AR, Raedt R, Steenland HW, Sprengers M, Bzymek K, Navratilova Z, Mesina L, Xie J, Lapointe V, Kloosterman F, Vonck K, Boon PAJM, Soltesz I, McNaughton BL, Luczak A (2017) Involvement of fast-spiking cells in ictal sequences during spontaneous seizures in rats with chronic temporal lobe epilepsy. Brain 140:2355–2369.
- Ngugi AK, Bottomley C, Kleinschmidt I, Sander JW, Newton CR (2010) Estimation of the burden of active and life-time epilepsy: A meta-analytic approach. Epilepsia 51:883–890.
- Otsu Y, Donneger F, Schwartz EJ, Poncer JC (2020) Cation-chloride cotransporters and the polarity of GABA signalling in mouse hippocampal parvalbumin interneurons. The Journal of Physiology Available at: https://physoc.onlinelibrary.wiley.com/doi/abs/10.1113/JP279221 [Accessed February 6, 2020].
- Perucca P, Dubeau F, Gotman J (2014) Intracranial electroencephalographic seizure-onset patterns: effect of underlying pathology. Brain 137:183–196.
- Pitkänen A, Ekolle Ndode-Ekane X, Lapinlampi N, Puhakka N (2019) Epilepsy biomarkers Toward etiology and pathology specificity. Neurobiology of Disease 123:42–58.
- Pohlen MS, Jin J, Tobias RS, Maheshwari A (2017) Pharmacoresistance with newer anti-epileptic drugs in mesial temporal lobe epilepsy with hippocampal sclerosis. Epilepsy Research 137:56–60.
- Prince DA, Wilder BJ (1967) Control Mechanisms in Cortical Epileptogenic Foci*: Surround Inhibition. Arch Neurol 16:194–202.

- Puskarjov M, Seja P, Heron SE, Williams TC, Ahmad F, Iona X, Oliver KL, Grinton BE, Vutskits L, Scheffer IE, Petrou S, Blaesse P, Dibbens LM, Berkovic SF, Kaila K (2014) A variant of KCC2 from patients with febrile seizures impairs neuronal Cl– extrusion and dendritic spine formation. EMBO reports 15:723–729.
- Quesney LF (1986) Clinical and EEG features of complex partial seizures of temporal lobe origin. Epilepsia 27 Suppl 2:S27-45.
- Saito T, Ishii A, Sugai K, Sasaki M, Hirose S (2017) A de novo missense mutation in SLC12A5 found in a compound heterozygote patient with epilepsy of infancy with migrating focal seizures. Clinical Genetics 92:654–658.
- Saitsu H, Watanabe M, Akita T, Ohba C, Sugai K, Ong WP, Shiraishi H, Yuasa S, Matsumoto H, Beng KT, Saitoh S, Miyatake S, Nakashima M, Miyake N, Kato M, Fukuda A, Matsumoto N (2016) Impaired neuronal KCC2 function by biallelic *SLC12A5* mutations in migrating focal seizures and severe developmental delay. Scientific Reports 6:30072.
- Schevon CA, Weiss SA, McKhann G, Goodman RR, Yuste R, Emerson RG, Trevelyan AJ (2012) Evidence of an inhibitory restraint of seizure activity in humans. Nat Commun 3:1–11.
- Schmidt RP, Thomas LB, Ward AA (1959) The hyper-excitable neurone. microelectrode studies of chronic epileptic foci in monkey. Journal of Neurophysiology 22:285–296.
- Sedigh-Sarvestani M, Thuku GI, Sunderam S, Parkar A, Weinstein SL, Schiff SJ, Gluckman BJ (2014) Rapid eye movement sleep and hippocampal theta oscillations precede seizure onset in the tetanus toxin model of temporal lobe epilepsy. J Neurosci 34:1105–1114.
- Semah F, Picot MC, Adam C, Broglin D, Arzimanoglou A, Bazin B, Cavalcanti D, Baulac M (1998) Is the underlying cause of epilepsy a major prognostic factor for recurrence? Neurology 51:1256–1262.
- Sessolo M, Marcon I, Bovetti S, Losi G, Cammarota M, Ratto GM, Fellin T, Carmignoto G (2015) Parvalbumin-Positive Inhibitory Interneurons Oppose Propagation But Favor Generation of Focal Epileptiform Activity. J Neurosci 35:9544–9557.
- Shiri Z, Manseau F, Lévesque M, Williams S, Avoli M (2015) Interneuron activity leads to initiation of low-voltage fast-onset seizures. Annals of Neurology 77:541–546.
- Shiri Z, Manseau F, Lévesque M, Williams S, Avoli M (2016) Activation of specific neuronal networks leads to different seizure onset types. Ann Neurol 79:354–365.
- Sivakumaran S, Cardarelli RA, Maguire J, Kelley MR, Silayeva L, Morrow DH, Mukherjee J, Moore YE, Mather RJ, Duggan ME, Brandon NJ, Dunlop J, Zicha S, Moss SJ, Deeb TZ (2015) Selective Inhibition of KCC2 Leads to Hyperexcitability and Epileptiform Discharges in Hippocampal Slices and In Vivo. J Neurosci 35:8291–8296.
- Spencer SS, Spencer DD (1994) Entorhinal-Hippocampal Interactions in Medial Temporal Lobe Epilepsy. Epilepsia 35:721–727.

- Stephen LJ, Kwan P, Brodie MJ (2001) Does the Cause of Localisation-Related Epilepsy Influence the Response to Antiepileptic Drug Treatment? Epilepsia 42:357–362.
- Stödberg T et al. (2015) Mutations in *SLC12A5* in epilepsy of infancy with migrating focal seizures. Nature Communications 6:8038.
- Till Á, Szalai R, Hegyi M, Kövesdi E, Büki G, Hadzsiev K, Melegh B (2019) [A rare form of ion channel gene mutation identified as underlying cause of generalized epilepsy]. Orv Hetil 160:835–838.
- Toyoda I, Fujita S, Thamattoor AK, Buckmaster PS (2015) Unit Activity of Hippocampal Interneurons before Spontaneous Seizures in an Animal Model of Temporal Lobe Epilepsy. J Neurosci 35:6600–6618.
- Truccolo W, Donoghue JA, Hochberg LR, Eskandar EN, Madsen JR, Anderson WS, Brown EN, Halgren E, Cash SS (2011) Single-neuron dynamics in human focal epilepsy. Nature Neuroscience 14:635–641.
- Verzeano M, Crandall PH, Dymond A (1971) Neuronal activity of the amygdala in patients with psychomotor epilepsy. Neuropsychologia 9:331–344.
- Viitanen T, Ruusuvuori E, Kaila K, Voipio J (2010) The K+–Cl– cotransporter KCC2 promotes GABAergic excitation in the mature rat hippocampus. The Journal of Physiology 588:1527–1540.
- Weiss SA, Alvarado-Rojas C, Bragin A, Behnke E, Fields T, Fried I, Engel J, Staba R (2016) Ictal onset patterns of local field potentials, high frequency oscillations, and unit activity in human mesial temporal lobe epilepsy. Epilepsia 57:111–121.
- Weiss SA, Banks GP, McKhann GM, Goodman RR, Emerson RG, Trevelyan AJ, Schevon CA (2013) Ictal high frequency oscillations distinguish two types of seizure territories in humans. Brain 136:3796–3808.
- Wennberg R, Arruda F, Quesney LF, Olivier A (2002) Preeminence of Extrahippocampal Structures in the Generation of Mesial Temporal Seizures: Evidence from Human Depth Electrode Recordings. Epilepsia 43:716–726.
- Wenzel M, Hamm JP, Peterka DS, Yuste R (2019) Acute Focal Seizures Start As Local Synchronizations of Neuronal Ensembles. J Neurosci 39:8562–8575.
- Wiebe S, Blume WT, Girvin JP, Eliasziw M, Effectiveness and Efficiency of Surgery for Temporal Lobe Epilepsy Study Group (2001) A randomized, controlled trial of surgery for temporal lobe epilepsy. N Engl J Med 345:311–318.
- Wyler AR, Ojemann GA, Ward AA (1982) Neurons in human epileptic cortex: Correlation between unit and EEG activity. Annals of Neurology 11:301–308.

Yekhlef L, Breschi GL, Lagostena L, Russo G, Taverna S (2015) Selective activation of parvalbumin- or somatostatin-expressing interneurons triggers epileptic seizurelike activity in mouse medial entorhinal cortex. Journal of Neurophysiology 113:1616–1630.